The influence of petrogenetic processes on the composition of Ocean Island Basalts: Studies of lavas from Hawaii and Tubuai Islands

Dissertation

Zur Erlangung des Grades

"Doktor des Naturwissenschaften"

Am Fachbereich

Chemie, Pharmazie und Geowissenschaften

der Johannes Gutenberg-Universität Mainz

Marie Jamais

Geb. am 06.12.1976 in Nancy, Frankreich

Mainz, 2006

All views and results in this thesis are those of the authors, unless stated otherwise.

Ich versichere hiermit, die vorliegende Arbeit selbständig verfasst zu haben und alle benutzen Hilfsmittel und Quellen in der Arbeit angegeben zu haben.

à mon père,

et à son éternelle soif de connaissance

Abstract

Ocean Island Basalts (OIB) provide important information on the chemical and physical characteristics of their mantle sources. However, the geochemical composition of a generated magma is significantly affected by partial melting and/or subsequent fractional crystallization processes. In addition, the isotopic composition of an ascending magma may be modified during transport through the oceanic crust. The influence of these different processes on the chemical and isotopic composition of OIB from two different localities, Hawaii and Tubuai in the Pacific Ocean, are investigated here.

In a first chapter, the Os-isotope variations in suites of lavas from Kohala Volcano, Hawaii, are examined to constrain the role of melt/crust interactions on the evolution of these lavas. As $^{187}Os/^{188}Os$ sensitivity to any radiogenic contaminant strongly depend on the Os content in the melt, Os and other PGE variations are investigated first. This study reveals that Os and other PGE behavior change during the Hawaiian magma differentiation. While PGE concentrations are relatively constant in lavas with relatively primitive compositions, all PGE contents strongly decrease in the melt as it evolved through ~ 8% MgO. This likely reflects the sulfur saturation of the Hawaiian magma and the onset of sulfide fractionation at around 8% MgO. Kohala tholeiites with more than 8% MgO and rich in Os have homogeneous $^{187}Os/^{188}Os$ values likely to represent the mantle signature of Kohala lavas. However, Os isotopic ratios become more radiogenic with decreasing MgO and Os contents in the lavas, which reflects assimilation of local crust material during fractional crystallization processes. Less than 8% upper oceanic crust assimilation could have produced the most radiogenic Os-isotope ratios recorded in the shield lavas. However, these small amounts of upper crust assimilation have only negligible effects on Sr and Nd isotopic ratios and therefore, are not responsible for the Sr and Nd isotopic heterogeneities observed in Kohala lavas.

In a second chapter, fractional crystallization and partial melting processes are constrained using major and trace element variations in the same suites of lavas from Kohala Volcano, Hawaii. This inverse modeling approach allows the estimation of most of the trace element composition of the Hawaiian mantle source. The calculated initial trace element pattern shows slight depletion of the concentrations from LREE to the most incompatible elements, which indicates that the incompatible element enrichments described by the Hawaiian melt patterns are entirely produced by partial melting processes. The “Kea trend” signature of lavas from Kohala

Volcano is also confirmed, with Kohala lavas having lower Sr/Nd and La/Th ratios than lavas from Mauna Loa Volcano.

Finally, the magmatic evolution of Tubuai Island is investigated in a last chapter using the trace element and Sr, Nd, Hf isotopic variations in mafic lava suites. The Sr, Nd and Hf isotopic data are homogeneous and typical for the HIMU-type OIB and confirms the cogenetic nature of the different mafic lavas from Tubuai Island. The trace element patterns show progressive enrichment of incompatible trace elements with increasing alkali content in the lavas, which reflect progressive decrease in the degree of partial melting towards the later volcanic events. In addition, this enrichment of incompatible trace elements is associated with relative depletion of Rb, Ba, K, Nb, Ta and Ti in the lavas, which require the presence of small amount of residual phlogopite and of a Ti-bearing phase (ilmenite or rutile) during formation of the younger analcitic and nephelinitic magmas.

Zusammenfassung

Ozeaninselbasalte liefern wichtige Informationen über die chemischen und physikalischen Eigenschaften ihrer Ausgangsgesteine im Erdmantel. Die chemische Zusammensetzung von Mantelschmelzen wird jedoch entscheidend während des partiellen Schmelzens und der anschließenden fraktionierten Kristallisation verändert. Zudem kann auch die isotopische Zusammensetzung von Mantelschmelzen während des Transports durch die ozeanische Kruste verändert werden. Anhand von Laven zweier ozeanischer Inseln, Hawaii und Tubuai im Pazifischen Ozean, wird in dieser Dissertation der Einfluss dieser sekundären Prozesse auf die chemische und isotopische Zusammensetzung von Schmelzen des Erdmantels untersucht.

Im ersten Kapitel wird untersucht welchen Einfluss die Wechselwirkung zwischen Schmelzen des Kohala Vulkans (Hawaii) und der umgebenden Kruste während des Magmentransports und der Magmendifferenzierung auf die Os Isotopenzusammensetzung der Schmelze hat. Da die Os Konzentration der Schmelze entscheidend dafür ist wie stark die $^{187}Os/^{188}Os$ Werte durch Assimilation von umgebendem Krustenmaterial beeinflusst werden, werden in einem ersten Schritt die Variation der Konzentrationen der Platin Gruppen Elemente während der magmatischen Differenzierung untersucht. Dabei zeigt sich, dass sich das Verhalten von Os und anderen Platingruppenelementen während der Magmendifferenzierung ändert. Die Konzentrationen der Paltingruppenelemente in Laven mit primitiver Zusammensetzung bleiben relativ konstant, nehmen aber stark ab sobald die Laven einen MgO

Gehalt von etwa 8wt. % unterschreiten. Dieser Effekt geht wahrscheinlich auf die Schwefelsättigung und die damit beginnende Schwefelfraktionierung der Magmen bei etwa 8% MgO zurück. Tholeiite mit mehr als 8% MgO und hohen Os Gehalten haben homogene $^{187}Os/^{188}Os$ Werte, die sehr wahrscheinlich der des aufschmelzenden Erdmantels unter Kohala entsprechen. Die Os Isotopenverhältnisse steigen allerdings mit abnehmendem Os Gehalt der Magmen an, was ein Hinweis für Assimilation der lokalen Kruste während der fraktionierten Kristallisation ist. Assimilation von weniger als 8% der oberen ozeanischen Kruste ist ausreichend um die radiogensten Osmium-Isotopeverhältnisse der Kohala Laven zu erklären. Da solch relative geringe Mengen an assimilierter Kruste keinen nennenswerten Effekt auf die Sr und Nd Isotopenverhältnisse haben, kann die beobachtete Variation der Sr und Nd Isotopenverhältnisse nicht allein auf diesen Effekt zurückgeführt werden.

Im zweiten Kapitel werden die Auswirkungen von partieller Schmelzbildung und fraktionierter Kristallisation auf die Haupt- und Spurenelementkonzentrationen der Kohala Laven untersucht. Mit Hilfe von inversen Spurenelementmodellierungen wurden zudem die Spurenelementkonzentrationen in der Mantelquelle geschätzt. Die errechneten Spurenelementkonzentrationen zeigen eine leichte Verarmung der leichten Seltenen Erd Elemente gegenüber den inkompatibelsten Spurenelementen, was zeigt dass deren Anreicherung in den Schmelzen allein ein Resultat der partiellen Schmelzbildung ist und nicht auf eine Anreicherung dieser Element relativ zu den leichten Seltenen Erd Elemente in der Mantelquelle zurückzuführen ist. Die niedrigeren Sr/Nd und La/Th Verhältnisse der Kohala Laven im Vergleich zu Laven von Mauna Loa zeigen zudem, dass diese Laven den Laven des sogenannten “Kea Trends” zuzuordnen sind.

Im letzten Kapitel wird die chemische Entwicklung mafischer Laven von Tubuai anhand deren Spurenelement- und Sr, Nd, Hf Isotopenvariationen untersucht. Die Sr, Nd, und Hf Isotopenverhältnisse in allen Laven sind homogen, was auf den Ursprung der Laven aus einer homogenen Mantelquelle hindeutet. Sie sind typisch für Ozeaninselbasalte des HIMU Typs. Die zunehmende Anreicherung an inkompatiblen Spurenelementen mit zunehmender Alkalinität der Laven lässt auf Entstehung durch zunehmend niedrigere partielle Schmelzgrade schließen. Die damit einhergehende relative Verarmung an Rb, Ba, K, Nb, Ta and Ti ist ein Hinweis auf eine geringe Menge an residualem Phlogopit und einer Ti-führenden Mineralphase (Ilmenit oder Rutil) während der Schmelzbildung der Analcite and Nephelinite.

Contents

Introduction

1. Mantle signatures in oceanic basalts

Mantle-derived magmas provide important information on the geochemical composition of the Earth's mantle and its evolution into different "mantle reservoirs". The development of different mantle reservoirs is ultimately related to the formation of new oceanic crust and the concurrent depletion of the upper mantle composition at mid oceanic ridges, and to the subsequent recycling of the oceanic and/or continental crust through the mantle. Oceanic basalts provide particularly accurate information on mantle composition because the oceanic crust is very thin (5 – 6 km) compared to the continental crust (30 – 40 km), which reduces the risk of contamination during magma transport to the surface. Ocean basalts mainly include Mid-Ocean Ridge Basalts (MORB) and Ocean Island Basalts (OIB). MORB are thought to sample the upper depleted mantle (DMM) while OIB may derive from deeper layers down to the 660 km seismic boundary or even to the core - mantle boundary (2900 km e.g. Hofmann, 1997).

As inferred from geochemical and isotopic studies, the composition of OIB possibly reflects a mixture of several mantle components such as undepleted lower mantle, recycled oceanic lithosphere or recycled subcontinental sediments (e.g. Hofmann and White, 1982; White, 1985; Zindler and Hart, 1986; Hart, 1988; Hart et al., 1992). At least five isotopically extreme components have been invoked: HIMU, two enriched mantle components EM-1 and EM-2, the depleted MORB mantle (DMM) and FOZO. The HIMU component (Zindler and Hart, 1986) has the highest Pb-isotope ratios and the lowest Sr-isotope ratios of any OIB and has most often been interpreted as reflecting recycled altered oceanic crust (Chase, 1981; Hofmann and White, 1982; Weaver, 1991; Chauvel et al., 1992) (Fig. 1). The origin of the EM-1 and EM-2 components is more controversial. The EM-1 component (Zindler and Hart, 1986) exhibits very low $^{143}Nd/^{144}Nd$, relatively low $^{87}Sr/^{86}Sr$ and low Pb-isotopes ratios (Fig. 1) and is thought to originate either from recycling of subcontinental lithosphere (e.g. McKenzie and O'nions, 1983; Mahoney et al., 1991; Milner and Le Roex, 1996), from recycling of ancient pelagic sediment (Ben Othman et al., 1989; Weaver, 1991; Chauvel et al., 1992; Rehkämper and Hofmann, 1997; Plank and Langmuir, 1998; Eisele et al., 2002) or from lower continental crust material (Willbold and Stracke, 2006). The EM-2 component has the highest $^{87}Sr/^{86}Sr$ (Fig. 1) and relatively high $^{207}Pb/^{204}Pb$ ratios and is though to be formed by recycling of oceanic crust plus small amounts of terrigeneous sediments (e.g. Zindler and Hart, 1986) or , alternatively , by metasomatized oceanic lithosphere (Workman et al., 2004). The DMM component is defined by

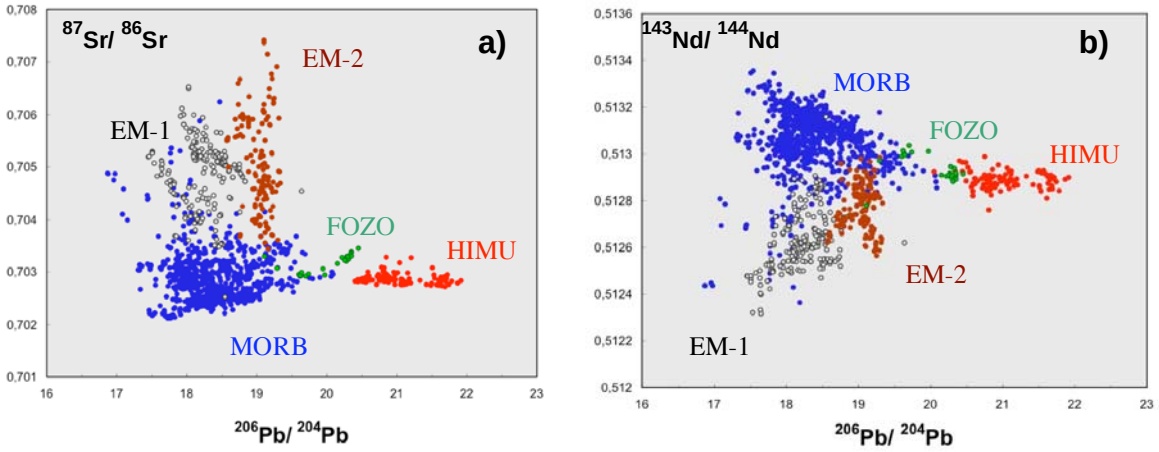

Fig. 1: a) *$^{206}Pb/^{204}Pb$ versus $^{87}Sr/^{86}Sr$ diagram and* ***b)*** *$^{206}Pb/^{204}Pb$ versus $^{143}Nd/^{144}Nd$ diagram showing isotopic compositions of the different mantle reservoir sampled by OIB (EM-1, EM-2, HIMU and FOZO) plotted together with MORB. Figure modified from figure 1 of Stracke et al. (2003) and Stracke et al. (2005).*

the most depleted MORB samples, with the highest $^{143}Nd/^{144}Nd$ and the lowest Sr- and Pb-isotopes ratios. Finally, the FOZO component (for FOcus ZOne) has been defined as the point of convergence of Sr-Nd-Pb isotope arrays for individual ocean islands (Hart et al., 1992), and recently redefined as being the radiogenic end of the trend of MORB in a $^{206}Pb/^{204}Pb$ versus $^{87}Sr/^{86}Sr$ diagram (Fig. 1) (Stracke et al., 2005). FOZO has slightly less radiogenic Pb-isotope ratios and more radiogenic Sr-isotope ratios than the HIMU component (Stracke et al., 2005).

Although the isotopic signature of the mantle source is relatively well preserved during magma genesis and ascent of the melt to the surface, the geochemical composition of the generated melts is significantly affected by partial melting and/or subsequent fractional crystallization and potential assimilation processes. Partial melting concentrates the most incompatible elements (i.e. elements that are the most difficult to incorporate into the crystal structure of common mantle minerals) into the melts, an affect that is most pronounced at low degrees of partial melting. When magmas reach the mantle – crust boundary, the density contrast between mantle peridotites and lower crustal gabbros leads to stalling and differentiation of the cooling magmas into magma chamber. Mineral phases fractionate from magmas as their temperature decrease, inducing changes in their major and trace element compositions. In addition, mantle-derived melts may assimilate small quantities of surrounding crustal material, which could potentially modify their geochemical and also isotopic signatures. In order to decipher the mantle composition recorded in ocean basalts, numerous studies have been developed over the last 40 years on the behavior of major and trace elements during petrogenetic processes and on the partitioning of major and trace elements between the different

mineral phases and melts. Various inverse modeling approaches have also been developed to constrain partial melting (Shaw, 1970; Minster and Allègre, 1978; Hofmann and Feigenson, 1983; Mckenzie, 1985), fractional crystallization (Hofmann and Feigenson, 1983; Danyushevsky et al., 2000) or assimilation / fractional crystallization (DePaolo, 1981) processes.

In this thesis, chemical and isotopic data of OIB from two different localities, Hawaii in the North Pacific and Tubuai Island, Cook-Austral chain in the South Pacific (Fig. 2) are used in conjunction with previously developed petrogenetic models to evaluate their effects on the geochemical and isotopic compositions of the erupted lavas.

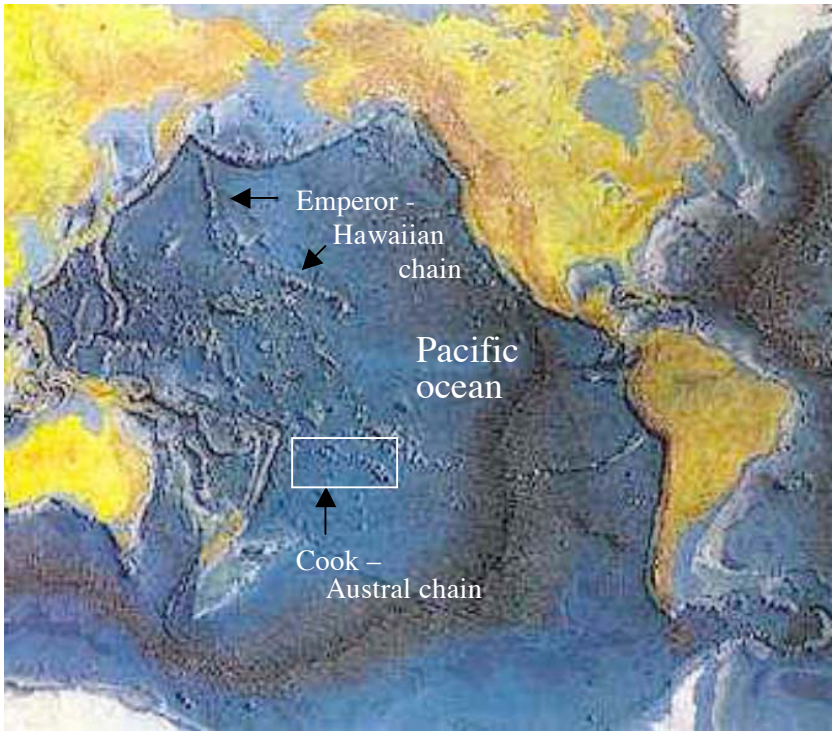

Fig. 2: *Map of the Pacific Ocean's floor showing the location of the Hawaiian-Emperor chain in the north and of the Cook-Austral chain in the south. Extract from the world ocean floor map (http://platetectonics.com/oceanfloors/index.asp).*

2. The Hawaiian mantle plume

The Hawaiian Islands are situated at the Southeast end of the Hawaiian-Emperor chain that stretches over 6000 km in the North Pacific Ocean (Fig. 2), and represent one of the most actively studied hot-spot localities on Earth. The linear volcanic islands and seamounts that form the Hawaiian-Emperor chain show a regular age progression from the active Loihi, Kilauea and

Mauna Loa volcanoes, located at the southeastern end, to the 75-80 Ma old volcanoes located at the northwestern end of the chain. The direction of alignment changes from SE-NW in the Hawaiian chain to S-N in the Emperor chain (Fig. 2). The alignment of these volcanic islands and seamounts over 70 Ma has been shown to reflect the motion of the Pacific plate above a stationary hotspot (Wilson, 1963; Clague and Dalrymple, 1987; Sharp and Clague, 2006). Combined geophysical and isotopic studies suggest that the Hawaiian lavas are the production of a deep-seated mantle plume, rising up from the lower mantle (e.g. Morgan, 1972; Kurz et al., 1982; Kurz et al., 1983; Montelli et al., 2006).

Typically, the Hawaiian volcanoes evolve through four stages of volcanic activities as the pacific plate moves above the hotspot: preshield, main shield or shield building, postshield and rejuvenated stage (MacDonald, 1968; Clague and Dalrymple, 1987). The alkalic preshield lavas are usually buried under the shield stage lavas and are rarely exposed subaerially. The preshield stage corresponds to the current volcanic stage of the Loihi seamount. The tholeiitic shield stage produces most of the volcano's volume and is followed by the postshield stage that erupt silica rich alkalic lavas. After a short period of no activity (0.25 – 2.5 Ma), small quantities of silica poor lavas are generally produced and form the rejuvenated stage. According to their geochemical and isotopic characteristics, the Hawaiian volcanoes are generally separated into two main trends, the "Loa trend" and the "Kea trend" (Jackson et al., 1972) (Fig. 3). The Kea trend lavas have on average lower $^{87}Sr/^{86}Sr$, higher $^{143}Nd/^{144}Nd$ and higher $^{206}Pb/^{204}Pb$ ratios compared to the Loa trend lavas (e.g. Stille et al., 1986; Lassiter et al., 1996; Abouchami et al., 2005). They are also more enriched in incompatible elements, indicating that they were formed by lower degrees of partial melting than the Loa trend lavas (Hofmann and Jochum, 1996; Lassiter et al., 1996). The most recent studies have demonstrated that the Loa and Kea end-members could sample different parts of recycled oceanic lithosphere. The Loa trend lavas show features of recycled lower crust (Sobolev et al., 2000) while the Kea component may contain recycled lithospheric mantle (Lassiter and Hauri, 1998).

According to its Sr and Nd isotopic composition, the Kohala volcano, situated at the northern end of the big Island of Hawaii (Fig. 3), belongs to the Kea trend volcanoes (Feigenson et al., 1983; Hofmann et al., 1987; Lanphere and Frey, 1987). It provides relatively long stratigraphic sequences of lava from both the main shield and the postshield stages of volcanic activity, ideal to study the compositional variations during the magmatic evolution of a single volcano. In a first chapter, the Os-isotope variations within suites of lavas from Kohala volcano

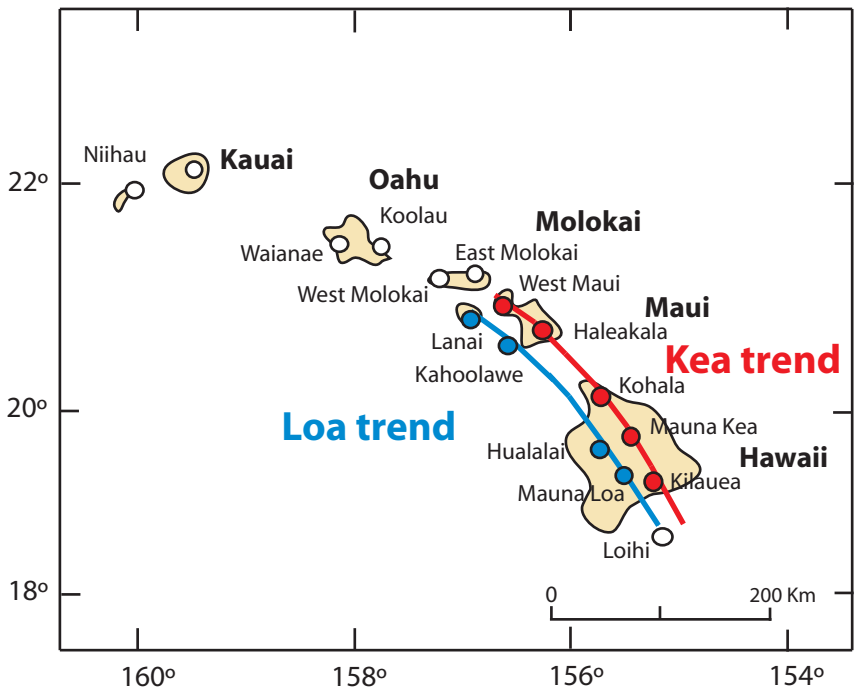

Fig. 3: *Map of the Hawaiian Islands showing the spacial distinction between the " Loa trend" and the "Kea trend" volcanoes. Figure modifed from Abouchami (2005).*

are used to constrain the effects of possible assimilation of local crust material into the Hawaiian magmas during their differentiation. As Os-isotopes mostly depend on the Os content of the melt, the behavior of Os and other Platinum Group Elements (PGE) during fractional crystallization processes will be investigated first.

The trace element variations within the same lava suites will be studied in a second chapter in order to constrain the trace element composition of the source of these lavas. The inverse modeling method proposed in Hofmann and Feigenson (1983) have been previously applied on the same suites of lavas from Kohala volcano using Rare Earth Element (REE) variations (Feigenson et al., 1983). The method is extended here to highly incompatible elements in order to further constrain the mantle source composition of Kohala lavas.

3. Tubuai Island and the HIMU component

In contrast to the Hawaiian-Emperor chain, the origin of the Cook-Austral chain in the South Pacific is more controversial (Fig. 2). The age progression among the volcanic islands and seamounts is far more irregular (Dalrymple et al., 1975; Duncan and Mcdougall, 1976; Bellon et al., 1980; Turner and Jarrard, 1982) and has become increasingly difficult to reconcile with the plume theory (e.g. Diraison, 1991; Chauvel et al., 1997; Mcnutt et al., 1997). The geochemical

and isotopic signatures of the lavas are highly variable between the different islands and also vary within single islands such as Rurutu, Rimatara and Raivavae (Nakamura and Tatsumoto, 1988; Chauvel et al., 1997; Schiano et al., 2001; Lassiter et al., 2003) (Fig. 4). The isotopically extreme HIMU-type OIB have been identified in several islands situated in the central part of the chain (Mangaia, Rimatara, Rurutu (old volcanics), Tubuai, Raevavae), while EM-type OIB have been observed both in the southern (Rapa, Marotiri, MacDonald) and the northern islands (Rarotonga, Atiu, Aitutaki) (Fig. 4). Another signature has been described, presenting characteristics less extreme than the previous HIMU component and recently termed FOZO in Stracke et al. (2005). This FOZO-type signature most often occurs during the younger phases of volcanism of the HIMU islands (Mauke, Rimatara, Rurutu (young volcanics), Raevavae) (e.g. Chauvel et al., 1997). Among the various signature observed along the Cook-Austral chain, the HIMU signature is particularly intriguing because it has been described in only two places in the world: at the Cook-Austral islands and at St Helena Island in the South Atlantic. The term HIMU signifies high time integrated $^{238}U/^{204}Pb$ (high μ = high $^{238}U/^{204}Pb$), which is generally thought to be the result of the presence of recycled oceanic crust in their mantle source that has lost most of its Pb (and Rb, K) during subduction or alteration processes and has consequently developed high 238U/204Pb ratios (Chase, 1981; Hofmann and White, 1982; Zindler and Hart, 1986; Halliday et al., 1988; Hart, 1988; Nakamura and Tatsumoto, 1988; Vidal et al., 1989; Weaver, 1991;

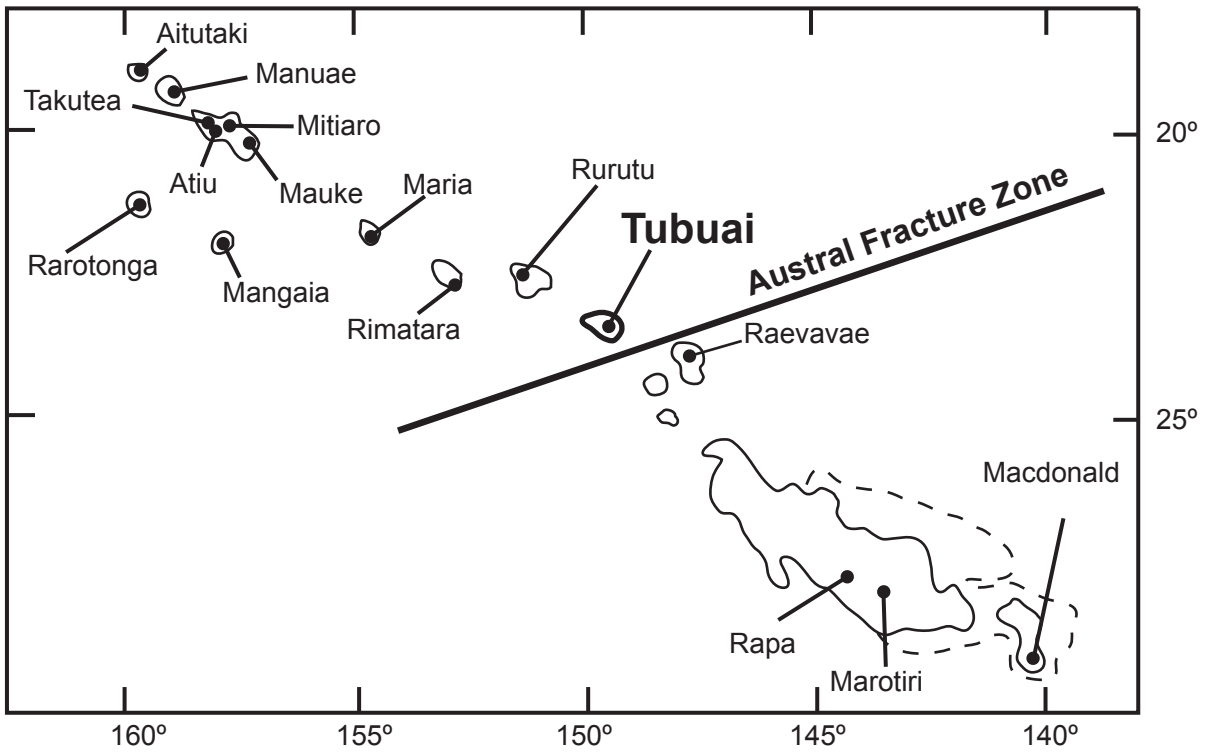

Fig. 4: *General map of the Cook-Austral Islands chain in the South Pacific.*

Chauvel et al., 1992; Chauvel et al., 1997; Salters and White, 1998; Stracke et al., 2003; Stracke et al., 2005). Contrary to FOZO, EM-1, EM-2 and DMM, the HIMU component appears to be restricted exclusively to the source of HIMU-type OIB (Stracke et al., 2005) and may thus be related to an exceptional and rare mantle reservoir. The second part of this dissertation, investigates the magmatic evolution of one of the HIMU-type islands of the Cook-Austral chain, Tubuai Island. Trace element and Sr, Nd, Hf isotopic analyses have been performed on suites of progressively more alkaline lavas from Tubuai in order to constrain the isotopic and geochemical differences between the mafic lavas from Tubuai Island.

References

Abouchami W., Hofmann A. W., Galer S. J. G., Frey F. A., Eisele J. and Feigenson M. D. (2005) Lead isotopes reveal bilateral asymmetry and vertical continuity in the Hawaiian mantle plume. *Nature* 434, 851-856.

Bellon H., Brousse R. and Pantaloni A. (1980) Ages de l'ile de Tubuai: l'alignement des Australes et des Cook. . *Cahiers Indo-Pacifique* 2(4), 219-240.

Ben Othman D., White W. M. and Patchett J. (1989) The geochemistry of marine sediments, island arc magma genesis and crust-mantle recycling. *Earth Planet Sci Lett* 94, 1-21.

Chase C. G. (1981) Oceanic island Pb: two-stage histories and mantle evolution. *Earth Planet. Sci. Lett.* 52, 227-284.

Chauvel C., Hofmann A. W. and Vidal P. (1992) HIMU-EM: The French Polynesian connection. *Earth Planet Sci Lett* 110, 99-119.

Chauvel C., McDonough W., Guille G., Maury R. and Duncan R. (1997) Contrasting old and young volcanism in Rurutu Island, Austral chain. *Chem. Geol.* 139, 125-143.

Clague D. A. and Dalrymple G. B. (1987) The Hawaiian-Emperor volcanic chain, I, Geologic evolution. *U.S. Geol. Surv. Prof. Pap.* 1350, 5-54.

Dalrymple G. B., Jarrard R. D. and Clague D. A. (1975) K-Ar ages of some volcanic rocks from the Cook and Austral Islands. *Geol. Sci. Amer. Bull.* 86, 1463-1467.

Danyushevsky L. V., Della-Pasqua F. N. and Sokolov S. (2000) Re-equilibration of melt inclusions trapped by magnesian olivine phenocrysts from subduction – related magmas : petrological implications. . *Contrib Mineral petrol* 138, 68-83.

DePaolo D. J. (1981) Trace element isotopic effects of combined wallrock assimilation and fractional crystallisation. *Earth Planet Sci Lett* 53, 189-202.

Diraison C. (1991) Le volcanisme aerien des archipelss polynesiens de la Societe, des Marquises et des Australes-Cook. Tephrostratigraphie, datation isotopique et geochimique comparees. Contribution a l'etude des origines du volcanisme intraplaque du pacifique centrale., Univ. Bretagne Occidentale.

Duncan R. and McDougall I. (1976) Linear volcanism in French Polynesia. *Journ. Volcanol. Geoth. Res.* 1, 197-227.

Eisele J., Sharma M., Galer S. J. G., Blichert-Toft J., Devey C. W. and Hofmann A. W. (2002) The role of sediment recycling in EM-1 inferred from Os, Pb, Hf, Nd, Sr isotope and trace element systematics of the Pitcairn hotspot. *Earth Planet. Sci. Lett.* 196, 197-212.

Feigenson M. D., Hofmann A. W. and Spera F. J. (1983) Case studies on the origin of basalt II. The transition from Tholeiitic to alkalic volcanism on Kohala Volcano, Hawaii. . *Contrib Mineral petrol* 84, 390-405.

Halliday A. N., Dickin A. P., Fallick A. E. and Fitton J. G. (1988) Mantle dynamics: a Nd, Sr, Pb and O isotopic study of the Cameroon Line volcanic chain. *J. Petrol.* 29, 181-211.

Hart S. R. (1988) Heterogeneous mantle domains: Signatures, genesis and mixing chronologies. *Earth Planet. Sci. Lett.* 90, 273-296.

Hart S. R., Hauri E. H., Oschmann L. A. and Whitehead J. A. (1992) Mantle plumes and entrainment: Isotopic evidence. *Science* 256, 517-520.

Hofmann A. W. (1997) Mantle geochemistry: The message from oceanic volcanism. *Nature* 385, 219-229.

Hofmann A. W. and Feigenson M. D. (1983) Case studies on the origin ogf basalt. I. Theory and reassessment of Grenada basalts. *Contrib. Mineral. Petrol.* 84, 382-389.

Hofmann A. W., Feigenson M. D. and Raczek I. (1987) Kohala revisited. *Contrib Mineral petrol* 95, 114-122.

Hofmann A. W. and Jochum K. P. (1996) Source characteristics derived from very incompatible trace elements in Mauna Loa and Mauna Kea basalts, Hawaii Scientific Drilling Project. *Journal of geophysical research* 101, 11831-11839.

Hofmann A. W. and White W. M. (1982) Mantle plumes from ancient oceanic crust. *Earth Planet. Sci. Lett.* 57, 421-436.

Jackson E. D., Silver E. A. and Dalrymple G. B. (1972) Hawaiian-Emperor chain and its relation to Cenozoic circumpacific tectonics. *Geol. Soc. Am. Bull.* 83, 601-618.

Kurz M. D., Jenkins W. J. and Hart S. R. (1982) Helium isotopic systematics of ocean islands: Implications for mantle heterogeneity. *Nature* 297, 43-47.

Kurz M. D., Jenkins W. J., Hart S. R. and Clague D. A. (1983) Helium isotopic variations in Loihi Seamount and the Island of Hawaii. *Earth Planet Sci Lett* 66, 388-406.

Lanphere M. A. and Frey F. A. (1987) Geochemical evolution of Kohala Volcano, Hawaii. . *Contrib Mineral petrol* 95, 100-113.

Lassiter J. C., Blichert-Toft J., Hauri E. and Barsczus H. G. (2003) Isotope and trace element variations in lavas from Raivavae and Rapa, Cook-Austral islands: constraints on the nature of HIMU- and EM-mantle and the origin of mid-plate volcanismm in French Polynesia. *Chem. Geol.* 202, 115-138.

Lassiter J. C., DePaolo D. J. and Tatsumoto M. (1996) Isotopic evolution of Mauna Kea Volcano: results from the initial phase of the Hawaii Scientific Drilling Project. *J Geophys. Res.* 101, 11769-11780.

Lassiter J. C. and Hauri E. H. (1998) Osmium-isotope variations in Hawaiian lavas : evidence for recycled oceanic lithosphere in the Hawaiian plume. *Earth Planet Sci Lett* 164, 483-496.

MacDonald G. A. (1968) Composition and origin of Hawaiian lavas. In *Studies in volcanology*, Vol. 116 (ed. R. E. Coats, R. L. Hay, and C. A. Anderson), pp. 477-522.

Mahoney J. C., Nicollet J. C. and Dupuy C. (1991) Madagascar basalts: tracking oceanic and continental sources. *Earth Planet Sci Lett* 104, 350-363.

McKenzie D. (1985) The extraction of magma from the crust and mantle. *Earth Planet Sci Lett* 74, 81-91.

McKenzie D. and O'Nions. (1983) Mantle reservoirs and ocean island basalts. *Nature* 301, 229-231.

McNutt M. K., Caress D. W., Reynolds J., Jordahl K. A. and Duncan R. (1997) Failure of the plume theory to explain midplate volcanism in the southern Austral islands. *Nature* 389, 479-482.

Milner S. C. and Le Roex A. P. (1996) Isotope characteristics of the Okenyena igneous complex, northewestern namibia: constraints on the composition of the early Tristan plume and the origin of the EM 1 mantle component. *Earth Planet Sci Lett* 141, 277-291.

Minster J.-F. and Allègre C. J. (1978) Systematic use of trace elements in igneous processes, part III. Inverse problem of batch melting in volcanic suites. *Contrib Mineral petrol* 68, 37-52.

Montelli R., Nolet G., Dahlen F. A. and Masters G. (2006) A catalogue of deep mantle plume: New results from finite-frequency tomography. *Geochem Geophys Geosyst* 7(11).

Morgan W. J. (1972) Deep mantle convection plumes and plate motions. *Bull. Amer. Assoc. Petrol. Geol.* 56, 203-213.

Nakamura Y. and Tatsumoto M. (1988) Pb, Nd, and Sr isotopic evidence for a multicomponent source for rocks of Cook-Austral Islands and heterogeneities of mantle plumes. *Geochim. Cosmochim. Acta* 52, 2909-2924.

Plank T. and Langmuir C. H. (1998) The chemical composition of subducting sediment and its consequences for the crust and mantle. *Chemical Geology* 145, 325-394.

Rehkämper M. and Hofmann A. W. (1997) Recycled ocean crust and sediment in Indian Ocean MORB. *Earth Planet Sci Lett* 147, 93-106.

Salters V. J. M. and White W. M. (1998) Hf isotope constraints on mantle evolution. *Chem. Geol.* 145, 447-460.

Schiano P., Burton K. W., Dupre B., Birck J. L., Guille G. and Allegre C. J. (2001) Correlated Os-Pb-Nd-Sr isotopes in the Austral-Cook chain basalts: the nature of mantle components in plume sources. *Earth Planet. Sci. Lett.* 186(527-537).

Sharp W. D. and Clague D. A. (2006) 50-Ma initiation of Hawaiian-Emperor bend records major change in Pacific plate motion. *Science* 313, 1281-1284.

Shaw D. M. (1970) Trace element fractionation during anatexis. *Geochim. Cosmochim. Acta* 34, 237-243.

Sobolev A. V., Hofmann A. W. and Nikogosian I. K. (2000) Recycled oceanic crust observed in "ghost plagioclase" within the source of Mauna Loa lavas. *nature* 404, 986-989.

Stille P., Unruh D. M. and Tatsumoto M. (1986) Pb, Sr, and Nd isotopic constraints on the origin of Hawaiian basalts and evidence for a unique mantle source. *Geochim Cosmochim Acta* 50, 2303-2319.

Stracke A., Bizimis M. and Salters V. J. M. (2003) Recycling oceanic crust: Quantitative constraints. *Geochem. Geophys. Geosystems* 4(3).

Stracke A., Hofmann A. W. and Hart S. R. (2005) FOZO, HIMU, and the rest of the mantle zoo. *Geochem. Geophys. Geosystems* 6(5).

Turner D. L. and Jarrard R. D. (1982) K-Ar dating of the Cook-Austral Island chain: a test of the hot-spot hypothesis. *Journ. Volcanol. Geoth. Res.* 12, 187-220.

Vidal P., Rocaboy A. and Dupuy C. (1989) Composition du manteau: le reservoir HIMU. *C.R. Acad. Sci. Paris* 308(2), 635-639.

Weaver B. L. (1991) The origin of ocean island basalt end-member compositions: Trace element and isotopic constraints. *Earth Planet. Sci. Lett.* 104, 381-397.

White W. M. (1985) Sources of oceanic basalts: Radiogenic isotopic evidence. *Geology* 13, 115-118.

Willbold M. and Stracke A. (2006) Trace element composition of mantle end-members: Implications for recycling of oceanic and upper and lower continental crust. *Geochem. Geophys. Geosystems* 7(4).

Wilson J. T. (1963) Evidence from islands of the spreading of the ocean floors. *Nature* 197, 536-538.

Workman R. K., Hart S. R., Jackson M., Regelous M., Farley K. A., Blusztajn J., Kurz M. D. and Staudigel H. (2004) Recycled metasomatized lithosphere as the origin of the Enriched Mantle II (EM2) end-member: Evidence from the Samoan Volcanic Chain. *Geochem Geophys Geosyst* 5(4).

Zindler A. and Hart S. R. (1986) Chemical geodynamics. *Annu. Rev. Earth Planet. Sci.* 14, 493-571.

Part I

Studies of lavas from Kohala Volcano, Hawaii

Chapter 1

PGE and Os isotopic variations in lavas from Kohala Volcano, Hawaii: Constraints on PGE behavior and melt / crust interaction

M. JAMAIS, J. C. LASSITER, G. BRUEGMAN

Abstract

We have examined the Os-isotope variations in suites of variably-fractionated lavas from Kohala Volcano, Hawaii, in order to evaluate the effects of melt / crust interaction on the mantle isotopic signature of these lavas. As $^{187}Os/^{188}Os$ sensitivity to any radiogenic contaminant strongly depend on the Os content in the melt, the Re and PGE variations during the Hawaiian magma differentiation have been first examined. This study reveals that Os and other PGE behavior change during magma differentiation and that all PGE contents strongly decrease in the melt as it evolves through ~ 8% MgO. The distribution also indicates a strong increase of the bulk partition coefficients values for PGE in lavas with less than 8% MgO (D_{PGE} = 30 - 50) compared to values in more primitive lavas (> 8% MgO, $D_{PGE} \leq 6$). This sudden change in PGE behavior most likely reflects the sulfur saturation of the Hawaiian magma and the onset of sulfide fractionation at around 8% MgO. Using bulk partition coefficients calculated in this study and partition coefficients between sulfide and silicate melt reported in literature, we estimated that 0.1 - 0.3% sulfide fractionation would be necessary to explain the observed decline of PGE concentrations in the evolved Hawaiian magmas.

The more primitive compositions (> 8% MgO), rich in Os, display a narrow range of $^{187}Os/^{188}Os$ values (0.130 - 0.132), which are similar to values in high-MgO lavas from Mauna Kea and Haleakala Volcanoes and are likely to represent the mantle signature of Kohala lavas. However, Os isotopic ratios become more radiogenic with decreasing MgO and Os contents in evolved lavas, ranging from 0.130 to 0.196 in the shield stage Pololu basalts and from 0.131 to 0.223 in the Postshield Hawi lavas. This reflects assimilation of local crust material during fractional crystallization of the magma at shallow level. AFC modeling suggests that less than 8% upper oceanic crust assimilation could have produced the most radiogenic Os-isotope ratios recorded in the Pololu lavas. However, these small amounts of upper crust assimilation have only negligible effect on Sr and Nd isotopic ratios and therefore, are not responsible for the Sr and Nd isotopic heterogeneities observed in Kohala lavas.

1. Introduction

Ocean Island Basalts provide important information on the chemical and physical characteristics of their mantle sources. However, the composition of an ascending magma may be modified during transport through the oceanic crust. Shallow-level assimilation processes have been demonstrated to happen in different places (Reisberg et al., 1993; Martin et al., 1994; Roy-Barman and Allegre, 1995; Widom and Shirey, 1996; Caroff et al., 1999) and some authors have proposed that much of the chemical and isotopic heterogeneities recorded within individual ocean islands reflect interaction of the melt with lithospheric material (Halliday et al., 1995; Eiler et al., 1996; Class and Goldstein, 1997). In order to extract accurate information regarding the mantle sources of ocean island basalts, it is therefore necessary to constrain the extent to which melt / crust interaction has affected isotope ratios in individual basalt suites.

Os isotopes are very sensitive to any mantle-derived melt / old crust interaction because of the extreme fractionation of the Re / Os ratio between the earth's crust and mantle. An old oceanic crust such as the one surrounding the Hawaiian Islands presents much more radiogenic Os-isotope ratios than a mantle-derived magma. In contrast, Sr and Nd-isotope ratios, commonly employed to define mantle signatures, display small differences between oceanic crust and mantle.

Therefore, we propose to study Os-isotopes variations in a suite of variably fractionated lavas from Kohala Volcano, Hawaii, in order to constrain the amount of crustal material assimilated by the Hawaiian magmas. Hence, the effect of such a process could be evaluated on other isotopic tracers such as Sr and Nd. However, the sensitivity of Os-isotope ratios depends largely on the Os content in the magma. Consequently, it is first necessary to systematically study the Os and other PGE distribution produced during fractional crystallization processes in order to unfold the $^{187}Os/^{188}Os$ variations caused by assimilation.

The study of PGE variations in Kohala lavas will reveal the strong decrease of all PGE concentrations in evolved lavas due to the sulfur saturation of the Hawaiian magma and the onset of sulfide phases at around 8 - 9% MgO. The good MgO – PGE correlations described by evolved Kohala lavas will provide bulk distribution coefficient for PGE between 35 and 50, much higher than in primitive Hawaiian basalts. Thereafter, Os variations in Kohala lavas will reveal the occurrence of small amount of local upper oceanic crust assimilation during the

Kohala magma evolution. However, we will see that such amount of assimilation has only negligible effect on the Sr and Nd isotopic compositions of Kohala lavas.

2. Magmatic evolution of Kohala Volcano

Kohala Volcano is the northernmost and the oldest of the five major shield Volcanoes of Big Island, Hawaii (Fig. 1). Kohala is an extinct volcano, 35 km long and 24 km wide, and consists of an eroded dome. The northern flank of the mountain is particularly eroded, with numerous large river valleys, which provide an easy access to a relatively long stratigraphic sequence.

Lava flows are 455 to 62 ka old (Mcdougall and Swenson, 1972) and were erupted during two stages of volcanic activity (Stearn and Macdonald, 1946): the shield-building stage named "Pololu volcanics", which form roughly 99 percent of the subaerial volume of the volcano (455 to 260 Ka), and a post-shield-building stage named "Hawi Volcanics" that overlaps the first event (232 to 62 ka) (Spengler and Garcia, 1988) (Fig. 1). These two units are separated by an erosional unconformity on the wet northeastern slopes of the mountain and by a red soil zone on the dry western slopes. Pololu volcanics are dominantly tholeiitic in composition, but grade into alkalic basalts within the upper 100 meters of the unit. Hawi volcanics are highly-fractionated alkaline lavas ranging in composition from hawaiites to trachytes (Stearn and Macdonald, 1946). Previous studies have suggested that the transition from tholeiitic to alkalic volcanism in the Pololu unit can be explained by a gradual decrease in the degree of partial melting of identical source material (Hofmann and Feigenson, 1983; Hofmann et al., 1987). In contrast, the alkaline Hawi lavas from the post-shield-building stage of volcanism are isotopically and compositionally distinct from the underlying Pololu lavas (Hofmann et al., 1987; Lanphere and Frey, 1987; Spengler and Garcia, 1988).

Phenocryst assemblage, major elements and transition metals variations suggest that olivine is the major crystallizing phase in tholeiites and that aluminous clinopyroxene is most likely to dominate over olivine in the crystallizing phase of the Pololu alkali basalts (Feigenson et al., 1983; Hofmann et al., 1987). Major and trace elements variations in the Hawi lavas indicate that plagioclase, clinopyroxene, Ti-magnetite, olivine and apatite have crystallized in the post-shield-building stage of Kohala volcanism (Spengler and Garcia, 1988).

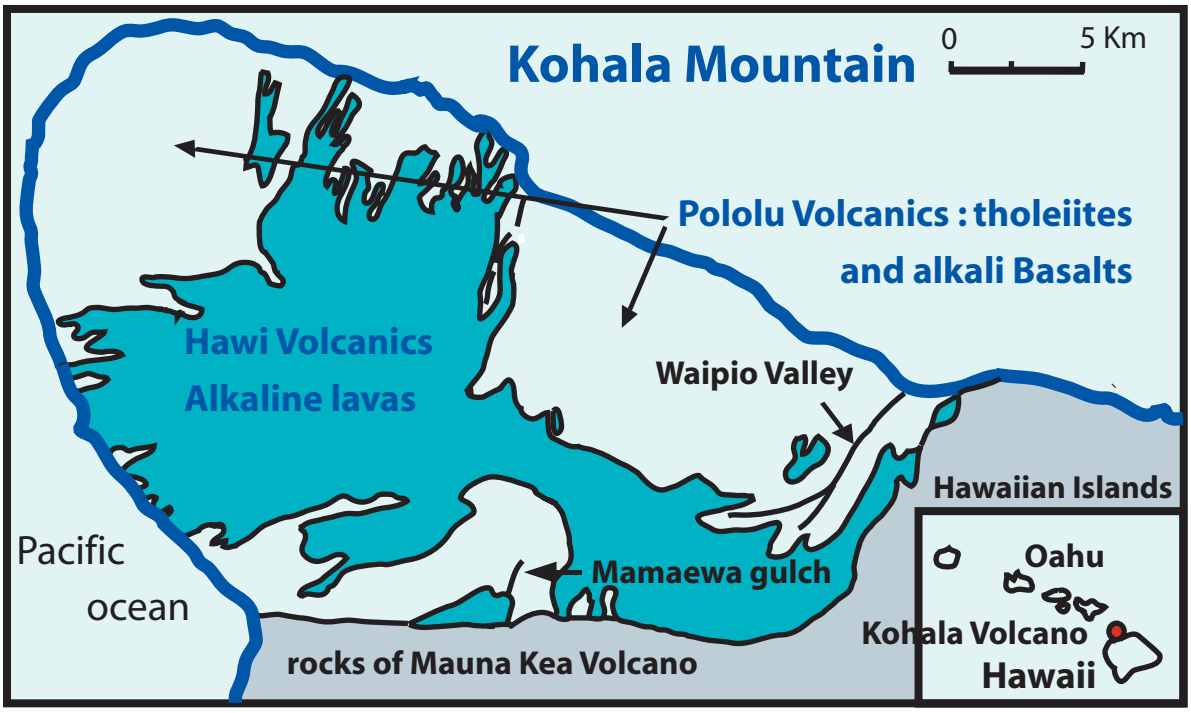

***Fig. 1**: Map of Kohala Volcano modified from Lanphere and Frey (1987). Tholeiite samples have been collected in the Waipio Valley while alkali basalt and Hawi lava samples have been collected in the Mamaewa gulch (Feigenson et al., 1983).*

Finally, the Sr- and Nd-isotope signatures of the shield-building stage of Kohala Volcano (Pololu series) are similar to those in lavas from other volcanoes of the "Kea trend" end member. Hawi lavas from the postshield-building stage have slightly more depleted Sr and Nd isotope signatures, i.e. higher Nd and lower Sr-isotope values, although there is no real gap between the Pololu and Hawi ranges of isotopic values (Hofmann et al., 1987; Lanphere and Frey, 1987). A similar shift to more depleted isotope values in the overlying alkalic rocks has been also observed at Haleakala, Mauna Kea and Kauai Volcanoes (Chen and Frey, 1983; Feigenson, 1984; Chen and Frey, 1985; Kennedy et al., 1991; Lassiter et al., 1996).

3. Samples and Analytical Methods

The lava suite investigated here consists of a total of 15 samples from Kohala: 9 from the Pololu and 6 from the Hawi lava flows. The major and trace element composition of these samples is reported in Feigenson et al. (1983). Sr and Nd isotopic compositions as well as transition metal compositions on a subset of these samples are also presented in Feigenson et al. (1983) and Hofmann et al. (1987). Petrographic descriptions of these samples and location of

sampling can be found in Feigenson et al. (1983).

These Kohala lavas, and particularly the alkaline series, have relatively fractionated compositions, with Mg number between 63 and 47 in the tholeiite series and only up to 47 in the alkaline series. Thus, an additional batch of four Hawaiian lava samples has been analyzed together with the Kohala series in order to extend the range of compositions and better constrain PGE behavior during magma differentiation. This lavas suite is from Kauai Island, the second oldest and northernmost island of the major Hawaiian chain, and comprises one tholeiite with a Mg number of 66 and three alkaline lavas (Basanites) with Mg numbers from 49 up to 70. The major and trace element composition of these samples is reported in Feigenson (1984). In the present study, we measured Re, PGE abundances and Os isotopic compositions on these Kauai lavas, but only the PGE abundances will be discussed here.

Os isotope compositions as well as Re, Os, Ir, Ru and Pt abundances were determined at the Max-Plank Institut für Chemie in Mainz. Two grams of whole rock powders were dissolved in sealed quartz vessels together with a mixed Re / PGE spike (^{185}Re, ^{190}Os, ^{191}Ir, ^{101}Ru, ^{198}Pt) and reverse aqua regia (4ml conc. HCl and 6ml conc. HNO_3) for 16 h at 300°C and 100 bar using a high-pressure asher (Meisel et al., 2001). Re and PGE were separated from the matrix using the procedure described in Brügmann et al. (1999). Osmium was extracted from the Re- and PGE-bearing solution as OsO_4 into liquid bromine and trapped in HBr. The Os-fraction was further purified via micro-distillation (Birck et al., 1997). Afterwards, Ru, Re, Ir and Pt were sequentially extracted from the solution in anion exchange columns, using a technique modified after Rehkämper and Halliday (1997) and described in Büchl et al. (2004).

Os isotopic compositions were measured by ion counting on a Finnigan MAT-262 thermal ionisation mass spectrometer in negative ion mode (NTIMS). Total analytical blank are less than 1pg. In-run analytical uncertainties for Os-isotopic composition are reported for each sample in Table 1. Repeated analyses of a standard containing 100 pg Os (n = 80) yielded a 2σ external precision for the ^{187}Os/^{188}Os better than 0.3%. Duplicate analyses of several samples were performed, each starting with digestion of a separate aliquant of sample powder. The results of these duplicates agreed within 0.6% for ^{187}Os/^{188}Os and from 5 to 60 % for Os concentrations. According to the good reproducibility of ^{187}Os/^{188}Os ratios, we suspect the high heterogeneity of Os contents measured in our samples to be due to inhomogeneous distribution of Os-bearing phases, such as sulfides, in the lavas. However, this heterogeneity has only minor effects on the model developed in this study.

Table 1: Re, PGE and isotopic compositions of Kohala lavas, Re and PGE compositions of Kauai lavas.

	MgO (Wt%) a	$^{87}Sr/^{86}Sr$ a	$^{143}Nd/^{144}Nd$ a	$^{187}Os/^{188}Os$	Os (ppb)	Ir (ppb)	Ru (ppb)	Pt (ppb)	Re (ppb)
KOHALA									
Pololu Lavas									
Tholeiites									
W4	8.75	0.703676	0.512956	0.13016 ± 4	0.117	0.089	0.14	2.7	0.322
W4-dup				0.13011 ± 3	0.238				
W22	8.48	0.703601	0.512973	0.13045 ± 5	0.138	0.109	4.58	33.7	0.546
W11	7.57	0.703841	0.512944	0.13309 ± 3	0.219	0.223	3.29	11.5	0.62
dup-W11				0.13325 ± 2	0.204	0.227	3.59	4.2	0.607
W1	7.48	0.703672	0.512974	0.13156 ± 4	0.085	0.044	2.94	25.3	0.298
MG0	6.94	0.703689	0.512962	0.15453 ± 16	0.009	0.013	1.45	0.7	0.219
KH16	6.43	0.703621	0.512969	0.14178 ± 4	0.021				
MG3	5.94	0.703612	0.512966	0.16130 ± 5	0.007	0.062	0.57	1.7	0.391
dup-MG3				0.16157 ± 9	0.003				
Alkali Basalts									
H1	5.29			0.13665 ± 11	0.009				
MG1	5.25	0.703668	0.512972	0.19560 ± 10	0.008	0.021	0.17	4,00	0.618
Hawi Lavas									
KH5	4.93			0.14454 ± 4	0.011	0.013	0.2	1.4	0.077
H3	4.29	0.70349	0.513012	0.13067 ± 4	0.036				
KH13	3.25			0.17758 ± 9	0.008				
KH1	1.73	0.703514	0.513	0.21682 ± 10	0.003				
KH19	1.17	0.703554	0.513018	0.22279 ± 7	0.005				
KAUAI									
Tholeiite									
N7	11.55				0.252	0.078	0.61	1.69	0.33
dup-N7					0.386	0.081	0.56	1.85	0.24
Alkaline Lavas									
GQ1	15.97				0.772	0.265	0.29	1.24	0.114
N8	11.48				0.361	0.099	0.38	2.09	0.397
N6	6.28				0.012	0.009	0.14	0.85	0.448

a : data from Feigenson et al. (1983), Feigenson (1984) and Hofmann et al. (1987)

The quality of Os data from the Mainz laboratory was also confirmed based in a comparative analytical study of serpentinite standard UB-N (Meisel et al., 2001; Büchl et al., 2004). The Re, Ir, Ru and Pt abundances were measured on a Nu Plasma Multi-Collector ICPMS (MC-ICPMS) at the MPI. External precision (2σ) of standard solution (10 - 25 ng/g) measurements was 0.1 - 0.2% for Re, Pt and Ir, and 0.6% for Ru. Reagent blanks for Ir, Ru, Re, Pt and Pd were less than 0.025 ng/g, 0.030 ng/g, 0.010 ng/g, 0.020 ng/g, and 0.100 ng/g, respectively. PGE values in two duplicate analyses agreed within 6%.

4. Results

4.1 Lavas from Kohala Volcano

Rhenium and PGE abundances as well as Os isotopic compositions of Kohala lavas are reported in Table 1. The Pololu samples investigated here range from relatively "primitive" tholeiites having MgO > 7% to differentiated tholeiites and alkali basalts with MgO between 7 and 5 wt.% (Table 1). All Hawi samples are highly differentiated alkaline rocks with MgO content between 5 and 1 wt.%.

Kohala lavas have variable Os concentrations ranging from about 10 up to 250 ppt in the Pololu basalts, and from 3 to 35 ppt in the Hawi lavas. Concentrations in the Pololu basalts are within the range of those previously obtained on variably-fractionated basalts from Haleakala Volcano (Martin et al., 1994). Os concentrations of both Pololu and Hawi lavas decrease with indices of fractionation (e.g. decreasing MgO, Ni and Cr content in Pololu lavas and decreasing MgO, TiO_2 and Sc content in Hawi lavas), consistent with the compatible behavior of Os during fractional crystallization (Fig. 2). The decrease of Os content is sharp in Pololu basalts, with values from 250 ppt in lavas with ~ 8% MgO to 10 ppt in lavas with ~ 5% MgO. This Os decrease is more gradual in the highly-fractionated Hawi lavas, with values ranging from 35 ppt in lavas with ~ 5% MgO to 3 ppt in lavas with ~ 1% MgO (Fig. 2).

The least fractionated tholeiites from Pololu Volcanics (with MgO >7%) have primitive mantle (PM)-normalized PGE patterns similar to those previously reported for relatively primitive tholeiites from Mauna Loa and Kilauea Volcanoes (Tatsumi et al., 1999; Bennett et al., 2000; Crocket, 2000) (Fig. 3a). In these studies, Hawaiian lavas have been shown to be more

depleted in I-PGE (Ir, Os and Ru) compared to peridotites and komatiites but enriched in all PGE compared to MORBs. We note however that Kohala lavas have slightly lower Ir contents than most Mauna Loa and Kilauea lavas. In contrast, all PGE abundances in evolved Pololu and Hawi lavas are more depleted compared to primitive Hawaiian tholeiites with the most differentiated compositions exhibiting MORB-like abundances (Fig. 3b). Finally, rhenium abundances in the Pololu lavas vary from 261 to 618 ppm, but contrary to PGE abundances, are not clearly correlated with MgO contents.

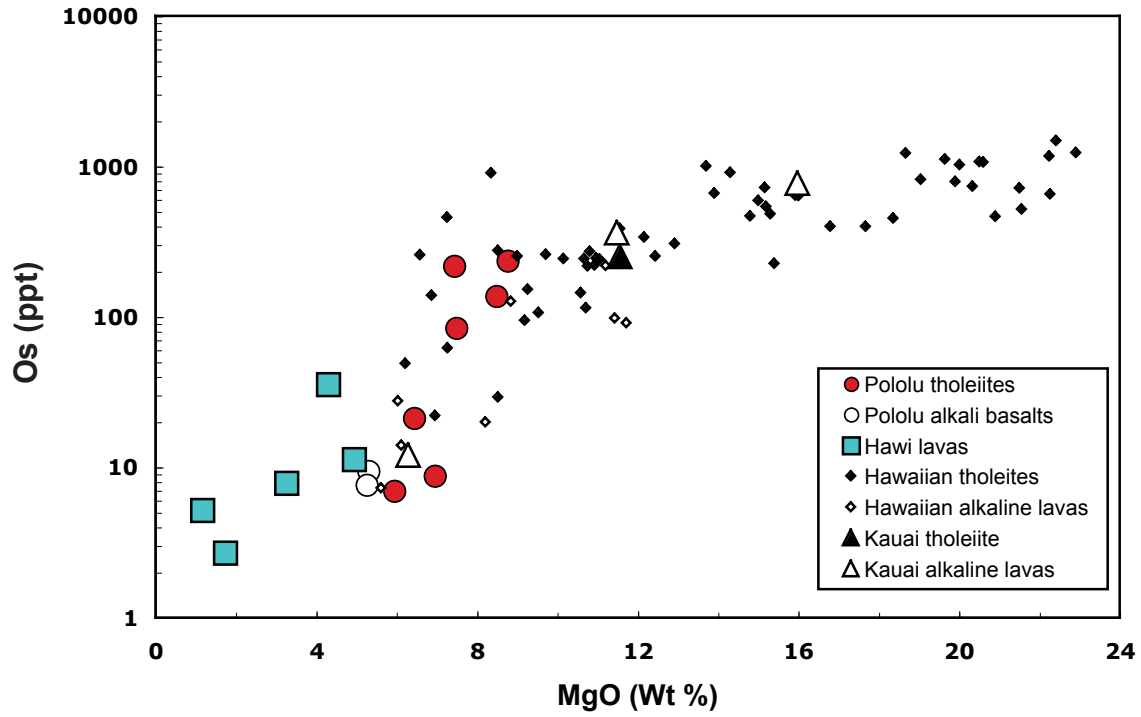

Fig. 2: *MgO - Os variations in Kohala and Kauai lavas as well as in other Hawaiian lavas. Additional data are from Martin et al. (1994), Hauri et al. (1996) and (1997), Bennett et al. (1996) and (2000) and Lassiter et al. (1998). The new data emphasize a change in Os behavior during the Hawaiian magma evolution and the strong decrease of Os concentrations in evolved lavas.*

$^{187}Os/^{188}Os$ ratios range from 0.130 to 0.196 in the shield-stage Pololu basalts and from 0.131 to 0.223 in the Post-shield Hawi lavas. In the Pololu Volcanics, tholeiites with more than 7% MgO span a narrow range of values (0.130 - 0.133) while evolved tholeiites and alkalic basalts extend to more radiogenic Os-isotopes ratios (0.137 - 0.196). In these evolved Pololu basalts as well as in the Hawi lavas, Os-isotopes ratios are inversely correlated with MgO and Os concentrations.

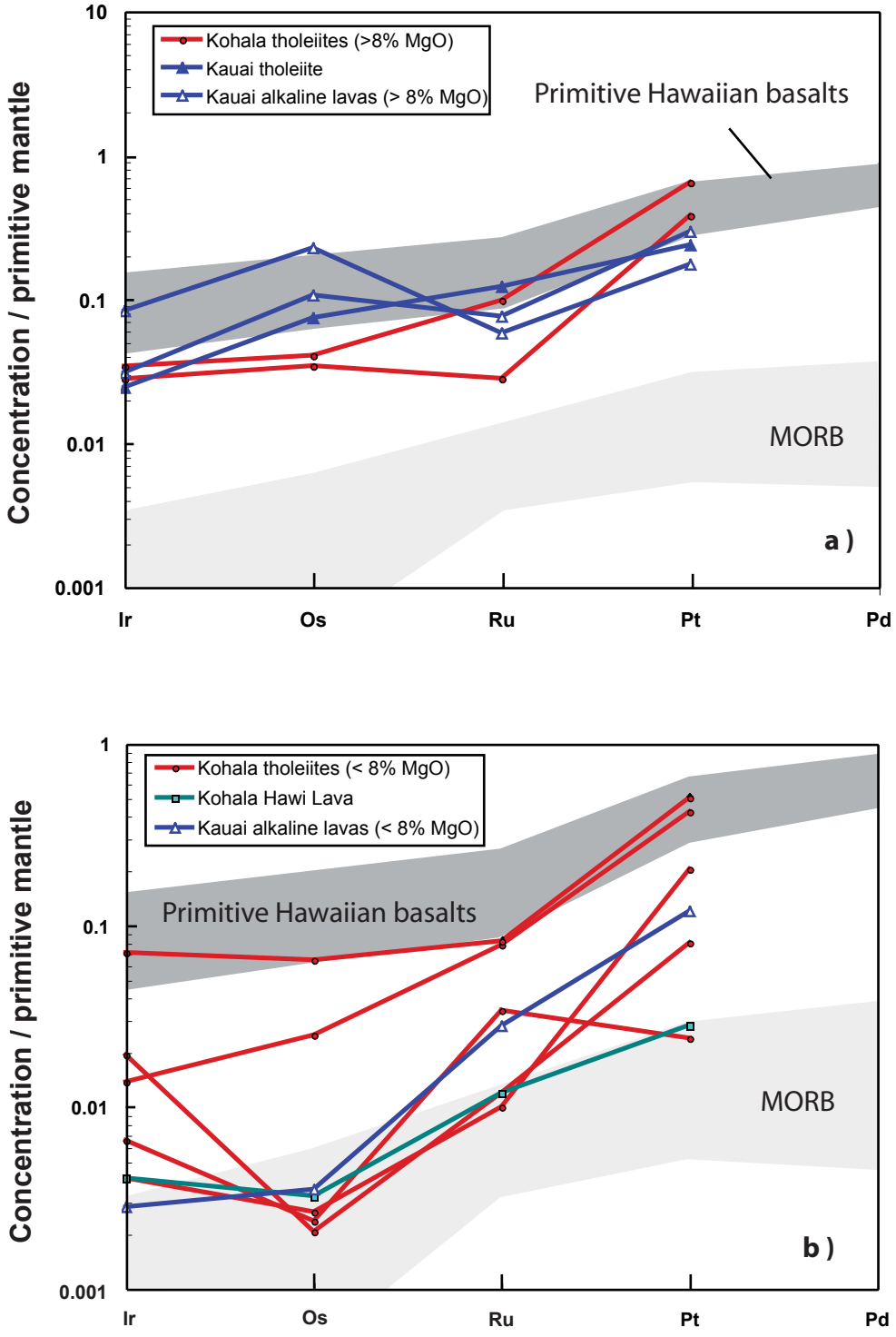

Fig. 3: *Primitive-mantle normalized PGE patterns for Kohala and Kauai lavas. Primitive hawaiian basalt field and MORB field are also shown for comparison. The primitive Hawaiian field is based on data reported in Tatsumi et al. (1999) and Bennett et al. (2000) for high-MgO tholeiites from Mauna Loa and Kilauea Volcano. The MORB field is based on data reported in Tatsumi et al. (1999) for pacific MORB.* ***a)*** *The relatively primitive lavas (> 8% MgO) from Kohala and Kauai Volcanoes display similar PGE patterns than others primitive Hawaiian lavas.* ***b)*** *In contrast, lavas with less than 8 % MgO have more depleted PGE compositions and their PGE patterns partly overpap the MORB field.*

4.2 Additional lavas from Kauai Island

Os abundances in Kauai lavas range from 12 to 772 ppt. These compositions fit in the MgO-Os correlation described by all the lavas from Hawaiian Islands (Fig. 2) and show that the alkaline series overlap the tholeiitic series from primitive to evolved compositions. Ir, Ru and Pt content obtained on primitive lavas N7, N8 and GQ1 are in the range of values displayed by primitive Hawaiian tholeiites. However, the alkaline lava GQ1 shows lower Pt content than the Hawaiian picrites (Fig. 3a). Finally, the PGE pattern of the evolved alkaline lava N6 ranges among the evolved and alkaline rocks of Kohala Volcano (Fig. 3b).

5. Os and PGE behavior during magma evolution

5.1 PGE variation in Pololu basalts and S-saturation of the Hawaiian magma

Osmium content sharply decreases during fractional crystallization of the Pololu magma. When compared to previous data obtained on other Hawaiian basalts (Fig. 2), these new results emphasize a sudden change around 8 – 9 % MgO in the slope of the MgO - Os correlation described by the Hawaiian trend; Os content decreases much more moderately in melt with higher MgO content. This break in slope between primitive and evolved lavas indicate a shift in the Os compatibility and reveals the onset of a new crystallizing phase around 8% MgO which has a strong control on Os variations.

Fig. 4 shows bi-variate plots of MgO vs Ir, Ru and Pt for Kohala tholeiites and previous literature data on Hawaiian lavas. As for Os variations, results obtained on Kohala tholeiites emphasize a change in Ir, Ru and Pt behavior during fractional crystallization of the Hawaiian magma. In the primitive Hawaiian lava suites (> 9% MgO), Ir, Ru and Pt abundances are rather constant during magma evolution, though we note a slight increase of Pt and a slight decrease of Ru as the magma composition evolves from 16 to 9 % MgO. Conversely, all concentrations strongly decrease as the magma evolves towards lower MgO.

This sudden depletion of Ir, Os, Ru and Pt starting at the same degree of melt differentiation, at around 8 – 9 % MgO, most likely reflects the sulfur saturation of the Hawaiian melt and the onset of sulfide fractionation. PGE are extremely compatible in sulfide,

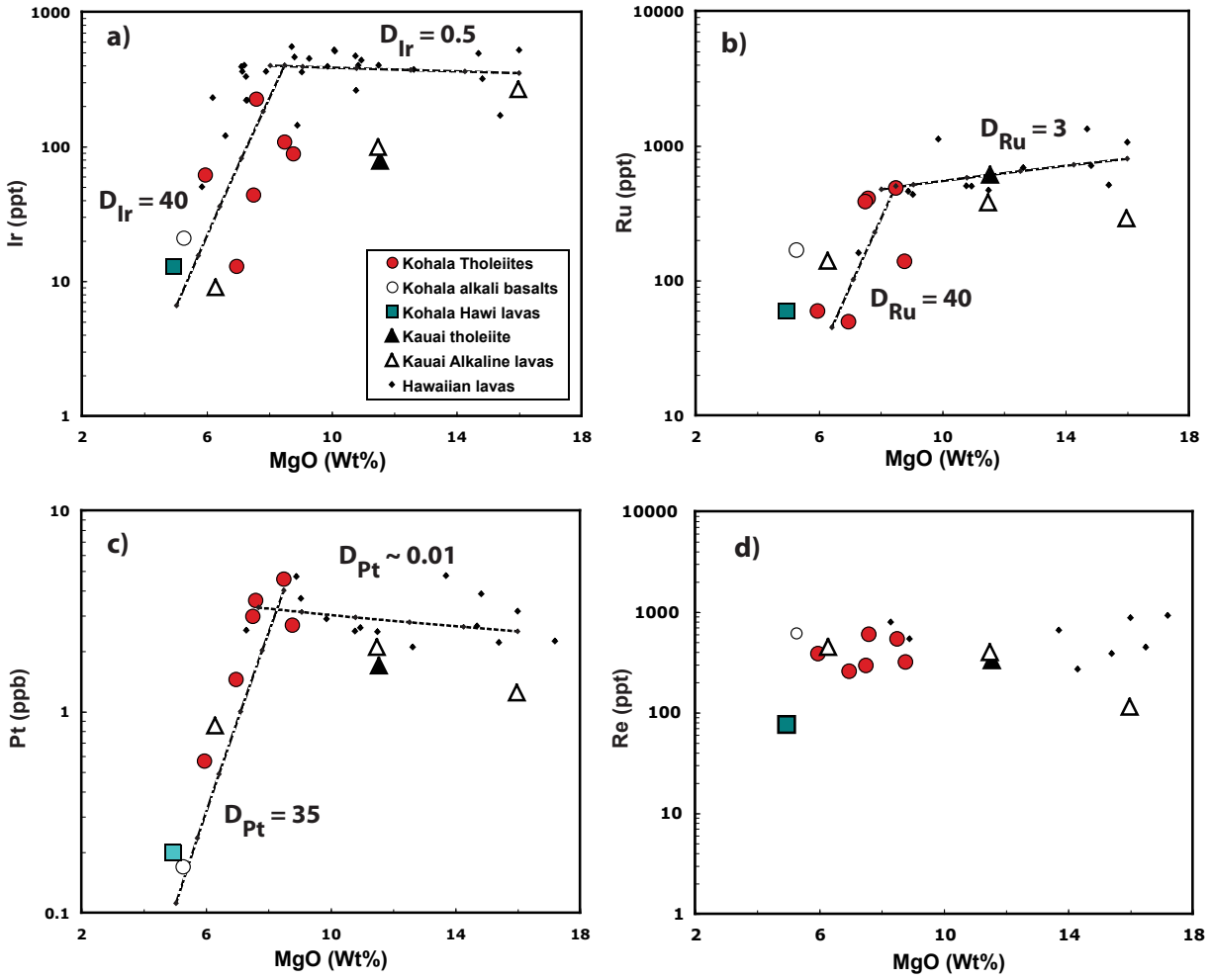

Fig. 4: *Plots of Ir, Ru, Pt and Re as a function of MgO in Kohala and Kauai lavas, together with previous data on Hawaiian basalts (Tatsumi et al., 1999; Crocket, 2000; Bennett et al., 2000). These plots reveal the change of PGE behavior during differentiation of the Hawaiian magma at around 8% MgO and the strong decline of these elements in evolved lavas.* ***a)*** *MgO-Ir variations suggesting a change of* D_{Ir} *from 0.5 in primitive compositions to 40 in evolved lavas.* ***b)*** *MgO-Ru variations suggesting a change of* D_{Ru} *from 3 in primitive compositions to 40 in evolved lavas.* ***c)*** *MgO-Pt variations suggesting a change of* D_{Pt} *from 0.01 in primitive compositions to 35 in evolved lavas.* ***d)*** *MgO-Re variations indicating that Re do not clearly correlate with MgO, which is most likely due to the volatile nature of Re and massive loss before subaerial erruption (see text).*

with sulfide / silicate melt partition coefficients in the range of 10^3 – 10^5 (Keays and Campbell, 1981; Peach et al., 1990; Fleet and Stone, 1991; Peach et al., 1994; Fleet et al., 1996; Roy-Barman et al., 1998). Previous studies have shown that some PGE can be fractionated by silicate / oxide phases (Barnes et al., 1985; Brügmann et al., 1987) or segregated into different PGE-bearing alloys and metal clusters (Peck and Keays, 1990a, 1990b; Merckle, 1992; Tredoux et al., 1995) but sulfide is the only phase that strongly collects all PGE. The good correlation of PGE variations with indices of fractionation also indicates that this segregation occurs during magma evolution at a shallow level and is not due to earlier processes such as random catching of PGE by mantle sulfides during the ascent of the melt towards the magma chamber

(Ballhaus and Ryan, 1995). In addition, the regular and simultaneous decline of Ir, Os and Pt concentrations also rules out random catching of PGE into sulfide phases belonging to the surrounding material during magma evolution (Fig. 4).

Conversely, Re abundances in Kohala tholeiites do not clearly correlate with either MgO or other PGE (Fig. 4), although Re have been shown to be compatible in sulfides (Jones and Drake, 1986; Roy-Barman et al., 1998). However, much of the Re (at least 80%) contained in subaerial lavas has been suspected to be lost during magma degassing prior to eruption (Lassiter, 2003). Thus, Re variations are unlikely to be informative in our lava set and will not be discussed further.

Experimental studies on sulfur solubility in silicate melt have shown that cooling and olivine fractionation within the magmatic chamber drive silicate melts to reach sulfur saturation (Mathez, 1976; Holzheid and Grove, 2002). The sulfur saturation of a melt is particularly visible on Pt and Pd variations because these elements are essentially fractionated by sulfide (Keays, 1995). Thus, when a magma is sulfur under-saturated, these elements behave rather incompatibly and their contents would slightly increase during magma evolution. In contrast, when a magma reaches sulfur saturation, Pt and Pd would preferentially partition into sulfide ($D_{Pt,}$ and $D_{Pd} = 10^4$) and their contents would clearly decrease.

Pd variations were previously studied on variably-fractionated lavas series from Kilauea Volcano (Crocket, 2000) and the MgO-Pd variation plot obtained are reported in Fig. 5. These data show that Pd abundances are rather constant in MgO-rich Kilauea lavas, but decrease strongly in evolved lavas with less than 8% MgO. Thus, these additional data obtained on Kilauea tholeiites reveal the coupled segregation of Pt and Pd in evolved magma compositions and confirm the previous idea that the Hawaiian magma reaches sulfur saturation around 8 - 9% MgO.

The good MgO - PGE correlations described by the whole set of Hawaiian lavas (Fig. 2, 4 and 5) give us the opportunity to estimate the bulk distribution coefficients for PGE during both early and late stages of magma differentiation. These calculations will thereby emphasize the change in PGE behavior outlined above.

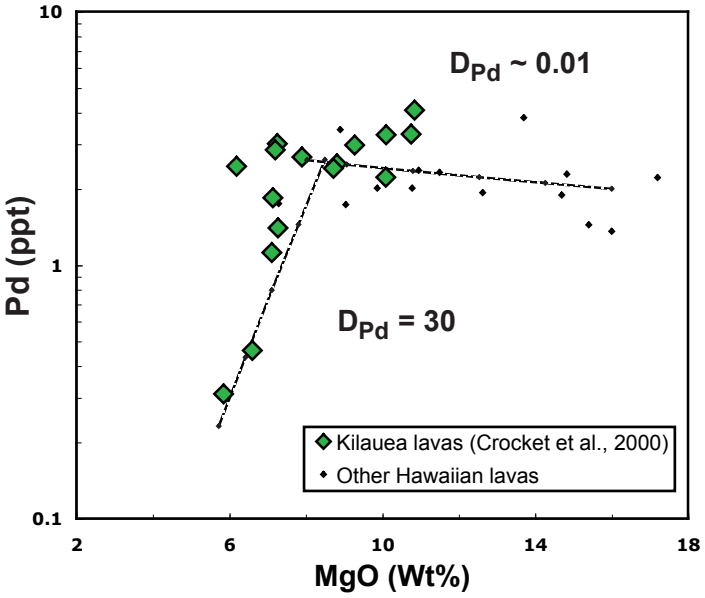

Fig. 5: *MgO - Pd variations in Kilauea lavas such as reported in Crocket (2000) as well as in other Hawaiian basalts (Tatsumi et al., 1999; Bennett et al., 2000). Contrary to a moderate increase of Pd in primitive lavas, a strong decline of Pd appears in evolved Hawaiian lavas with less than 8 % MgO. The strong mobilization of Pd in evolved lavas emphasizes the presence of sulfide in the Hawaiian melt and the onset of these phases at around 8 % MgO.*

5.2 Bulk distribution coefficient calculation

In order to determine bulk distribution coefficients for PGE, the estimate of a primary magma composition for Hawaiian lavas was first necessary. A primary magma composition for Kohala tholeiites has been estimated using the model of reverse olivine crystallization proposed by Danyushevsky et al. (2000). For this, we considered that olivine in equilibrium with the primary melt composition has $F_O = 90$, as proposed in Bennett et al. (2000), and applied a step calculation with 0.1% increment on 22 Kohala tholeiite compositions (from Feigenson et al. (1983)). At each step (adding of 0.1% olivine), compositions of the new melt and olivine in equilibrium were re-evaluated (see Danyushevsky et al., 2000). The average primary composition obtained has 16 % MgO and is consistent with an Os content of 600 ppt according to the Hawaiian trend (Fig. 2).

Thereafter, a bulk distribution coefficient for Os during the early stage of magmatic differentiation was evaluated from the slope of the MgO - Os correlation described by the Hawaiian trend. From the primary composition calculated above, fractional crystallization trends were calculated for different D_{Os} values using the Rayleigh fractionation law:

$$C_m = C_0*(1 - F)^{(D-1)}$$

where C_m is the Os concentration in the melt, C_o is the initial concentration of Os in the melt (600 ppt), F is the degree of fractionation and D the bulk distribution coefficient for Os. Relation

between MgO content in the melt and its degree of fractionation is given in the reverse fractionation model. Fig. 6 shows that the MgO - Os correlation defined by primitive Hawaiian lavas is thus best matched by fractional crystallization trend using a D_{Os} of 6 (± 2). In the same way, a bulk distribution coefficient for Os during the late stage of fractional crystallization was estimated from the slope of the correlation defined by Kohala tholeiites. Fractional crystallization trends were calculated from a starting composition with 8.5% MgO and 180 ppt Os using different values of D_{Os}. The MgO - Os correlation defined by Kohala tholeiites is thus best matched by fractionation of an assemblage with D_{Os} = 50 (± 10)(Fig. 6). Thus, our calculations indicate that the bulk D_{Os} between mineral phases and melt shifts from about 6 in primitive magma compositions to about 50 in lavas with less than 8.5 % MgO (Fig. 6).

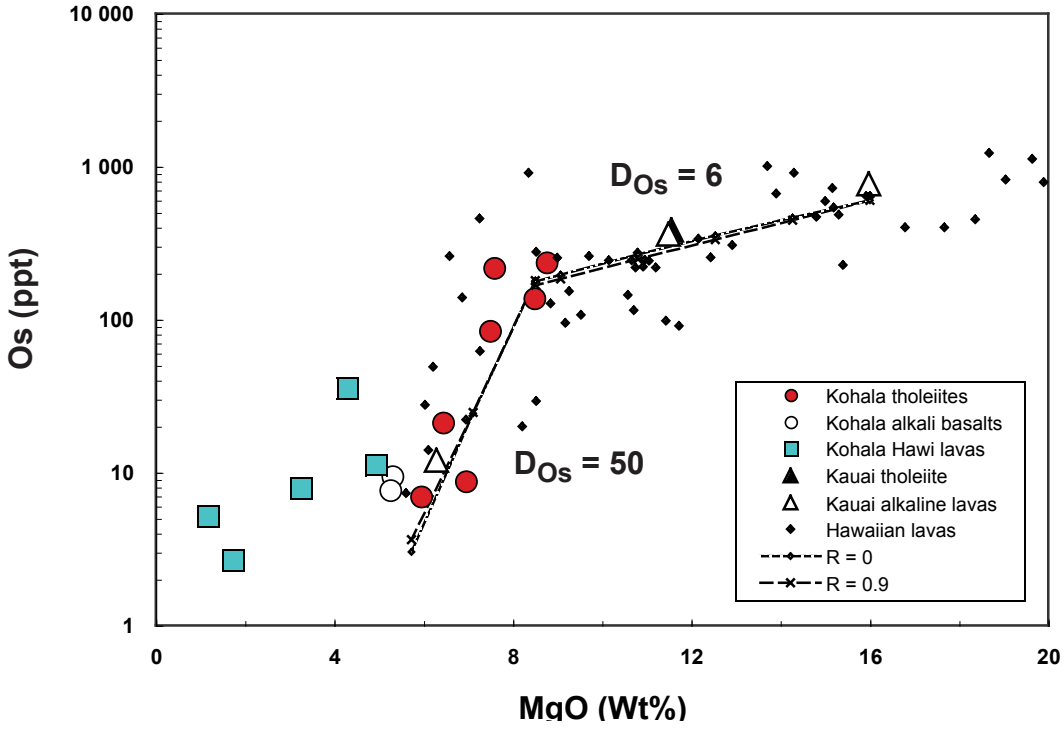

Fig. 6: *MgO - Os variations in Hawaiian lavas showing the estimates of bulk distribution coefficient for Os during the Hawaiian magma differentiation. The MgO - Os correlations described by Hawaiian lavas suggest a shift of D_{Os} from 6 in primitive compositions up to 50 in lavas with less than 8.5 % MgO. This emphasizes the strong mobilization of Os into sulfide phases during late stage of evolution due to sulfur saturation of the Hawaiian magma beyond 8.5 % MgO.*

The same calculations have been performed using assimilation and fractional crystallization trends (AFC equations of DePaolo (1981)) in order to measure the effect of any crust material assimilation on the bulk DOs value. We considered for that an oceanic crust assimilant with 21

ppt Os, as estimated in the following section (paragraph 6.2), and a maximum mass assimilated / mass fractionated ratio R = 0.9 (see paragraph 6.2). It appears then from Fig. 6 that assimilation processes have only negligible effect on Os partitioning and are not necessary to consider in these calculations.

The bulk D_{Os} value of 50 estimated for evolved lavas is much higher than the value previously suggested by Martin et al. (1994) on lava suites from Haleakala Volcano (D_{Os} =10 ± 5). However, their calculations were based on the assumption of a linear MgO - Os correlation from a hypothetical primary high-MgO magma composition to their most evolved lavas. But as outlined before, the actual set of published Os data on Hawaiian lavas reveals a change in Os behavior during fractional crystallization of the Hawaiian melt.

The partitioning of other PGE in Hawaiian lavas has also been evaluated in the same way (Fig. 4 and 5) and the result of these calculations is summarized in Table 2. Fractionation trends in evolved compositions have been calculated from a starting melt composition with 8.5 % MgO. We should emphasize that the small number of PGE data does not allow for a good precision on the exact starting point for the decline of all PGE and the slope of the MgO - PGE correlations (Fig. 4). However, this evaluation points out important changes in the bulk partition coefficient values for PGE between primitive and evolved lava compositions.

Table 2: Estimation of PGE partitioning during the Hawaiian magma differentiation

	Ir	Os	Ru	Pt	Pd
For a magma composition between 16 and 8.5 % MgO					
Starting composition	350 ppt	600 ppt	800 ppt	2.5 ppb	2 ppb
Bulk distribution coefficient D	0.5	6	3	< 0.5	< 0.5
For a magma composition with less than 8.5 % MgO					
Starting composition	400 ppt	180 ppt	500 ppt	4 ppt	2.6 ppb
Bulk distribution coefficient D	40	50	40	35	30

As for Os, the estimated bulk partition coefficient values for Ir, Ru, Pd and Pt are very high in evolved lavas (30 - 40) compared to values obtained on primitive lavas compositions (< 0.5 - 6). Therefore, the strong increase of PGE partitioning in lavas with less than ~ 8% MgO

confirm the sulfur saturation of the Hawaiian magma and the onset of sulfide phases at a composition around 8 % MgO.

5.3 PGE-bearing mineral phases before S-saturation of the Hawaiian magma

The MgO-PGE correlations defined by the Hawaiian trend also show slight decrease of Os and Ru during the early stage of magma differentiation (Fig. 4 and 6, Table 2). Although Ru and Os are well correlated with MgO and Ni, a number of studies have shown that olivine does not contain significant amount of Os and Ru and seems therefore unlikely to be responsible for the compatible behavior of these elements during magma evolution (Mitchell and Keays, 1981; Gueddari et al., 1996; Lorand et al., 1999; Burton et al., 2002). Other phases such as Cr-Spinel (Capobianco and Drake, 1990; Hart and Ravizza, 1996; Righter et al., 2004) or Ru-Ir-Os alloys (Stockman and Hlava, 1984; Merckle, 1992; Walker et al., 1996; Sattari et al., 2002) have been shown to host significant amount of I-PGE and could potentially control the PGE variations in the primitive Hawaiian lavas. However, precise partitioning of noble metals in these phases remains a subject of debate and the present data set does not allow for further constraints on the possible I-PGE-bearing phase present during early stages of magma differentiation.

5.4 Estimation of sulfide proportion in evolved Hawaiian magma

After the magma has reached sulfur saturation, sulfide is most likely to be the major host phase for all PGE. It is therefore possible to evaluate the proportion of sulfide present in the Hawaiian magma using the bulk distribution coefficients for PGE calculated above.
The bulk distribution coefficient for an element i is given by:

$$\text{Bulk } D_i = \sum X_j * P_{j\,/\,melt}$$

where X represents the proportion of the different mineral phases (j) in the melt and $P_{j\,/\,melt}$ represents the partition coefficient between each mineral phase j and the melt for the element i. Now if we consider sulfide to be the only host phase for at least Ir, Pt and Pd in the evolved Hawaiian magma (MgO < 8%), this equation is reduced for these elements to:

$$\text{Bulk } D_i = X_{\text{sulfides}} * P_{\text{sulfides / melt}}$$

On the other hand, the I-PGE-bearing phases present before sulfur saturation of the Hawaiian magma may potentially mobilize a small quantity of Os and Ru in the sulfur saturated melt as well. It is thus necessary to subtract the bulk D values obtained on primitive lavas from the bulk D values obtained on evolved lavas in order to eliminate this effect on Os and Ru partitioning. Os and Ru distributions between sulfide and the evolved Hawaiian melt are then:

$$X_{\text{sulfides}} * P_{\text{sulfides / melt}} = \text{bulk } D_{Os} - D_{Os\ (\text{silicate oxide})} = 50 - 6 = 44$$
$$X_{\text{sulfides}} * P_{\text{sulfides / melt}} = \text{bulk} D_{Ru} - D_{Ru\ (\text{silicate oxide})} = 40 - 3 = 37$$

Thus, using partition coefficients between sulfide and silicate melt for PGE reported in literature, we have calculated the proportion of sulfide responsible for PGE distribution in the evolved Hawaiian magma. For this evaluation, several references for PGE partitioning have been considered. The results are reported in Table 3.

Table 3: Evaluation of sulfide proportion in the evolved Hawaiian magma (< 8% MgO).

	Ir	**Os**	**Ru**	**Pt**	**Pd**
$D_{(\text{sulfides / silicate melt})}$	40	44	37	35	30
$P_{(\text{sulfides / silicate melt})}$ *a	25000	22000	46000	12000	15000
X_{sulfides}	0.2 %	0.2 %	0.1 %	0.3 %	0.2 %
$P_{(\text{sulfides / silicate melt})}$ *b		48000			
X_{sulfides}		0.1 %			
$P_{(\text{sulfides / silicate melt})}$ *c	35000	97000	35000		9180
X_{sulfides}	0.1 %	0.05 %	0.1 %		0.3 %

**a: Partition coefficients between sulfide and silicate melt reported in Fleet et al. (1996);*
**b: Partition coefficients between sulfide and silicate melt reported in Roy-barman et al. (1998);*
**c: Partition coefficients between sulfide and silicate melt reported in Sattari et al. (2002)*

It appears from this calculation that the proportion of sulfide required to explain the PGE partitioning in the Hawaiian magma is extremely low and is most probably situated between 0.1 and 0.3 %. This estimation of sulfide proportion agrees well with what we should expect for a sulfur-saturated and sulfide fractionating magma. For example, if we consider a sulfur content

of 1000 ppm in the Hawaiian magma at sulfur saturation point (see Mavrogenes and O'neill (1999)), 1 % crystallization in the melt would increase the sulfur content to around 1010 ppm. Because of the saturation, around 10 ppm of sulfur would be mobilized to form sulfide phases. Now if we consider a sulfur proportion of around 30 % weight in sulfide, around 30 ppm of sulfide would be generated by this "extra" 10 ppm of sulfur. Consequently, 1% crystallization of the magma at sulfur saturation point would induce around 30 ppm sulfide crystallization and a proportion of sulfide in the crystallizing phase of 30.10^{-6} / 1.10^{-2} = 3.10^{-3} or 0.3 %. Therefore, the above estimation of around 0.1 - 0.3% of sulfide in the evolved Hawaiian magma is another evidence for the mobilization of all PGE into sulfide phases in lavas with less than 8 % MgO.

We note finally that, in spite of slightly higher values on Pt and Pd, the different proportions of sulfide estimated above are relatively homogeneous. Therefore, this indicates that the distribution coefficient for PGE estimated graphically in this study agree relatively well with values of partition coefficient for PGE reported in literature (Fleet et al., 1996; Roy-Barman et al., 1998; Sattari et al., 2002).

5.5 Os and PGE behavior in the post-shield stage of Kohala Volcano

Osmium content is extremely low in the highly differentiated lavas from Hawi Volcanics. In addition, the low Ir, Ru and Pt concentrations obtained on sample KH5 suggest that the Hawi magma was sulfur saturated well before its composition reach 5% MgO (Fig. 4). On the other hand, the slope of the MgO-Os correlation defined by Hawi lavas seems weaker than those well defined by Pololu lavas (Fig. 6). Olivine is not the dominant silicate phase crystallizing from the Alkaline Hawi magma (Spengler and Garcia, 1988). Therefore, it is not possible to apply the reverse fractional crystallization calculation in order to constrain a primary magma composition and a bulk D_{Os} for these post-shield lavas.

However, the overlap of the alkaline lavas from Kauai with the field of the primitive Hawaiian tholeiites suggests a common MgO - Os trend for all Hawaiian magma (Fig. 6). Consequently, the MgO - Os trend defined by the Hawi lavas from Kohala Volcano is most probably linked to the field of the primitive Hawaiian tholeiites. Thus, a more moderate Os decline seems to have happen during the differentiation of the evolved Hawi magma. Now Os decrease in evolved Pololu lavas has been previously explained by the presence of sulfide in the

melt. Therefore, this more moderate Os decrease could indicate that sulfide phases were less abundant during the differentiation of the Hawi magma.

5.6 Conclusion

This study of Os, Ir, Ru and Pt variations in Kohala lavas has demonstrated that the PGE behavior change during the differentiation of the Hawaiian magma. While variations are rather constant in primitive Hawaiian tholeiites, a strong and simultaneous decline of all PGE concentrations are recorded in lavas with less than 8% MgO. The estimated bulk distribution coefficients in these evolved Kohala lavas range from 35 for Pt to 50 for Os and are very high compared to the estimates in primitive Hawaiian lavas (> 8% MgO).

This sudden decline of all PGE concentrations most likely reflects the sulfur saturation of the Hawaiian magma and the onset of sulfide fractionation at a melt composition ~ 8% MgO. From the calculated bulk partition coefficients for PGE and the partition coefficients between sulfide and silicate melt reported in Fleet et al. (1996), Roy-Barman et al. (1998) and Sattari et al. (2002), a sulfide proportion of 0.1 - 0.3 % in the fractionating assemblage has been estimated during the differentiation of the Kohala magma.

Finally, the extremely low Os and other PGE contents in the Hawi lavas suggest that the post-shield magma of Kohala Volcano was also sulfur saturated under compositions of 1 - 5 % MgO. However, Os decrease seems more moderate in these lavas, which suggests that the amount of sulfide was more moderate in the fractionating assemblage of the Hawi magma than it was in the Pololu magma.

6. Constraints on Assimilation and Fractional Crystallization (AFC) processes

6.1 Mantle signature and contamination of the melt at shallow level

Os isotopes in lavas from both shield building and post-shield-building stage of Kohala Volcano are very heterogeneous, ranging from values similar to those obtained on other Hawaiian basalts to highly radiogenic values (Fig. 7). Variation in Os isotopic ratios is also

inversely correlated with indices of fractionation, which suggests contamination of the melt during the fractional crystallization.

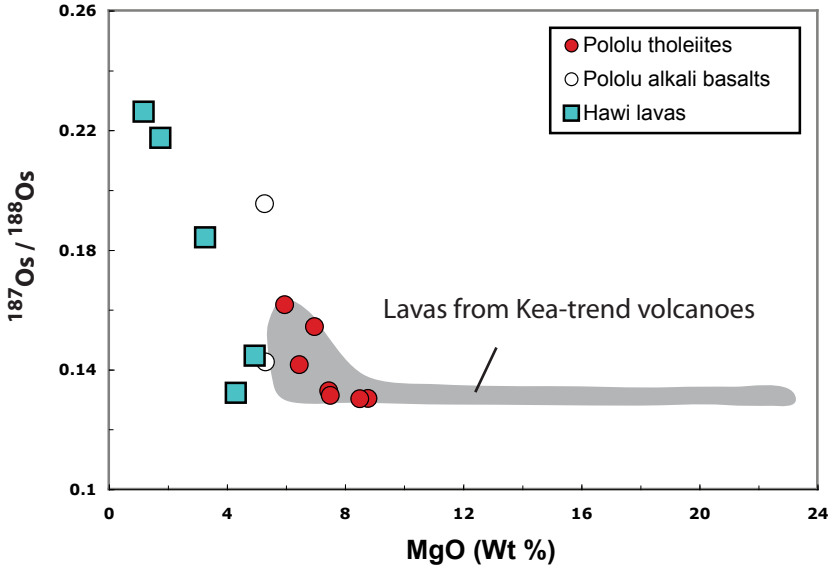

Fig. 7: *$^{187}Os/^{188}Os$ compositions plotted as a function of MgO concentrations in Kohala lavas. The field displayed by other lavas from Kea-trend Volcanoes, such as Mauna Kea, Haleakala and Kilauea volcanoes, is also reported form comparison. It is based on data from Martin et al. (1994), Lassiter and Hauri (1998) and Bennett et al. (1996) and (2000). Variations recorded in Kohala tholeiites overlap the field displayed by other Kea-trend lavas. Os-isotopes are very homogeneous in relatively primitive compositions and become radiogenic in evolved compositions. Lavas from the Post-shield stage of Kohala Volcano present a very large range of $^{187}Os/^{188}Os$, inversely correlated with MgO content.*

In the Pololu Volcanics, the less fractionated tholeiites have homogeneous $^{187}Os/^{188}Os$ ratios, with an average of 0.131. These values are similar to those obtained on high-MgO lavas from Haleakala, Kilauea and Mauna Kea Volcanoes (Martin, 1991; Martin et al., 1994; Lassiter and Hauri, 1998; Brandon et al., 1999), which are thought to represent the mantle source of these Kea-trend Volcanoes. In contrast, $^{187}Os/^{188}Os$ ratios are scattered and more radiogenic in evolved Pololu basalts having low Os content (less than 30 ppt) (Fig. 7). In the previous part, we have seen that Os and other PGE abundances exhibit a strong decline within a narrow range of MgO values (8 - 5% MgO), which are most likely due to the sulfur saturation of the melt and segregation of these elements into sulfide phases. Consequently, this drop of Os content during fractional crystallization would enhance the sensitivity of Os isotopes to any contamination with radiogenic materials. In fact, $^{187}Os/^{188}Os$ values in the Pololu basalts gradually increase with the decrease of Os concentrations, reflecting a progressive contamination of these isotopic ratios as the magma evolves (Fig. 8). We note also that Os concentrations in evolved lavas are comparable with the low Os concentrations reported for oceanic crust materials (1 - 35 ppt)

(Lassiter and Hauri, 1998; Blusztajn et al., 2000; Peucker-Ehrenbrink et al., 2003). Thus, interactions with radiogenic wall-rock materials during magma differentiation are likely to influence the Os isotopic composition of the most evolved magma. Consequently, radiogenic $^{187}Os/^{188}Os$ ratios recorded in evolved Pololu basalts are most probably due to coupled processes of oceanic crust assimilation and fractional crystallization.

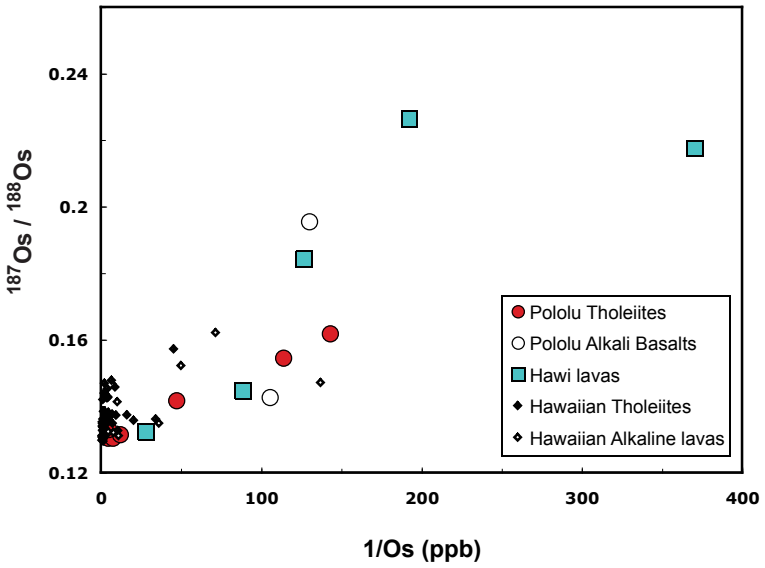

Fig. 8: *1/Os - $^{187}Os/^{188}Os$ variations in Kohala lavas and other Hawaiian lavas showing the inverse correlation of Os-isotopes and Os concentrations in evolved Hawaiian lavas. This reflects contamination of the melt during fractional crystallization at shallow level. Additional data are from Martin et al. (1994), Lassiter and Hauri (1998), Bennett et al. (1996) and (2000).*

6.2 Assimilation in the post shield lavas from Kohala Volcano

The highly-fractionated lavas from Hawi Volcanics also exhibit a very large range of Os isotopic ratios, with extremely radiogenic values in the most fractionated compositions ($^{187}Os/^{188}Os$ up to 0.223, see Fig. 7). The low Os concentrations (3 – 35 ppt) and the very good correlation displayed between MgO contents and Os isotopic ratios in these lavas suggest that coupled processes of assimilation and fractional crystallization (AFC) are also responsible for their elevated $^{187}Os/^{188}Os$ ratios.

However, we observe a clear distinction in the MgO - $^{187}Os/^{188}Os$ correlation between lavas from the shield stage and lavas from the post-shield stage of Kohala Volcano (Fig.7). Although Hawi lavas samples have more evolved compositions than all Pololu basalts samples, the range of their isotopic ratios starts from similar values than those displayed by the less fractionated Pololu tholeiites. We saw previously that Os decrease was more moderate during differentiation of the evolved Hawi magma than it was during differentiation of the evolved Pololu magma (with < 8% MgO). The sensitivity of Os-isotopes strongly depends on Os content in the

lavas. Consequently, a more moderate decrease in Os during fractional crystallization of the Hawi magma may have reduced the effect of AFC on the Os-isotopes.

We note also that the correlation between Os isotopic ratios and Os concentrations is more scattered in the highly differentiated lavas from Hawi Volcanics. This scatter reflects most likely the "nugget effect" on Os concentrations induced by the presence of sulfide in the lavas. As outlined in paragraph 3, Osmium is strongly concentrated in sulfide phases, which would most likely produce very heterogeneous Os content in the rock. This effect would be particularly visible in these differentiated lavas as Os content is extremely low. Finally, our set of data does not clearly constrain the mantle signature of the Hawi lavas. However, the overlap of the Hawi lavas trend and the Pololu lavas trend in the 1/Os - $^{187}Os/^{188}Os$ variations diagram (Fig. 8) suggests that Hawi and Pololu lavas have similar Os-isotopes mantle signatures and that these ratios were affected by the same radiogenic material.

In the following, we examine the nature and the quantity of radiogenic material that was assimilated during evolution of the Pololu magma. After an overview of the possible assimilated materials and their geochemical characteristics, the 1 / Os - $^{187}Os/^{188}Os$ correlation will be used to constrain the extent of coupled assimilation / fractional Crystallization.

6.3 Magma chamber location and possible assimilated materials

The exact location of the magma chamber under Kohala Volcano is not known. The Hawaiian magma could then have been contaminated either by mantle lithospheric material, lower oceanic crust material or upper oceanic crust material during its differentiation. Studies on abyssal peridotites have revealed that lithospheric mantle material possesses very low values of $^{187}Os/^{188}Os$ ratios (~ 0.125) compared to values obtained on Hawaiian basalts (> 0.129) (Martin, 1991; Roy-Barman and Allegre, 1994; Snow and Reisberg, 1995). Therefore, interactions between the Hawaiian plume and upper mantle material cannot be responsible for the radiogenic Os isotopic ratios recorded in the evolved Kohala lavas. In contrast, the old oceanic crust surrounding the Hawaiian Islands (110 ± 2 Ma Waggoner, 1993)) should possess highly radiogenic Os-isotopes and low Os concentrations and appears to be the most suitable candidate for contaminating Kohala magma during its evolution. Because of the coupled compatible behavior of Os and incompatible behavior of Re during partial melting processes, the earth's crust possesses lower Os concentrations and higher Re / Os ratios than the earth's mantle. With

time, ^{187}Re decay produces an increase of $^{187}Os/^{188}Os$ ratios in the crust, resulting in highly radiogenic Os-isotopic ratios compared to mantle-derived magmas.

The existence of shallow magma reservoirs within active Hawaiian volcanoes has been documented. Geodetic and seismic studies have suggested crustal magma chamber at ~ 3 - 4 km depth in Mauna Loa Volcano (Decker et al., 1983) and at ~ 3 - 6 km depth in Kilauea Volcano (Klein et al., 1987). Other seismic studies have inferred even shallower magma chamber in Kilauea Volcano, between 0 and 2 km depth (Ryan et al., 1981; Thurber, 1984, 1987; Rowan and Clayton, 1993). Finally, greater magma chamber depths have been estimated in Loihi seamount. Based on entrapment depth for melt inclusions in xenolith bodies, Roedder (1983) and Clague (1988) estimated a summit magma reservoir between 8 and 17 km depth, while Garcia et al. (1998) gave petrological and seismic evidence for a "8-to-9-km-deep" magma chamber. However, this greater depth of Loihi's magma chamber compared to other active Hawaiian volcanoes has been inferred to the cooler thermal regime in this submarine volcano (Garcia et al., 1998).

6.4 Contaminant parameters

In the absence of precise location for a Kohala magma chamber within the oceanic crust, we have estimated geochemical parameters for both the upper and lower oceanic crust surrounding the Hawaiian Islands.

Parameters for a 110 Ma-old Upper oceanic crust have been determined from Os and Re average values reported in Peucker-Ehrenbrink et al. (2003) for a drilled section of Pacific oceanic crust (DSDP/ODP site 504B). In this study, Os and Re data have been analyzed on samples from different units of the upper oceanic crust. However, the sampling was judge disproportional according to the different units and the authors calculated average values of $^{187}Re/^{188}Os$, $^{187}Os/^{188}Os$ and Os content for each unit and for the entire upper oceanic crust using petrographic data. Each time, they calculated $^{187}Re/^{188}Os$ and $^{187}Os/^{188}Os$ ratios by taking differences in concentrations and isotopic compositions into account. We used these estimated average data for the entire oceanic crust and recalculated the $^{187}Os/^{188}Os$ ratios for a 110 Ma-old oceanic crust. Parameters obtained are Os = 21 ppt and $^{187}Os/^{188}Os$ = 0.821. Peucker-Ehrenbrink et al. (2003) emphasized large and unquantifiable uncertainties on their average

values estimation. Consequently, the same errors are afflicted to our upper oceanic crust parameters.

Parameters for a 110 Ma-old lower oceanic crust have been determined from Os and Re data reported for a drilled section of lower Indian oceanic crust (Blusztajn et al., 2000) as well as from data obtained on gabbroic xenolith in Hawaiian magma (Lassiter and Hauri, 1998). In the case of the lower Indian oceanic crust data, $^{187}Os/^{188}Os$ ratios of each sample were recalculated for a 110 Ma-old material, with the exception of one troctolitic sample. Troctolites are very rich in Os compared to other lower crust material and represent lithologically only 1% of the drilling core (Blusztajn et al., 2000). Thus, we did not use data on this sample in our calculations. We noted that the estimated $^{187}Os/^{188}Os$ ratios and Os contents for a 110 Ma-old material are often very similar to values reported for the Hawaiian gabbroic xenoliths (Lassiter and Hauri, 1998), which makes relevant the use of Indian crust material in our calculation. Thereafter, an average value of $^{187}Os/^{188}Os$ ratios was obtained by taking the Os content associated with each Os isotopic ratio into account, as follow:

$$\text{Average } ^{187}Os/^{188}Os = \sum ([Os] * {}^{187}Os/^{188}Os) / \sum [Os]$$

Parameters obtained for a 110 Ma-old Lower oceanic crust are Os = 15 ppt and $^{187}Os/^{188}Os = 0.432$. The range of estimated $^{187}Os/^{188}Os$ ratios for a Hawaiian lower crust is however very large (0.22 – 2.63) and highlights some heterogeneities within the gabbro level. Consequently, the small number of samples (8) considered in our calculation may not be representative enough and the determined Hawaiian lower crust parameters are thus also afflicted by large uncertainties. However, these upper and lower crust parameters make best use of the available geochemical data on oceanic crust material.

6.5 AFC modeling: nature and proportion of the assimilated material

Using these estimates for the surrounding crust material and equations proposed by DePaolo (1981), we have modeled AFC processes responsible for the 1/Os - $^{187}Os/^{188}Os$ correlations described by the Kohala lavas. Fig. 9 shows AFC trends calculated for an assumed $D_{Os} = 50$ (see paragraph 5.3) starting from a melt composition with 180 ppt of Os and $^{187}Os/^{188}Os = 0.132$. Assimilation of either upper oceanic crust or lower oceanic crust materials

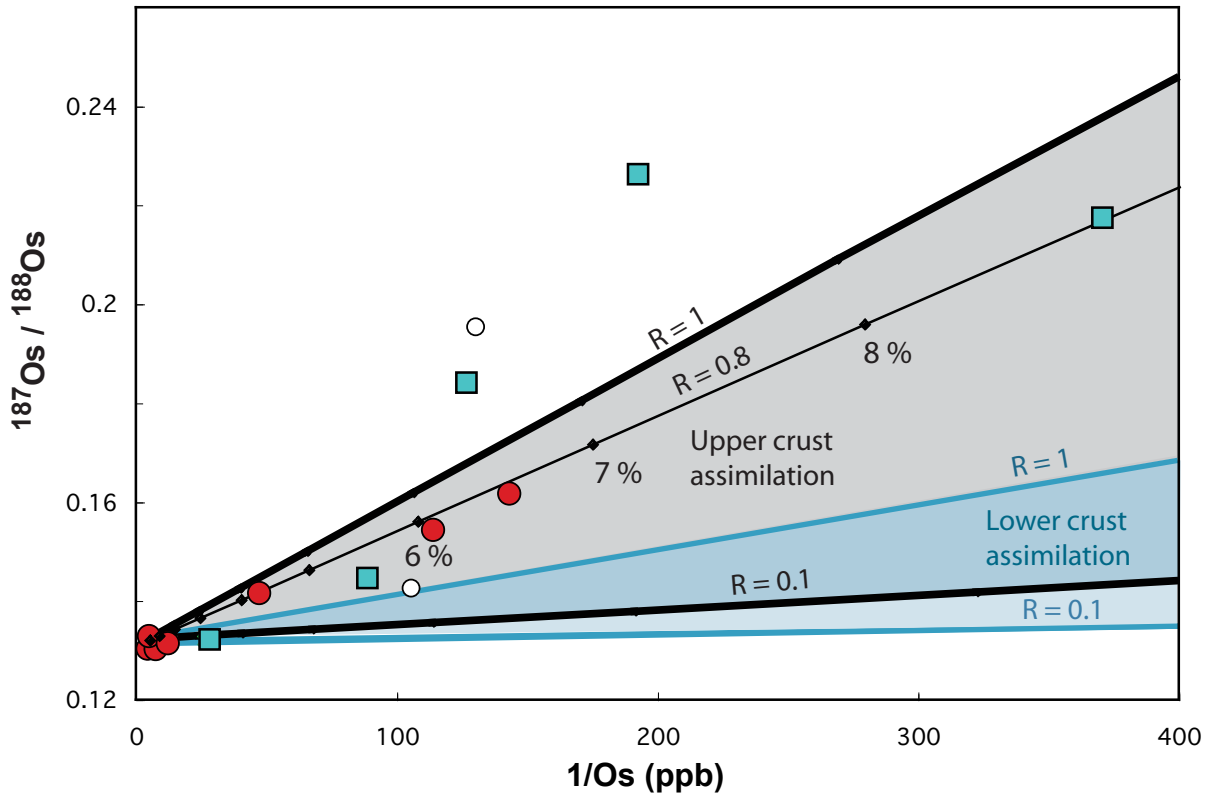

Fig. 9: *1/Os - $^{187}Os/^{188}Os$ variations in Kohala lavas showing assimilation and fractional crystallization (AFC) trends calculated for either upper or lower crust assimilation. For this modeling, we used an assumed D_{Os} = 50 and variable mass assimilated / mass fractionated ratios R . Parameters for a 110 Ma-old upper pacific crust are: $^{187}Os/^{188}Os$ = 0.821 and Os content = 21 ppt; parameters for a 110 Ma-old lower pacific crust are: $^{187}Os/^{188}Os$ = 0.432 and Os content = 15 ppt; parameters for the plume-derived melt are $^{187}Os/^{188}Os$ = 0.132 and Os content = 180 ppt. This AFC modeling suggests that upper crust assimilation rather than lower crust assimilation have occured during the evolution of the Kohala magma. The 1/Os - $^{187}Os/^{188}Os$ variations in Kohala tholeiites are best reproduced for a mass assimilated / mass fractionated ratio R = 0.8. Small dots in the AFC trend indicates the percentage of crystallisation from the starting composition with 8.5 % MgO. Thus, up to 7 % cristallization and then up to 6 % upper crust assimilation could explain the 1/Os - $^{187}Os/^{188}Os$ variations in Kohala tholeiites for a range of composition between 8.5 and 5 % MgO.*

have been considered using different mass assimilated / mass fractionated ratios R. As explained in DePaolo (1981) and Lassiter and Luhr (2001), this ratio R is < 1 under most natural conditions.

Fig. 9 indicates that assimilation of upper oceanic crust material can reproduce the radiogenic $^{187}Os/^{188}Os$ ratios observed in most of Pololu basalts using a mass assimilated / mass fractionated ratio R ~ 0.8. In contrast, assimilation trends for lower oceanic crust material cannot reproduce the range of $^{187}Os/^{188}Os$ ratios and Os content observed in Kohala basalts, except for unlikely values of R > 1. Consequently, this AFC modeling suggests that the magma chamber in Kohala Volcano is situated in the upper part of the oceanic crust rather than in the lower gabbro levels. This is in agreement with the shallow magma chambers indicated for

Mauna Loa and Kilauea volcanoes. The most radiogenic samples of Kohala tholeiites have experienced less than 7% of crystallization from a starting composition with 8.5% MgO. Therefore, this indicates that up to 6 % assimilation of upper crust material is most likely to have occurred in the Hawaiian magma for a range of composition between 8.5 and 5 % MgO (Fig. 9).

In order to estimate the total amount of assimilated material in these evolved Kohala lavas, we have applied this AFC modeling considering upper crust material assimilation for lavas with a range of composition between 16 and 8.5 % MgO. Fig. 10 shows AFC trends calculated for an assumed D_{Os} = 6 (see paragraph 5.3) starting from a melt composition with 600 ppt Os and $^{187}Os/^{188}Os$ = 0.131. The 1/Os - $^{187}Os/^{188}Os$ correlation described by primitive tholeiites from Kea-trend Volcanoes is then reproduced using a mass assimilated / mass fractionated ratio R = 0.1. We observe also that a composition with 180 ppt Os, estimated to be associated with 8.5% MgO in the melt, is reached slightly before 22 % crystallization in the magma for an Os-isotope

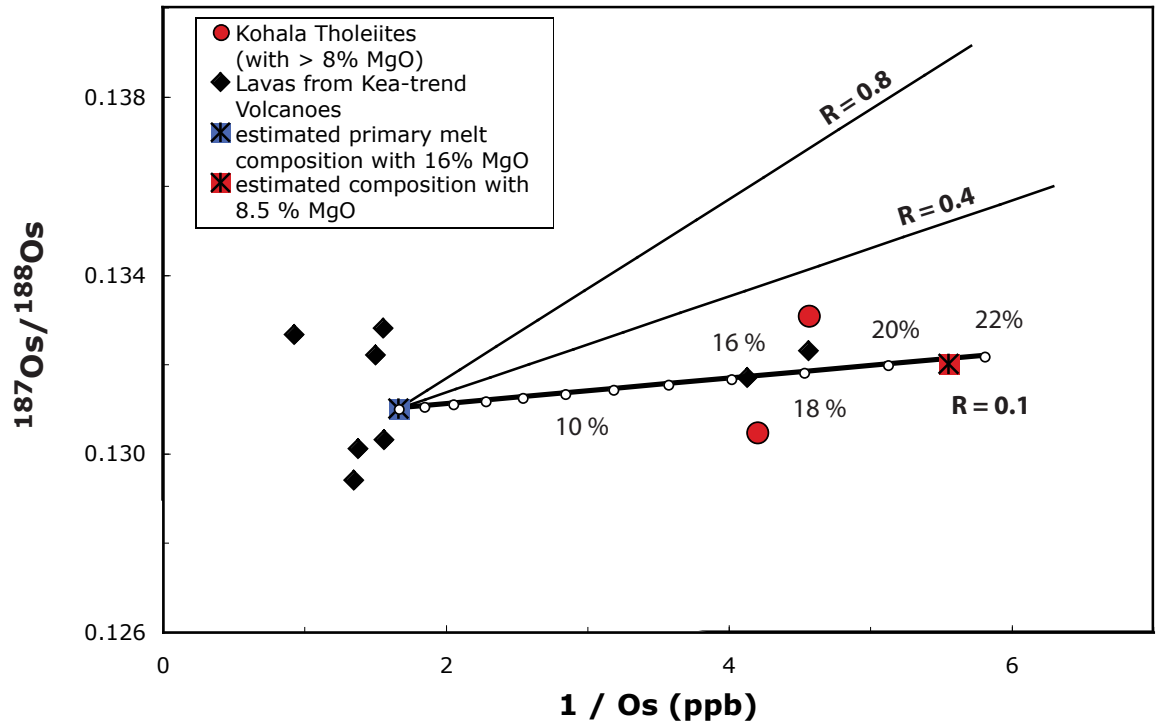

Fig. 10: *Plot of 1/Os - $^{187}Os/^{188}Os$ variations showing AFC trends for upper crust assimilation calculated from a primary melt composition with 600 ppt Os and $^{187}Os/^{188}Os$ = 0.131 using an assumed D_{Os} = 6 and different values of R. Os compositions and Os-isotopic ratios of relatively primitive Kohala tholeiites are best matched when considering a mass assimilated / mass fractionated ratio R = 0.1. Small dots in the AFC curve indicate 2 % fractional crystallization. Thus, such a model indicates that a magma with 8.5% MgO and ~200 ppt Os would have undergone slightly less than 22% olivine crystallization, and consequently ~2% assimilation. The Os-isotopic ratios would also have slightly increased from 0.131 to 0.132. Additional Hawaiian lavas are from Haleakala (Martin et al., 1994), Mauna Kea (Lassiter and Hauri, 1998) and Kilauea Volcanoes (Bennett et al, 2000).*

composition of 0.132. Therefore, this reveals that up to 2 % assimilation of upper crust material is most likely to have occurred in the Hawaiian magma for a range of composition between 16 and 8.5 % MgO.

Consequently, this AFC modeling applied to primitive and evolved composition indicates that the most evolved tholeiitic composition from Kohala Volcano may have assimilated up to 8% of upper crust material.

6.6 Impacts of oceanic crust assimilation on Sr- and Nd-isotopes

In order to examine the effect of such amount of assimilation on the Sr and Nd isotopic compositions of Kohala lavas, we have performed the same AFC modeling using Sr and Nd isotopic data. For the assimilant parameters, we have used Sr and Nd data reported for the same drilled section of pacific upper oceanic crust used for Os data (DSDP/ODP site 504B) (Alt et al., 1996; Pedersen and Furnes, 2001). As for Os, Sr and Nd isotopic ratios were recalculated for a 110 Ma old material and average values have been deduced considering the concentrations associated with each isotopic ratio. Parameters obtained for a 110 Ma-old upper oceanic crust are $^{87}Sr/^{86}Sr = 0.70278$, Sr = 56 ppm, $^{143}Nd/^{144}Nd = 0.51324$ and Nd = 7 ppm.

For this AFC modeling, we have considered a mass assimilated / mass fractionated ratio R = 0.1 until the magma reach 20 % crystallization and a mass assimilated / mass fractionated ratio R = 0.8 afterwards. Bulk distribution coefficients for Sr and Nd of 0.1 have been assumed. Finally, parameters for the plume-derived melt have been calculated from data reported in Hofmann et al. (1987 for relatively primitive Kohala tholeiites (MgO > 8%). Average values obtained are $(^{87}Sr/^{86}Sr)_{melt} = 0.70365$, Sr = 300 ppm, $(^{143}Nd/^{144}Nd)_{melt} = 0.512966$ and Nd = 20 ppm. Fig. 11 shows $^{87}Sr/^{86}Sr$ versus $^{187}Os/^{188}Os$ compositions and $^{143}Nd/^{144}Nd$ versus $^{187}Os/^{188}Os$ compositions for Kohala lavas and the AFC trends calculated. This AFC modeling reveals that 8% assimilation, corresponding to 27% crystallization in the Pololu magma, would produce only negligible changes on the $^{87}Sr/^{86}Sr$ and $^{143}Nd/^{144}Nd$ composition of the primitive Hawaiian melt. The average Sr isotopic value would decreases of around 1.10^{5} (0.70365 to 0.70364) while the average Nd isotopic value would increases of around 4.10^{6} (0.512966 to 0.512970). We note that these minor changes produced by 8% upper crust assimilation on both Sr- and Nd-isotopes are within the measurement error usually obtained on these isotopic ratios and are consequently negligible compared to isotopic heterogeneities within the primitive

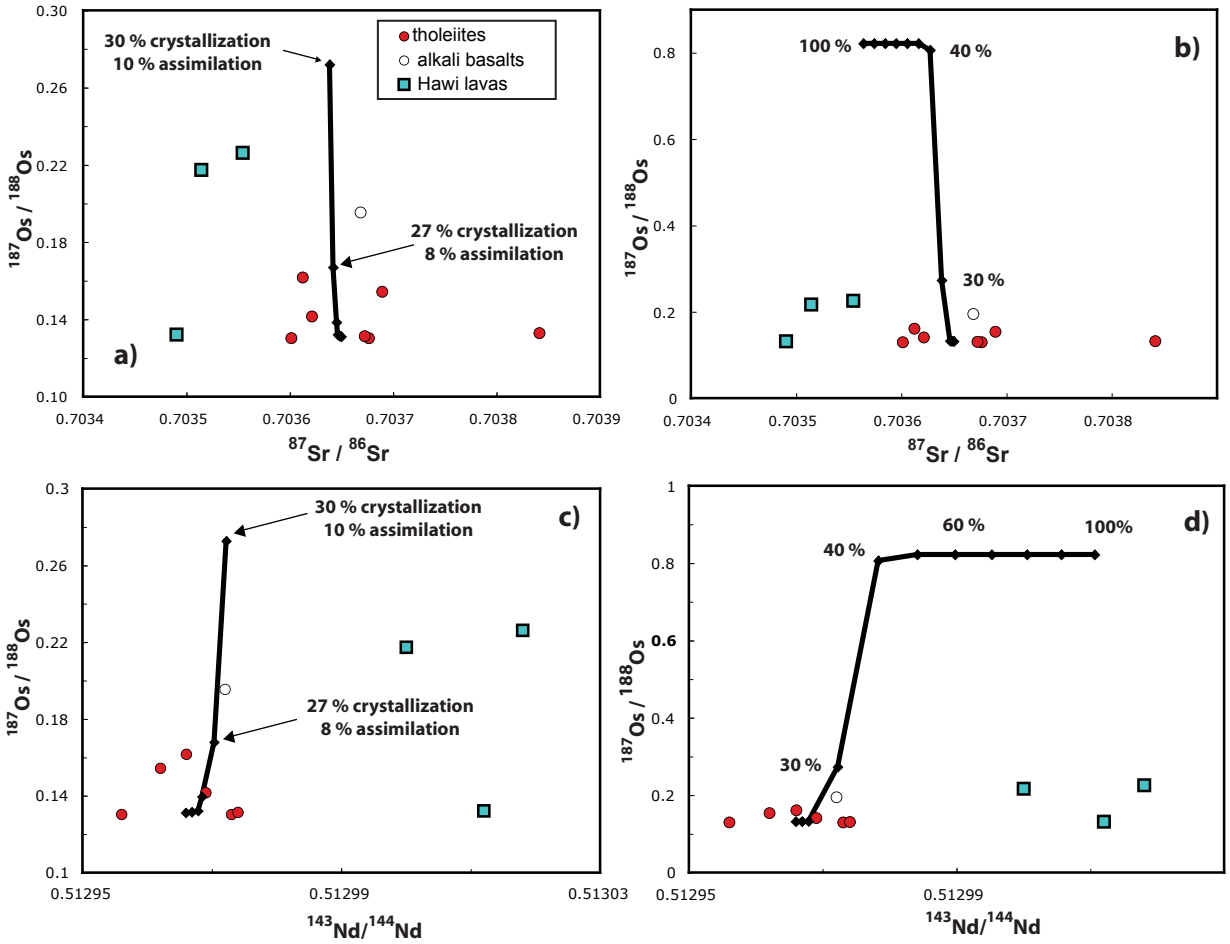

Fig. 11: *^{87}Sr / ^{86} Sr versus ^{187}Os / ^{188}Os and ^{143}Nd / ^{144}Nd versus ^{187}Os/ ^{188}Os diagrams showing the effect of upper oceanic crust material assimilation on the isotopic compositions of the Hawaiian magma. Parameters for a 110 Ma-old upper pacific crust are: $^{187}Os/^{188}Os$ = 0.821, Os content = 21 ppt, $^{87}Sr/^{86}Sr$ = 0.70278, Sr = 60 ppm, $^{143}Nd/^{144}Nd$ = 0.51324 and Nd = 7 ppm; parameters for the plume-derived melt are $^{187}Os/^{188}Os$ = 0.131, Os content = 600 ppt, $^{87}Sr/^{86}Sr$ = 0.70365, Sr = 285 ppm, $^{143}Nd/^{144}Nd$ = 0.51297 and Nd = 20 ppm. For this modeling, we used a D_{Os} = 6 and R = 0.1 up to 20% crystallization in the melt and then D_{Os} = 50 and R = 0.8 for the evolved magma (see text for more detailed). Plots **a)** and **c)** show AFC trends calculated for up to 10 % assimilation. Contrary to Os-isotopes, there is no significant change in Sr- and Nd-isotope compositions of the melt for such small amount of upper crust assimilation. Plots **b)** and **d)** show AFC trends calculated up to entire crystallization of the magma. This AFC modeling suggests that the Sr and Nd isotopic compositions of the Hawaiian magma would only change significantly beyond 40% crystallization, corresponding to 34 % assimilation in the melt.*

Kohala tholeiites ($^{87}Sr / ^{86}Sr$ = 0.70360 - 0.70374 and $^{143}Nd / ^{144}Nd$ = 0.51296 - 0.51300, see Fig. 11).

In fact, Fig. 11b and 11d show that, in contrast to Os isotopic ratios, AFC processes constrained in Kohala lavas would only significantly affect Sr and Nd isotopic ratios beyond 40% crystallization and then beyond 34% assimilation in the magma. But then such amount of assimilation would generate extremely radiogenic Os isotopic ratios in the melt of around 0.8. However, such an extreme value for Os isotopes has not been measured on any of the Kohala lavas and has even not yet been reported for any lava from the Kea trend volcanoes. Therefore,

interactions between the Kohala magma and local oceanic crust material are not responsible for the Sr and Nd isotopic heterogeneities within the Kohala lavas, which indicate that even the most evolved compositions are likely to reflect the Sr and Nd isotopic signature of their mantle source.

Thus, this study demonstrates that AFC processes have only negligible effects on the Sr and Nd isotopic compositions of Kohala lavas and thereby makes invalid models that propose to explain most of isotopic heterogeneities recorded within individual volcanoes by shallow level assimilation (Halliday et al., 1995; Eiler et al., 1996; Class and Goldstein, 1997).

6.7 Conclusion

This present study of $^{187}Os/^{188}Os$ variations on a set of variably-fractionated lavas from Kohala Volcano reveals first that coupled processes of assimilation and fractional crystallization have happened during both shield-buiding and post-shield building events of Kohala volcanic activity. Relatively primitive tholeiitic compositions (with > 8% MgO) display homogeneous $^{187}Os/^{188}Os$ ratios with an average value of 0.131 that constrain the mantle signature of Kohala basalts. In contrast, evolved Kohala lavas present radiogenic $^{187}Os/^{188}Os$ ratios, which are inversely correlated with both Os and MgO concentrations in the lavas. The Hawi lava series analyzed do not clearly constrain the mantle signature of the post-shield stage of Kohala Volcano. However, the range of Os-isotopes obtained on these lavas suggests a mantle signature with similar Os-isotope ratios than those of the shield building stage of volcanism.

An AFC modeling explains further the good correlation between Os concentrations and $^{187}Os/^{188}Os$ ratios observed in Pololu basalts by assimilation of small quantities of local upper oceanic crust material during magma differentiation. This suggests that the Kohala magma chamber is situated in the upper level of the oceanic crust, which is in agreement with previous geophysical estimations of shallow magma reservoir in Mauna Loa and Kilauea Volcanoes (Ryan et al., 1981; Decker et al., 1983; Thurber, 1984, 1987; Rowan and Clayton, 1993).

This AFC modeling suggests also that less than 8% upper crust assimilation is likely to have produced the most radiogenic Os-isotope ratios recorded in Pololu lavas. This small amount of upper crust assimilation has only negligible effect on Sr and Nd isotopic ratios, which are only susceptible to change significantly beyond 30 % of upper crust assimilation. Therefore, this study demonstrates that shallow level assimilation processes are not responsible for the Sr

and Nd isotopic heterogeneities observed within the Kohala lavas and more generally within individual Hawaiian Volcanoes.

References

Alt J. C., Teagle D. A. H., Bach W., Halliday A. N. and Erzinger J. (1996) Stable and strontium isotopic profiles through hydrothermally altered upper oceanic crust, Hole 504B. *Proc. ODP, scientific Results* 148, 57-69.

Ballhaus C. and Ryan C. G. (1995) Platinum-group elements in the Merensky Reef: I. PGE in solid solution in base metal sulfides and the down-temperature equilibration history of Merensky ores. *Contrib. Mineral. Petrol.* 122, 241-251.

Barnes S. J., Naldrett A. J. and Gorton A. P. (1985) The origin of the fractionation of Platinum-Group elements in terrestrial magmas. *Chemical Geology* 53, 303-323.

Bennett V. C., Esat T. M. and Norman M. D. (1996) Two mantle-plume components in Hawaiian picrites inferred from correlated Os-Pb isotopes. *Nature* 381, 221-224.

Bennett V. C., Norman M. D. and Garcia M. O. (2000) Rhenium and platinum group element abundances correlated with mantle source components in Hawaiian picrites: sulphides in the plume. *Earth Planet Sci Lett* 183, 513-521.

Birck J. L., Roy-Barman M. and Capmas M. (1997) Re-Os isotopic measurements at the femtomole level in natural samples. *Geostand. Newsl.* 21, 19-27.

Blusztajn J., Hart S. R., Ravizza G. and Dick H. J. B. (2000) Platinum-group elelments and Os isotopic characteristics of the lower oceanic crust. *Chemical Geology* 168, 113-122.

Brandon A. D., Norman M. D., Walker R. J. and Morgan J. W. (1999) 186Os - 187Os systematics of Hawaiian picrites. *Earth Planet Sci Lett* 174, 25-42.

Brügmann G. E., Arndt N. T., Hofmann A. W. and Tobschall A. J. (1987) Noble metal abundances in komatiite from Alexo, Ontario, and Gorgona Island, Columbia. . *Geochim Cosmochim Acta* 51, 2159-2169.

Brügmann G. E., Yang J. H., Snow J. E., Rehkämper M. and Mezger K. (1999) Gemeinsame Bestimmung der Os-Isotopie und der Edelmetall-konzentrationen in Peridotiten, Basalten,

Sulfiden und Eisenmeteoriten. *Kolloquium des DFG-Schwerpunktprogramms 'Ocean Drilling Programm and Deep Sea Drilling Project' Tagungsprogramm und Abstracts*, 21-22.

Büchl A., Brügmann G. E., Batanova V. G., Munker C. and Hofmann A. W. (2004) Melt percolation monitored by Os isotopes and HSE abundances: a case study from the mantle section of the Troodos Ophiolite. *Earth Planet Sci Lett* 204(385-402).

Burton K. W., Gannoun A., Birck J. L., Allegre C. J., Schiano P., Clocchiatti R. and Alard O. (2002) The compatibility of rhenium and osmium in natural olivine and their behaviour during mantle melting and basalt genesis. *Earth Planet Sci Lett* 198, 63-76.

Capobianco C. J. and Drake M. J. (1990) Partitioning of ruthenium, rhodium, and palladium between spinel and silicate melt and implications for platinum group element fractionation trends. . *Geochim Cosmochim Acta* 61, 4139-4149.

Caroff M., Guillou H., Lamieux M., Maury R. C., Guille G. and Cotten J. (1999) Assimilation of ocean crust by hawaiitic and mugearitic magmas: an exemple from Eiao (Marquesas). . *Lithos* 46, 235-258.

Chen C. Y. and Frey F. A. (1983) Origin of Hawaiian tholeiites and alkalic basalt. . *Nature* 302, 785-789.

Chen C. Y. and Frey F. A. (1985) Trace element and isotopic geochemistry of lavas from Haleakala Volcano, east Maui, Hawaii: Implications for the origin of Hawaiian basalts. *Journal of geophysical research* 90, 8743-8768.

Clague D. A. (1988) Petrology of ultramafic xenoliths from Loihi seamount, Hawaii. *J Petrol* 29, 1161-1186.

Class C. and Goldstein S. L. (1997) Plume-lithosphere interactions in the ocean basins: constraints from the source mineralogy. *Earth Planet. Sci. Lett.* 150, 245-260.

Crocket J. L. (2000) PGE fresh basalt, hydrothermal alteration products, and volcanic incrustations of Kilauea Volcano. *Geochim Cosmochim Acta* 64(10), 1791-1807.

Danyushevsky L. V., Della-Pasqua F. N. and Sokolov S. (2000) Re-equilibration of melt inclusions trapped by magnesian olivine phenocrysts from subduction – related magmas : petrological implications. . *Contrib Mineral petrol* 138, 68-83.

Decker R. W., Koyanagi R. Y., Dvorak J. J., Lockwood J. P., Okamura A. T., Yamashita K. M. and Tanigawa W. R. (1983) Seismicity and surface deformation of Mauna Loa Volcano, Hawaii. *EOS* 64, 545-547.

DePaolo D. J. (1981) Trace element isotopic effects of combined wallrock assimilation and fractional crystallisation. *Earth Planet Sci Lett* 53, 189-202.

Eiler J. M., Valley J. W. and Stolper E. M. (1996) Oxygen isotope ratios in Olivin from the Hawaii Scientific Drilling Project. *J Geophys. Res.* 101, 11807-11813.

Feigenson M. D. (1984) Geochemistry of Kauai volcanics and a mixing model for the origin of Hawaiian alkali basalts. *Contrib. Mineral. Petrol.* 87, 109-119.

Feigenson M. D., Hofmann A. W. and Spera F. J. (1983) Case studies on the origin of basalt II. The transition from Tholeiitic to alkalic volcanism on Kohala Volcano, Hawaii. . *Contrib Mineral petrol* 84, 390-405.

Fleet M. E., Crocket J. L. and Stone W. E. (1996) Partitioning of platinum-group elements (Ir, Os, Ru, Pt, Pd) and Gold between sulfide liquid and basalt melt. *Geochim Cosmochim Acta* 60, 2397-2412.

Fleet M. E. and Stone W. E. (1991) Partitioning of platinum-group elements in the Fe-Ni-S systemand their fractionation in nature. *Geochim Cosmochim Acta* 55, 245-253.

Garcia M. O., Rubin K. H., Norman M. D., Rhodes J. M., Graham D. W., Muenow D. W. and Spencer K. (1998) Petrololgy and geochronology of basalt breccia from the 1996 earthquake swarm of Loihi seamount, Hawaii: magmatic history of its 1996 eruption. *Bull Volcanol* 59, 577-592.

Gueddari K., Piboule M. and Amosse J. (1996) Differentiation of Platinum Group Elements (PGE) and of gold during partial melting of peridotites in the lherzolitic massifs of the Betico-Rifean range (Ronda and Beni Bousera). . *Chemical Geology* 134, 181-197.

Halliday A., Lee D. C., Tommasini S., Davies G. R., Paslick C. R., Fitton J. G. and James D. E. (1995) Incompatible trace elements in OIB and MORB and source enrichment in the sub-oceanic mantle. . *Earth Planet Sci Lett* 133, 379-395.

Hart S. R. and Ravizza G. (1996) *Os partitioning between phases in lherzolites and basalts.*

Hauri E., Lassiter J. C. and DePaolo D. J. (1996) Osmium isotope systematics of drilled lavas from Mauna Loa, Hawaii. *J. Geophys. Res.* 101, 11793-11806.

Hauri E. H. and Kurz M. D. (1997) Melt migration and mantle chromatography, 2: a time-deries Os isotope study of Mauna Loa Volcano, Hawaii. *Earth Planet Sci Lett* 153, 21-36.

Hofmann A. W. and Feigenson M. D. (1983) Case studies on the origin ogf basalt. I. Theory and reassessment of Grenada basalts. *Contrib Mineral petrol* 84, 382-389.

Hofmann A. W., Feigenson M. D. and Raczek I. (1987) Kohala revisited. *Contrib Mineral petrol* 95, 114-122.

Holzheid A. and Grove T. L. (2002) Sulfur saturation limits in silicate melts and their implications for core formation scenarios for terrestrial planets. *American Mineralogist* 87, 227-237.

Jones J. H. and Drake M. J. (1986) Geochemical constraints on core formation in the earth. . *Nature* 322, 221-228.

Keays R. R. (1995) The role of komatiitic and picritic magmatism and S-saturation in the formation of ores deposits. *Lithos* 34, 1-18.

Keays R. R. and Campbell I. E. (1981) Precious metals in the Jimberlana Intrusion, Western Australia: implications for the genesis of platiniferous ores in layered intrusions. *Econ. Geol.* 76, 1118-1141.

Kennedy A., Kwon S. T., Frey F. A. and West H. B. (1991) The isotopic composition of postshield lavas from Mauna-Kea Volcano, Hawaii. . *Earth Planet Sci Lett* 103, 339-353.

Klein F. W., Koyanagi R. Y., Nakata J. S. and Tanigawa W. R. (1987) The seismicity of Kilauea's magma system. *US Geol Surv Prof Pap* 1350, 1019-1185.

Lanphere M. A. and Frey F. A. (1987) Geochemical evolution of Kohala Volcano, Hawaii. . *Contrib Mineral petrol* 95, 100-113.

Lassiter J. C. (2003) Rhenium volatility in Subaerial Lavas : constraints from subaerial and submarine portions of the HSDP-2 Mauna Loa Drillcore. *Earth Planet Sci Lett* 214, 311-325.

Lassiter J. C., DePaolo D. J. and Tatsumoto M. (1996) Isotopic evolution of Mauna Kea Volcano: results from the initial phase of the Hawaii Scientific Drilling Project. *J Geophys. Res.* 101, 11769-11780.

Lassiter J. C. and Hauri E. H. (1998) Osmium-isotope variations in Hawaiian lavas : evidence for recycled oceanic lithosphere in the Hawaiian plume. *Earth Planet Sci Lett* 164, 483-496.

Lassiter J. C. and Luhr J. F. (2001) Osmium abundance and isotope variations in mafic Mexican volcanic rocks: Evidence for crustal contamination and constraints on the geochemical behavior of Osmium during partial melting and fractional crystallization. *Geochem Geophys Geosyst* 2, 2000GC000116.

Lorand J. P., Pattou L. and Gros M. (1999) Fractionation of platinum-group elements and gold in the upper mantle: a detailed study in pyrenean orogenic lherzolites. *Journal of petrology* 10, 957-981.

Martin C. E. (1991) Osmium isotopic characteristics of matle-derived rocks. *Geochim Cosmochim Acta* 55, 1421-1434.

Martin C. E., Carlson R. W., Shirey S. B., Frey F. A. and Chen C. Y. (1994) Os isotopic variations in basalts from Haleakala Volcano, Maui, Hawaii : a record of magmatic processes in oceanic mantle and crust. . *Earth Planet Sci Lett* 128, 287-301.

Mathez E. A. (1976) Sulfur solubility and magmatic sulfides in submarine basalt glass. *J Geophys. Res.* 81, 4269-4275.

Mavrogenes J. A. and O'Neill H. S. C. (1999) The relative effects of pressure, temperature and oxygen fugacity on the solubility of sulfide in mafic magmas. *Geochim Cosmochim Acta* 63(7/8), 1173-1180.

McDougall I. and Swenson D. A. (1972) Potassium-Argon ages of lavas from Hawi and Pololu volcanics Series, Kohala Volcano, Hawaii. *Bull Geol Soc Am* 83, 3731-3738.

Meisel T., Walker R. J., Irving A. J. and Lorand J. P. (2001) Osmium isotopic compositions of mantle xenoliths: a global perspective. . *Geochim Cosmochim Acta* 65, 1311-1323.

Merckle R. K. W. (1992) Platinum-group minerals in the middle group of chromitites layers at Mirikana, western Bushveld complex: implication for collection mechanism and postmagmatic modification. . *Can. J. Earth Sci* 29, 209-221.

Mitchell R. H. and Keays R. R. (1981) Abundances and distribution of gold, paladium and iridium in some spinel and garnet lherzolites: implications for the nature and origin of precious metal-rich intergranular components in the upper mantle. . *Geochim Cosmochim Acta* 45, 2425-2442.

Peach C. L., Mathez E. A. and Keays R. R. (1990) Sulphide melt-silicate distribution coefficient for noble metals and other chalchophile elements as deduced from MORB : Implication for partial melting. . *Geochim Cosmochim Acta* 54, 3379-3389.

Peach C. L., Mathez E. A., Keays R. R. and Reeves S. J. (1994) Experimentally determined sulfide melt-silicate melt partition coefficients for iridium and palladium. . *Chemical Geology* 117, 361-377.

Peck D. C. and Keays R. R. (1990a) Insights into the behavior of precious metals ion primitive, S-undersaturated magmas: evidence from the Heazlewood River Complex, Tasmania. *Can. mineralogist* 28, 553-577.

Peck D. C. and Keays R. R. (1990b) Geology, geochemistry and origin of platinum-group element-chromitite occurences in the Heazlewood Rivel Complex, Tasmania. *Econ. Geol.* 85, 765-793.

Pedersen R. B. and Furnes H. (2001) Nd- and Pb-isotopic variations through the upper oceanic crust in DSDP?ODP Hole 504B, Costa Rica Rift. *Earth Planet Sci Lett* 189, 221-235.

Peucker-Ehrenbrink B., Bach W., Hart S. R., Blusztajn J. and Abbruzzese T. (2003) Rhenium-osmium isotope systematics and platinum group element concentrations in oceanic crust from DSDP/ODP Sites 504 and 417/418. *Geochem Geophys Geosyst* 4.

Rehkämper M. and Halliday A. N. (1997) Development and application of new ion-exchange techniques for the separation of the platinum group and other siderophile elements from geological samples. *Talanta* 44, 663-672.

Reisberg L. C., Zindler A., Marcantonio F., White W. M., Wyman D. and Weaver B. (1993) Os isotope systematics in ocean island basalts. *Earth Planet Sci Lett* 120, 149-167.

Righter K., Campbell A. J., Humayun M. and Hervig R. L. (2004) Partitioning of Ru, Rh, Pd, Re, Ir, and Au between Cr-bearing spinel, olivine, pyroxene and silicate melts. *Geochem Geophys Geosyst* 68(4), 867-880.

Roedder E. (1983) Geobarometry of ultramafic xenoliths from Loihi seamount, Hawaii, on the basis of CO2 inclusions in olivine. *Earth Planet Sci Lett* 66, 369-379.

Rowan L. R. and Clayton R. W. (1993) The three-dimensional structure of Kilauea Volcano, Hawaii, From travel time tomography. *J Geophys. Res.* 98, 4355-4375.

Roy-Barman M. and Allegre C. J. (1994) 187Os/188Os ratios of mid-ocean ridge basalts and abyssal peridotites. *Geochim Cosmochim Acta* 58, 5043-5054.

Roy-Barman M. and Allegre C. J. (1995) 187Os/186Os in oceanic island basalts: Tracing oceanic crust recycling in the mantle. *Earth Planet. Sci. Lett.* 129, 145-161.

Roy-Barman M., Wasserburg G. J., Papanastessiou D. A. and Chaussidon M. (1998) Osmium isotopic compositions and Os concentrations in sulfide globules from basaltic glasses. . *Earth Planet Sci Lett* 154, 331-347.

Ryan C. G., Koyanagi R. Y. and Fiske R. S. (1981) Modeling the three-dimensional structure of macroscopic magma transport systems: Applications to Kilauea Volcano, Hawaii. *J Geophys. Res.* 86, 7111-7129.

Sattari P., Brenan J. M., Horn I. and McDonough W. F. (2002) Experimental constraints on the Sulfide- and Chromite-Silicate melt: partitioning behavior of rhenium and platinum-group elements. *Econ. Geol.* 97, 385-398.

Snow J. E. and Reisberg L. C. (1995) Os isotopic systematics of the MORB mantle: results from altered abyssal peridotites. . *Earth Planet Sci Lett* 133, 411-421.

Spengler R. S. and Garcia M. O. (1988) Geochemistry of the Hawi lavas, Kohala Volcano, Hawaii. *Contrib Mineral petrol* 99, 90-104.

Stearn H. T. and Macdonald G. A. (1946) Geology and ground-water resources of the island of Hawaii. *Hawaii Div Hydrogr Bull* 9, 362.

Stockman H. W. and Hlava P. F. (1984) Platinum-group minerals in Alpine chromitites from south-western Oregon. *Econ. Geol.* 79, 491-508.

Tatsumi Y., Oguri K. and Shimoda G. (1999) The behaviour of platinum-group elements during magmatic differenciation in Hawaiian tholeiites. *Geochem Journal* 33, 237-247.

Thurber C. H. (1984) Seismic detection of the summit magma complex of Kilauea Volcano, Hawaii. *Science* 223, 165-167.

Thurber C. H. (1987) Seismic structure and tectonics of Kilauea Volcano, Hawaii. *US Geol Surv Prof Pap* 1350, 919-934.

Tredoux M., Lindsay N. M., Davies G. and McDonald I. (1995) The fractionation of platinum-group elements in magmatic systems, with the suggestion of a novel causal mechanism. *S. African J. Geol.* 98, 157-161.

Waggoner D. G. (1993) The age and alteration of central Pacific Oceanic Crust near Hawaii, site 843. *Proc. ODP, scientific Results* 136, 119-132.

Walker R. J., Hansky E. J., Vuollo J. and Lippo J. (1996) The Os isotopic composition of Proterozoic upper mantle: evidence for chondritic upper mantle from Outokumpu ophiolite, Finland. *Earth Planet Sci Lett* 141, 161-173.

Widom E. and Shirey S. B. (1996) Os isotope systematics in the Azores: implications for mantle plume sources. *Earth Planet Sci Lett* 142, 451-465.

Chapter 2

The source composition of basalts from Kohala Volcano, Hawaii

M. JAMAIS, A.W. HOFMANN

Abstract

The model of basalt genesis developed in Hofmann and Feigenson (1983) and applied to lava series from Kohala Volcano, Hawaii in Feigenson et al. (1983) is extended here using variations of more incompatible trace elements to better constrain the mantle source composition of these lavas. New trace element analyses were performed on ten Kohala basalts and first confirmed the Kea end-member signature of these lavas, with Sr/Nd and La/Th ratios overlapping the field of lavas from Mauna Kea Volcano.

According to the actual estimations of Hawaiian primary magmas, a primary composition was reassessed for lavas from the shield building stage (Pololu lavas) with 16% MgO. Updating the primary magma composition as well as partition coefficients and primitive mantle reference values did not, however, significantly change the shape of the calculated REE patterns of the source. The previous conclusions inferring the presence of residual clinopyroxene without or with small amount of residual garnet in the source of Kohala lavas are therefore confirmed by these new data. In addition, the calculated primitive mantle-normalized source patterns indicate slight and progressive decrease of concentrations from the LREE to Ba and emphasize the Hawaiian source depletion in incompatible elements.

Finally, primary compositions for the post shield lavas (Hawi lavas) and shield stage lavas (Pololu lavas), calculated for a common primitive major element composition, are well aligned in the process identification diagrams of Minster and Allègre (1978). This suggests that the source composition has undergone only minor changes during the post shield-building event of Kohala Volcano.

1. Introduction

One of the major constraints when studying the chemical composition of the earth's mantle is the extreme fractionation of the major and trace elements during petrogenetic processes. To overcome these problems, Allègre and Minster (1978) have proposed a model of basalt genesis using variations in the trace element concentrations of a cogenetic suite of lavas. Hofmann and Feigenson (1983) have further developed a simplified version of this model. The method consists of reversing petrogenetic processes such as fractional crystallization and partial melting in order to constrain initial melt compositions as well as source composition and mineralogy. This modeling has been tested on a suite of lavas covering the entire shield building and post-shield building stage of Kohala Volcano, Hawaii and has provided successful results (Feigenson et al., 1983). Indeed, the method has shown that the transition from tholeiitic to alkalic basalts in the shield building stage of volcanism can be explained by a gradual decrease in the degree of partial melting of identical source material. Furthermore, calculations of initial Rare Earth Element patterns have suggested the presence of residual clinopyroxene during formation of the Kohala magma.

The purpose of this study is to extend the application of this modeling to other incompatible elements and High-Field-Strength-Elements (HFSE) in order to better constrain the initial trace element pattern of Kohala lavas and enhance the information obtained on their source composition. We performed trace element analyses - incompatible and Rare Earth Elements - on several lava samples from the shield building stage and the post-shield building stage of Kohala Volcano and re-assessed the completed initial pattern with the same method of calculation. Parameters for the fractionation correction employed in Feigenson et al. (1983) have been re-evaluated according to the current knowledge on Hawaiian picrites and magma fractionation calculations. Our results show, however, that this updating have only small effects on the calculated source patterns and do not alter the previous conclusions about the limited role of garnet during formation of the Kohala magma. On the other hand, the new calculations on incompatible elements provide more information about the Hawaiian source composition, which appears slightly depleted in incompatible elements relative to MREE and HREE. Finally, the comparison of primary magma compositions for the Hawi and Pololu lavas suggests that the trace element compositions did not change significantly during the post-shield building stage of Kohala Volcano.

2. Samples and analytical method

New trace element analyses were performed on some of the lava samples previously studied by Feigenson et al. (1983). These samples consist of five tholeiites and one alkali basalt from the Pololu volcanics (shield building of Kohala volcano) and four alkaline lavas from the Hawi Volcanics (post-shield building). Major element concentrations and Sr and Nd-isotopes ratios have been presented by Feigenson et al. (1983) and Hofmann et al. (1987), together with the previous trace element measurements.

The new trace element measurements were performed by Laser-Ablation-ICP-MS at the Max Planck Institute for chemistry in Mainz. Following the procedure of Fedorowich et al. (1993), homogeneous samples were obtained by melting around 40 mg of rock powder to glass beads using an Iridium strip heater. The melting took place in a closed box under an argon atmosphere to suppress oxidation and to limit volatilization of elements with low boiling points Fedorowich et al. (1993); a constant temperature of 1500°C and a melting time of 10 s were imposed by a pyrometer placed above the box. USGS standards BHVO-1 and BHVO-2 were prepared in the same way and analyzed with the samples. Internal glass standard NISTSMR-612 and Hawaiian basalts MPI-ding (KL2-G, ML3B-G see Jochum et al., 2000) were also measured along the analyses and compared with reference values (taken from GEOREM: http://georem.mpch-mainz.gwdg.de/sample_query.asp).

The data obtained have been corrected relative to the NIST-612. However, systematically lower Pb concentrations were observed for the measured standards BHVO-1 and BHVO-2 when compared with reference values. These differences reveal a sensitivity problem during the preparation of samples into glass beads. The low boiling point of Pb may have caused a small loss of this element during the melting process, which was not taken into account by the NIST-612 values because of the synthetic nature of this glass standard. Consequently, Pb values of all samples and USGS standards were corrected relative to the measured Hawaiian basalts MPI-Ding, which were prepared in the same way as our samples and may record similar Pb loss. The USGS standard measurements are in good agreement with reference values (less than 5% standard deviation) except for the U value of BHVO-1 (11%). The standard deviation (σ) is generally less than 10 % for all elements. We note however larger values up to 16% for few measurements of Pb that might reflect small loss by volatilization during preparation of the samples. We note also larger standard deviation values

for U, Th and Cs measurements on few samples. We do not have clear explanation for that but will not use these data in the following.

3. Results

Analytical data of Kohala lavas are reported in Table 1, along with analyses of USGS standard basalts BHVO-1 and BHVO-2. Feigenson et al. (1983) pointed out the extremely low Cs and Rb content in some tholeiites that have been collected on the wet flank of Kohala Mountain (Waipio Valley, samples W4, W11, W22). They suggested that these elements have been affected by rainwater leaching, which however did not significantly alter the Ba, Sr and REE content of these lavas. The new data also reveal low and heterogeneous Cs and Rb concentrations in these samples and confirm the leaching feature of these elements. Consequently, Cs and Rb data were not taken into account in the modeling. The new set of data generally agrees within 10% with the trace element concentrations reported by Feigenson et al. (1983). Nonetheless, there is more scatter for the Ba, Dy and Yb contents (about 11%) obtained on sample W4 as well as for the Ba content (16%) obtained on sample W11. Data reported for the BHVO-1 standard in Feigenson et al. (1983) are in good agreement with our measurements (less than 6%) and the scatter observed on duplicate measurements are difficult to explain. However, these discrepancies have only minor effects on the model developed here as similar results were obtained, when considering the whole set of Kohala samples, compared to the previous study.

4. Trace elements signature of Kohala lavas

The extension of trace element data to more incompatible elements allows a better characterization of Kohala lavas with regards to the main end-member of the Hawaiian plume. The Hawaiian volcanoes are mainly separated into two trends, the Loa-trend and Kea-trend volcanoes, according to their isotopic signature. On this criterion, the Sr and Nd isotopic signatures of Kohala lavas indicate that this volcano belongs to the Kea-trend volcanoes (Feigenson et al., 1983; Hofmann et al., 1987).

Table 1: Trace element analyses of Kohala lavas and USGS standards (in ppm)

Samples	W4	W22	W11	KH16	MG3	H1	KH5	H3	KH13	KH19	BHVO-2	BHVO-2 (ref.)	BHVO-1	BHVO-1 (ref.)
Rb	4.53	0.305	0.414	9.28	10.8	22.5	24.1	30.41	20.9	64.0	9.25	9.40	9.56	9.40
Sr	310	253	303	529	465	637	1659	1687	730	1238	397	397	409	400
Y	27.3	30.6	29.6	28.1	34.8	42.2	52.5	52.9	35.6	44.2	25.0	26.4	24.4	26.4
Zr	149	166	141	209	233	375	295	375	320	571	172	175	166	174
Nb	10.1	12.7	9.49	22.1	23.5	46.7	49.3	59.3	40.1	90.0	18.2	17.7	18.4	18.4
Cs	0.052	0.042	-	0.066	0.134	0.089	0.295	0.188	0.222	0.340	0.091	0.112	0.105	0.102
Ba	77.0	63.2	61.2	201	191	399	504	645	349	917	132	128	134	129
La	10.1	12.2	10.4	18.7	23.3	38.6	50.7	58.9	37.0	71.5	15.0	14.8	15.5	15.2
Ce	24.8	28.9	24.6	44.5	49.9	80.0	116	135	80.6	147	36.4	37.0	36.8	37.0
Pr	3.76	4.51	3.96	6.05	7.50	11.7	17.0	18.1	10.4	17.8	5.05	5.30	5.30	5.30
Nd	18.9	22.5	20.2	28.4	34.9	53.0	81.4	83.4	46.3	72.1	24.0	24.2	25.0	24.3
Sm	5.46	6.27	5.75	6.86	8.59	12.1	18.5	18.0	9.81	13.6	5.92	6.10	6.21	6.40
Eu	1.89	2.18	2.05	2.25	2.75	3.80	5.68	5.55	2.74	3.99	2.00	2.09	2.07	2.14
Gd	6.04	6.76	6.40	6.72	8.60	11.3	16.93	16.1	8.82	11.0	6.05	6.10	6.13	6.30
Tb	0.931	1.03	0.967	0.986	1.27	1.60	2.19	2.09	1.21	1.51	0.879	0.89	0.890	0.89
Dy	5.81	6.32	5.91	5.82	7.52	9.11	12.0	11.4	6.94	8.59	5.26	5.50	5.28	5.40
Ho	1.09	1.19	1.12	1.06	1.38	1.62	2.07	1.96	1.23	1.579	0.947	0.92	0.965	0.98
Er	2.83	3.16	2.96	2.76	3.57	4.13	5.09	4.85	3.25	4.35	2.48	2.49	2.49	2.64
Tm	0.384	0.412	0.388	0.361	0.460	0.530	0.616	0.594	0.416	0.599	0.322	0.32	0.321	0.308
Yb	2.46	2.61	2.46	2.23	2.91	3.26	3.62	3.56	2.53	3.99	2.01	2.08	2.02	1.96
Lu	0.343	0.364	0.341	0.308	0.398	0.442	0.491	0.481	0.358	0.590	0.272	0.282	0.277	0.271
Hf	3.93	4.36	3.66	5.01	5.89	8.79	7.26	8.26	6.71	12.6	4.28	4.29	4.29	4.40
Ta	0.670	0.851	0.631	1.38	1.51	2.90	3.00	3.45	2.30	5.27	1.16	1.17	1.21	1.19
Pb	0.837	1.33	1.15	1.94	1.91	2.24	2.71	2.97	1.75	6.08	1.49	1.70	2.44	2.20
Th	0.709	0.785	0.557	1.29	1.52	2.94	2.70	3.62	2.66	6.75	1.21	1.13	1.22	1.25
U	0.245	0.226	0.177	0.409	0.531	0.883	0.907	1.124	0.801	2.59	0.399	0.390	0.474	0.409

(ref.) = reference values from Willbold et al. (2003)

However, other geochemical features also divide these two Hawaiian end-members such as trace element ratios. For example, higher Sr/Nd ratios are generally observed in lavas from Loa-trend volcanoes and have been ascribed to the presence of recycled oceanic gabbros by Hofmann and Jochum (1996) and Sobolev et al. (2000). It appears that this "gabbroic signature" is absent from Kea-trend volcanoes and represents consequently a good indicator to constrain the nature of the different volcanoes. Higher La/Th ratios are also generally observed in lavas from Loa-trend volcanoes. These lavas are less enriched in highly incompatible elements relative to more compatible elements, indicating that they were produced by higher degrees of partial melting than the Mauna Kea lavas (Hofmann and Jochum, 1996). In addition, Hofmann and Jochum (1996) indicated systematically lower Ce/Pb ratios in lavas from Mauna Loa Volcano compared to lavas from Mauna Kea volcano. Consequently, diagrams showing these trace element ratios would emphasize the distinction between the two lava types. Fig. 1 shows La/Th and Pb/Ce ratios plotted versus Sr/Nd ratios for lavas from Mauna Loa and Mauna Kea volcanoes reported in literature. Data obtained on lavas from the shield building stage of Kohala Volcano are also plotted for comparison. It appears from these diagrams that trace element signatures of Kohala lavas overlap the field of Mauna Kea lavas and are clearly distinct from the field of Mauna Loa basalts. The trace element data are thus in agreement with the isotopic signatures of Kohala lavas and confirm that Kohala Volcano possesses geochemical features belonging to the Kea trend of the Hawaiian Volcanoes. In particular, they do not show the geochemical signature of recycled gabbro that appears to characterize Loa-trend volcanoes.

5. The source composition of Pololu lavas

The use of the model proposed by Hofmann and Feigenson (1983) supposes that all the lavas studied are cogenetic. However, isotopic data on Kohala lavas have revealed slight changes in the source compositions during the post shield building stage of the volcanic activity (Hofmann et al., 1987; Lanphere and Frey, 1987). The model was therefore applied to the Pololu lavas alone, and we studied the nature of the Hawi lavas separately.

The first step of the trace element modeling proposed by Hofmann and Feigenson (1983) consists in correcting trace element concentrations from the effects of fractional

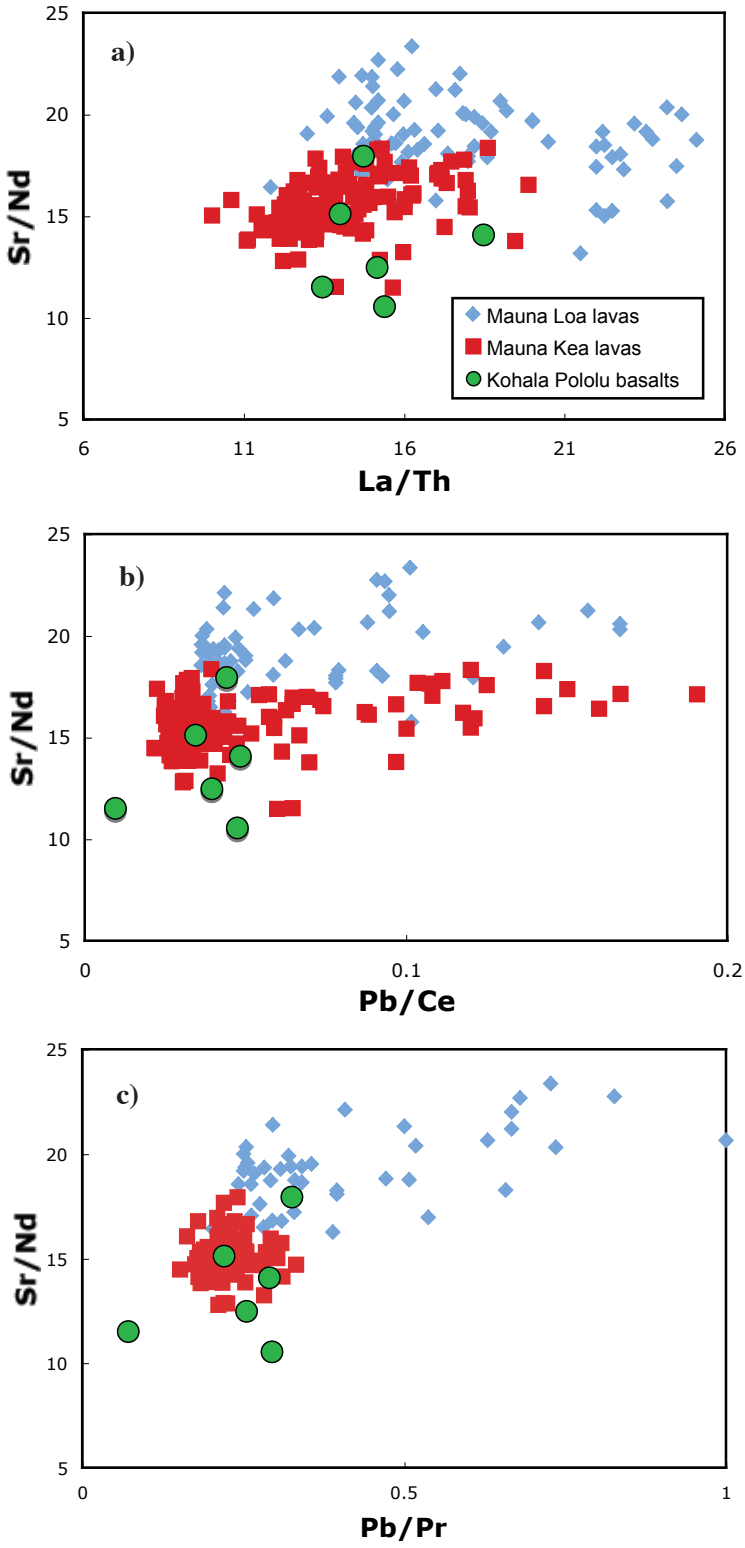

***Fig. 1**: Trace element ratios for lavas from Mauna Kea, Mauna Loa and the Pololu volcanics of Kohala Volcano. **a)** La/Th versus Sr/Nd diagram, **b)** Pb/Ce versus Sr/Nd diagram, and **c)** Pb/Pr versus Sr/Nd diagram highlighting the distinctions between Mauna Loa and Mauna Kea lavas. The Kohala lavas clearly overlap the field of the Mauna Kea lavas and confirm the "Mauna Kea" type signature of this volcano.*

crystallization. To use this correction, we need to estimate the major element composition of a common primary magma and calculate the amount of fractionating phases required to reproduce the major element composition of each lava sample. The previous estimation of a primary magma composition for Kohala lavas (12% MgO, see Feigenson et al., 1983) must be re-evaluated according to the actual knowledge on Hawaiian picrites. For example, Norman and Garcia (1999) have shown that olivine phenocrysts in Hawaiian picrites have forsterite contents up to 90 and suggested a parental Hawaiian melt with about 15 - 16 % MgO.

5.1 Re-assessment of a primary magma composition for the Pololu volcanics

The major element variations in Kohala tholeiites with relatively primitive compositions are dominantly controlled by olivine fractionation (Feigenson et al., 1983). Consequently, a primary magma composition for Kohala tholeiites has been estimated using the model of reverse olivine crystallization proposed by Danyushevsky et al. (2000). This model allows progressive addition of small amounts of olivine to a melt composition, with re-equilibration of the olivine composition with the new melt at each step. For this, we considered that olivine in equilibrium with the primary melt composition has Fo = 90, as proposed in Bennett et al., 2000, and applied a step calculation with 0.1% increment on 22 Kohala tholeiite compositions (reported in Feigenson et al., 1983), Waipio samples with MgO content > 7%). At each step (adding of 0.1% olivine), compositions of the new melt and olivine in equilibrium were re-evaluated (see Danyushevsky et al., 2000). To calculate olivine compositions, we considered the following approximation:

- The distribution coefficient relating the partitioning of iron and magnesium between olivine and silicate melt $K_D = (X_{Fe}^{Ol} / X_{Fe}^{L}) / (X_{Mg}^{Ol}/X_{Mg}^{L})$ is equal to 0.3 as determined in Roeder and Emslie (1970); X_i^A is the cationic fraction of element i in the phase A, Fe = Fe^{2+}, mg = mg^{2+}, Ol = olivine and L = liquid.

- $X_{Fe}^{Ol} + X_{Mg}^{Ol} = 2$ and $X_{Si}^{Ol} = 1$

Then, the previous equations are reduced to:

$$X_{Mg}^{Ol} = 2 / (1+ 0.3*X_{Fe}^{L} / X_{Mg}^{L}) \text{ and } X_{Fe}^{Ol} = 2 - X_{Mg}^{Ol}$$

The average composition of primary melt obtained through this calculation has 16 % MgO and is reported in Table 2.

Table 2: Major element compositions of primary magma and fractionating phases.

	Primary melt	Cpx [a]	Ilm [a]
SiO_2	48.3	47.31	2.39
TiO_2	1.79	0.97	22.3
Al_2O_3	11.7	10.99	2.04
FeO	11.7	8.08	68.4
MnO	0.170	0.16	1.53
MgO	16.1	14.86	2.02
CaO	8.37	14.23	0.192
Na_2O	1.63	1.67	0
K_2O	0.084	0	0
P_2O_5	0.182	0	0
Total	100	98.27	98.87

a: compositions used for fractionation correction calculations: Ilmenite is average composition phenocrysts for Kohala lavas reported in Feigenson et al. (1983); clinopyroxene is from Beeson and Jackson (1970) 68 SAL-7.

5.2 Magma fractionation calculation

In order to deduce the amount of olivine that has been removed to produce each tholeiite composition, olivine fractionation was further reproduced from this primary melt composition, using the inverse process of calculation and the same parameters as in the previous part. Melt compositions were calculated after Danyushevsky et al. (2000) as:

$$(\text{Wt\% in melt})_{old} = (\text{wt\% in melt})_{new} * (1\text{-}X) + (\text{wt\% in Olivine}) * X$$

with (wt% in olivine) now in equilibrium with $(\text{wt\% in melt})_{new}$. From this step calculation, degrees of fractionation were deduced for each tholeiitic composition having more than 7% MgO. The association of clinopyroxene and olivine fractionation is required to explain the

major element variations in Pololu lavas with more evolved compositions (Feigenson et al., 1983). Using the same least square regression method of Wright and Doherty (1970) as in the previous study, we re-calculated the different proportions of olivine and clinopyroxene removed from the re-assessed primary magma composition. For this calculation, we used olivine compositions in equilibrium with each lavas samples and the high-pressure clinopyroxene composition from Beeson and Jackson (1970) (Table 2). The amount of fractionating phases obtained for each Pololu lava sample are presented in Table 3.

5.3 Trace element concentrations in primary magmas

Trace element concentrations have been thus corrected for the effect of fractional crystallization using the Rayleigh fractionation law $c_1/c_0 = F^{(D-1)}$, where c_1 is the trace element concentration in the measured lava, c_0 is the pre-fractionation concentration, F is the amount of liquid remaining after fractionation and D is the mineral-melt partition coefficient (Table 5). Trace element concentrations of each primary melt obtained are reported in Table 3. The efficiency of this correction can be seen in Fig. 2, presenting the complete primitive-mantle-normalized patterns for Pololu basalts before and after fractionation correction. The corrected patterns appear more clustered and the scatter of concentrations is particularly reduced for the most incompatible elements and the HREEs.

The shape of the corrected REE patterns presented here is very similar to the one reported in Feigenson et al. (1983). As emphasized by the previous authors, olivine crystallization concentrates mostly all trace elements in the liquid and do not generate fractionation of the concentrations. Nonetheless, the removal of clinopyroxene fractionates the trace elements and we obtained sensibly lower H-REEs concentrations for the most evolved compositions. On the other hand, the trace element contents of Kohala lavas have been previously normalized to chondritic values that are two times lower than the actual primitive mantle values taken as reference in this study (McDonough and Sun, 1995). As a consequence, the deduced corrected trace element concentrations are also around two times lower than the previous estimation.

Table 3: Fractionation corrected trace elements abundances of Kohala lavas (in ppm), amount of fractionating phases and partition coefficients used for the correction.

Samples	W4	W22	W11	MG3	KH16	H1	KH5	H3	KH13	KH19	$D_{ol/melt}$ [a]	$D_{cpx/melt}$ [a]	$D_{ilm/melt}$ [a]
Rb	3.61	0.238	0.314	6.03	6.59	12.14	10.43	11.6	6.60	16.9	0.0003	0.0004	0
Sr	247	197	230	267	378	357	756	686	253	382	0.00004	0.18	0
Y	21.7	24.0	22.5	21.2	20.4	25.6	26.6	24.7	14.9	18.7	0.0099	0.54	0
Zr	118	130	107	133	149	208	133	150	109	175	0.0033	0.134	0
Nb	8.02	9.94	7.21	13.2	15.7	25.4	21.5	22.8	12.9	24.4	0.004	0.031	0
Cs	0.042	0.032	0	0.075	0.047	0.048	0.128	0.071	0.070	0.090	0.0015	0.0039	0
Ba	61.4	49.4	46.5	107	143	215	218	245	110	243	0.000005	0.0006	0
La	8.03	9.52	7.88	13.1	13.3	21.1	22.2	22.8	12.0	19.8	0.0005	0.0512	0
Ce	19.7	22.6	18.7	28.4	31.7	44.3	51.8	53.7	26.9	42.8	0.0003	0.112	0
Pr	2.99	3.53	3.01	4.32	4.33	6.56	7.73	7.35	3.61	5.49	0.0005	0.18	0
Nd	15.0	17.6	15.4	20.19	20.3	29.9	37.3	34.2	16.2	22.7	0.001	0.2	0
Sm	4.35	4.90	4.37	5.12	4.95	7.12	8.98	7.98	3.81	5.07	0.0013	0.4	0
Eu	1.50	1.70	1.55	1.65	1.63	2.28	2.83	2.53	1.12	1.60	0.0011	0.48	0
Gd	4.81	5.29	4.87	5.21	4.86	6.82	8.48	7.38	3.60	4.49	0.0011	0.5	0
Tb	0.742	0.809	0.735	0.771	0.714	0.968	1.10	0.966	0.499	0.626	0.0015	0.52	0
Dy	4.63	4.94	4.50	4.63	4.23	5.60	6.19	5.46	2.99	3.82	0.0027	0.6	0
Ho	0.867	0.931	0.854	0.850	0.771	1.00	1.08	0.942	0.538	0.715	0.0122	0.62	0
Er	2.26	2.47	2.25	2.21	2.01	2.56	2.65	2.34	1.42	1.98	0.0132	0.627	0
Tm	0.307	0.323	0.296	0.285	0.263	0.329	0.323	0.289	0.184	0.275	0.03	0.64	0
Yb	1.96	2.04	1.87	1.82	1.63	2.05	1.93	1.77	1.15	1.92	0.0305	0.691	0
Lu	0.274	0.285	0.260	0.25	0.225	0.279	0.264	0.241	0.165	0.289	0.0432	0.709	0
Hf	3.13	3.41	2.78	3.45	3.598	5.06	3.42	3.51	2.48	4.49	0.001	0.292	0
Ta	0.534	0.665	0.479	0.851	0.983	1.57	1.31	1.32	0.736	1.43	0.0005	0.031	0
Pb	0.667	1.04	0.875	1.07	1.38	1.21	1.18	1.14	0.556	1.62	0.003	0.01	0
Th	0.565	0.610	0.423	0.856	0.918	1.60	1.18	1.39	0.848	1.82	0.00005	0.023	0
U	0.195	0.177	0.134	0.298	0.291	0.479	0.395	0.431	0.255	0.700	0.00047	0.023	0
Ol [b]	0.203	0.218	0.24	0.17	0.18	0.11	0.218	0.23	0.215	0,00			
CPX				0.27	0.11	0.35	0.35	0.39	0.45	0.65			
Ilm									0.02	0.08			

a: Partition coefficients between mineral and silicate melt under 1 GPa based on Salters et al. (1999) and Hack et al. (1994). Ol = olivine, Cpx = clinopyroxene, Ilm = ilmenite
b: Ol, Cpx , and Ilm are amounts of those minerals added to each sample to obtain the major element content of the primary magma.

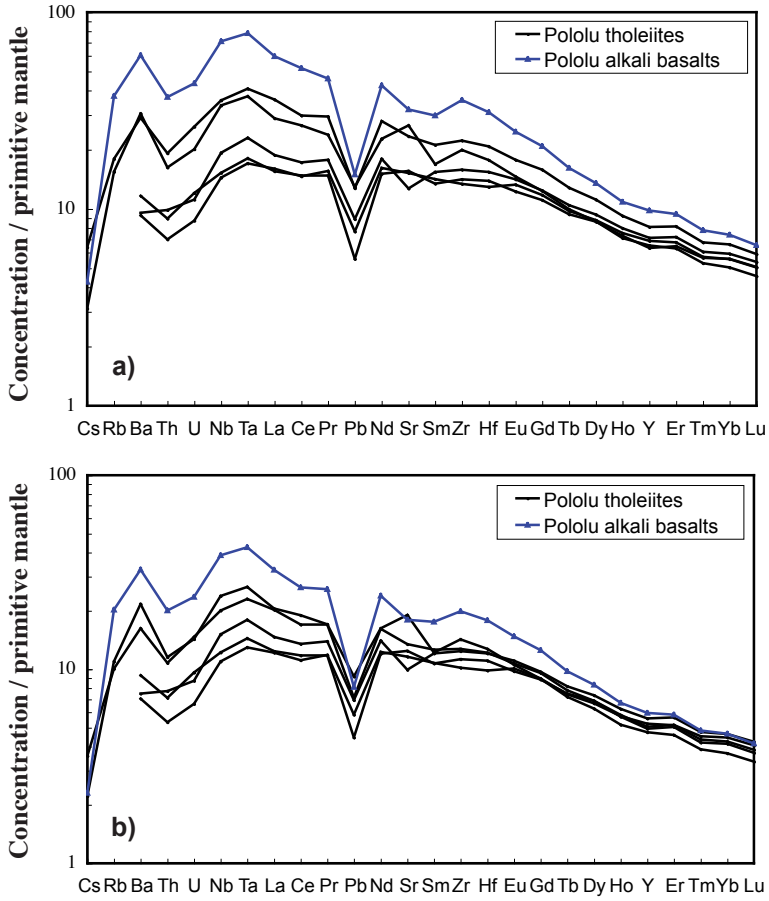

Fig. 2: a) *Trace element patterns for the Pololu basalts normalized to primitive mantle values (McDonough et al., 1995).* ***b)*** *Fractionation-corrected trace element patterns for the Pololu basalts normalized to primitive mantle values (McDonough et al., 1995). The correction for fractional crystallization reduces the scatter of concentrations.*

5.4 Initial concentrations and primary melt norm

The calculated trace element concentrations of primary melts were plotted on the process identification diagrams of Minster and Allègre (1978) (Fig. 3) and the deduced slope and intercepts are presented in Fig. 4. These diagrams represent another manner to verify the validity of the previous calculations because they emphasized lines for batch partial melting (Hofmann and Feigenson, 1983). The calculations are based on the equation for batch equilibrium partial melting:

$$C^i = C^i_o / D^i_o + F\,(1-P^i) \qquad \text{(Shaw, 1970)}$$

where C^i is the concentration of element i in the primary melt, C^i_o is the concentration of

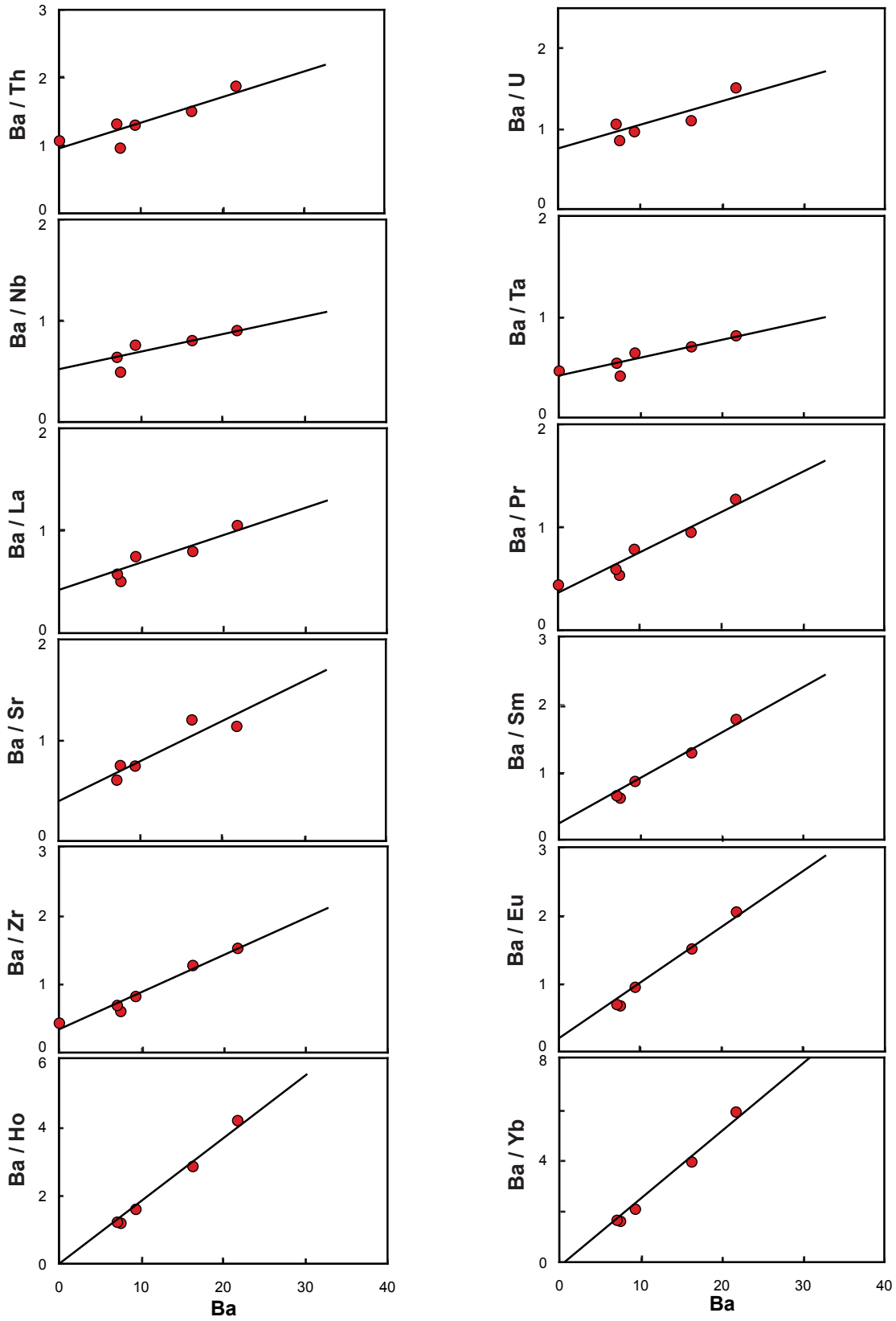

Fig. 3: *Process identification diagrams showing Ba content versus divers trace element ratios for Pololu lavas. The trace elements abundances used in these diagrams are corrected for fractionation and normalized to primitive mantle values. The correlations between trace element ratios and Ba are relatively good, particularly when MREE and HREE are involved in the ratios.*

element i in the source, D^i_o is the bulk partition coefficient for i in the source such as $D^i_o = F_\alpha D^i_\alpha + F_\beta D^i_\beta + \ldots$ with D^i_α the partition coefficient between mineral α and melt for element i and Fα the fraction of mineral a in the source, F is the fraction of residual liquid and Pi is the bulk partition coefficient for i in the melt such as $P^i = p_\alpha D^i_\alpha + p_\beta D^i_\beta + \ldots$with pα the fraction of mineral α in the melt. For a highly incompatible element such as Ba, $D^{Ba} = P^{Ba} = 0$ and then:

$$C^{Ba} / C^i = S^i C^{Ba}_o + I^i$$

where $S^i = D^i_o / C^i_o$ and $I^i = C^{Ba}_o / C^i_o (1 - P^i)$ are the slope and the intercept of the previous equation, plotted in the process identification diagrams.

Thus, if the data are sufficiently well corrected for fractional crystallization, they should form a single line, which conforms to a simple batch partial melting (see Feigenson et al., 1983). Good correlations are obtained between trace element ratios and Ba for all elements and justify consequently the previous magma fractionation calculations (Fig. 3). In contrast with the observations of Feigenson et al. (1983), errors on the intercepts of the process identification lines become larger towards the most incompatible elements and are very small on the Heavy

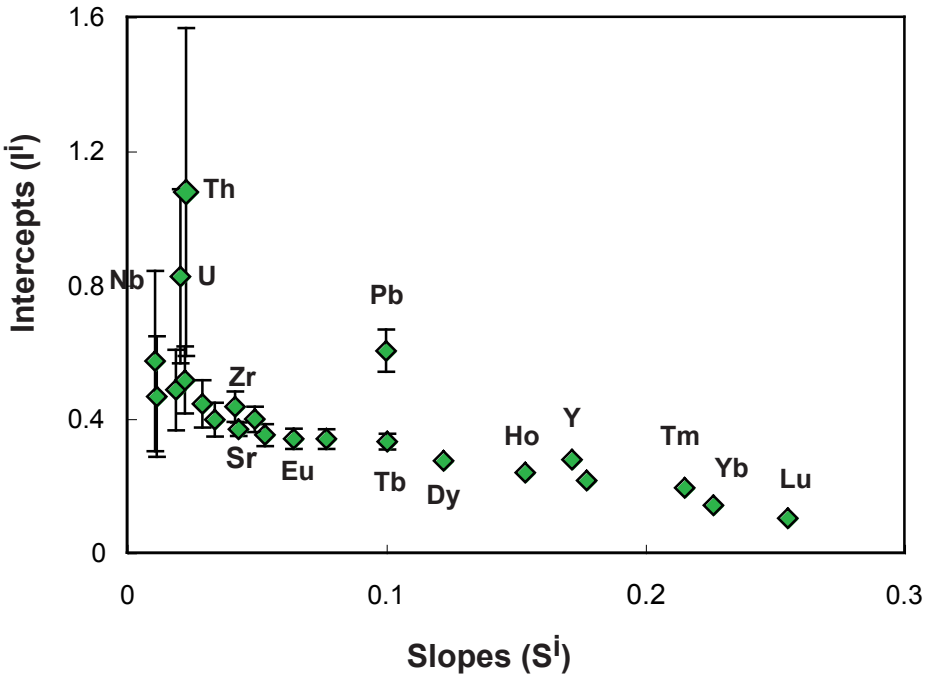

Fig. 4: *Slopes and intercepts of the process identification lines shown in Fig. 3. The error bars are given as one standard deviation of the intercept of the regression lines. The errors increase significantly toward the most incompatible elements and are very low on the HREE. The errors are smaller than the diameter of the dots, where no error bars are shown.*

REE. Reduction of the errors on the HREE is most likely due to stronger correction for fractionation applied on these elements. During magma differentiation, the removal of clinopyroxene fractionates the HREE from the LREE and highly incompatible elements in the melt, as the HREE are slightly more compatible than the other elements in this phase. Thus, the larger amount of fractionated phases estimated in this study allows a better correction of the HREE relative to incompatible elements compared to the previous work. On the other hand, the large errors obtained on the highly incompatible elements might be a consequence of minor source heterogeneities, which tend to be most pronounced for the most incompatible elements. Therefore, the corrected trace element patterns (Fig. 2) show more scatter on the highly incompatible element concentrations than on the REE contents.

The previous authors used the term "primary melt norm" for the proportion of mineral phases from the source that have formed the primary Kohala melts. In order to constrain as previously the presence or absence of garnet in the source of the Hawaiian lavas, two different mineralogies have been tested for the source, a garnet lherzolite and a spinel lherzolite. We re-calculated these primary melt norm following the same procedure than in Feigenson et al. (1983) and the same composition from xenolith 68 SAL-7, but using the primary melt composition presented in Table 2. The solutions of our calculations for both cases, garnet lherzolite and spinel lherzolite source compositions, are slightly different than in the previous study:

clinopyroxene = 0.449	clinopyroxene = 0.475
orthopyroxene = 0.551	orthopyroxene = 0.647
garnet = 0.118	spinel = 0.028
olivine = - 0.119	olivine = - 0.150
melt = 1.000	melt = 1.000

When considering either a garnet lherzolite or a spinel lherzolite source, our calculations yielded an amount of orthopyroxene and clinopyroxene entering the melt around 6% lower and an amount of olivine produced during partial melting two times lower than the previous estimations reported in Feigenson et al. (1983). The difference in olivine is at least in part the result of the assumption of a more magnesian primary melt composition. On the other hand,

the calculated amounts of garnet in the case of a garnet lherzolite source, and of spinel in the case of a garnet-free source, are quite similar to the previous estimations.

5.5 Source composition and mineralogy

The bulk partition coefficients of the melt P^i presented in Table 4 have been calculated from both type of primary melt norm, using the equation 9 of Hofmann and Feigenson (1983):

$$P^i = p_\alpha D^i_\alpha + p_\beta D^i_\beta + \ldots$$

where p_α is the fraction of mineral α entering in the melt and D^i_α is the partition coefficient between mineral α and melt for element i. The partition coefficients used in our calculations are reported in Table 4. Thereafter, from these bulk partition coefficients P^i, the slopes and intercepts values of Fig. 4, and equations reported above (paragraph 7.1 or equation (7)' and (10) of Hofmann and Feigenson (1983), we calculated the C_o^i/C_o^{Ba} and D_o^i/C_o^{Ba} shown in Fig. 5 and Fig. 6. As developed in Hofmann and Feigenson (1983), these values represent the initial concentrations and initial bulk distribution coefficients of the trace elements, relative to those of Ba. These initial patterns are here normalized to primitive mantle values and are deduced with the assumption of an initial Ba content equal to 1. Both models, supposing either garnet lherzolite or spinel lherzolite source composition, reproduce the same pattern for the majority of the trace elements and present only discrepancies for the most compatible elements (from Gd to Lu).

Fig. 6 shows the initial REE patterns estimated for the two models and normalized to primitive mantle values (Mcdonough and Sun, 1995). The bulk partition coefficient of the melt P^i and the bulk partition coefficient of the source relative to the initial Ba content D_o^i / C_o^{Ba} are also reported in these diagrams. As obtained in the previous study, the use of garnet lherzolite as source mineralogy produces a relatively flat source pattern on most of the REE (from La to Tm) and an apparently anomalous depletion on the most HREE (from Tm to Lu) with even negative concentrations on Lu (Fig. 6a). On the other hand, the initial REE pattern calculated for a spinel lherzolite source composition is also relatively flat on the LREE and MREE (from La to Tb) but increases progressively on the HREE (from Dy to Lu) (Fig. 6b).

Table 4: Bulk partition coefficients of the melt and distribution coefficients between mineral phases and melt during partial melting.

	Dol/melt [a]	D opx/melt [a]	D Cpx/melt [a]	D gt/melt [a]	D Sp/melt	Pi (Gt-Lh) [b]	Pi (Sp-Lh) [b]
Rb	0.0003	0.0002	0.0004	0.0002	0	0.0003	0.0003
Sr	0.00004	0.0007	0.091	0.0007	0	0.0414	0.0437
Y	0.018	0.05	0.14	2.5	0	0.3844	0.0962
Zr	0.0005	0.014	0.09	0.27	0	0.0800	0.0518
Nb	0.0005	0.004	0.01	0.015	0	0.0084	0.0073
Cs	0.0015	0.0001	0.0025	0.0001	0	0.0010	0.0010
Ba	0.000005	0.000006	0.0004	0.00007	0	0.0002	0.0002
La	0.0005	0.004	0.015	0.0007	0	0.0090	0.0096
Ce	0.0005	0.004	0.03	0.017	0	0.0176	0.0215
Pr	0.0005	0.008	0.07	0.03	0	0.0394	0.0384
Nd	0.00042	0.012	0.0884	0.064	0	0.0539	0.0497
Sm	0.0011	0.02	0.15	0.3	0	0.1138	0.0888
Eu	0.0011	0.06	0.16	0.8	0	0.19958	0.1147
Gd	0.0011	0.065	0.16	1.2	0	0.2497	0.1180
Tb	0.00324	0.065	0.165	1.4	0	0.2754	0.1200
Dy	0.0027	0.065	0.17	2	0	0.3488	0.12247
Ho	0.008	0.065	0.175	2.7	0	0.4333	0.1241
Er	0.013	0.065	0.18	3	0	0.4705	0.1257
Tm	0.02	0.07	0.23	3.5	0	0.5541	0.1516
Yb	0.02	0.08	0.25	5.5	0	0.8054	0.1676
Lu	0.02	0.12	0.276	7	0	1.0168	0.2059
Hf	0.0022	0.024	0.14	0.4	0	0.1233	0.0818
Ta	0.0005	0.004	0.01	0.015	0	0.0084	0.0073
Pb	0.003	0.009	0.009	0.005	0	0.0092	0.0097
Th	0.00005	0.002	0.006	0.009	0	0.0049	0.0040
U	0.00038	0.002	0.0113	0.028	0	0.0095	0.0066

a: distribution coefficients between mineral phases and silicate melt under 3 Gpa, based on Salters et al. (2002) and (2004).

b : Bulk partition coefficients of the melt calculated for the Garnet lherzolite (Gt-Lh) and the Spinel lherzolite (Sp-Lh) primary melt norm.

The anomalous depletion of Yb and Lu in the source pattern calculated for a garnet lherzolite mineralogy is accompanied by strong depletion of the source partition coefficient on the same elements, while the bulk partitioning in the melt is high and near to 1 for these elements. We should emphasize here that, although the process identification diagrams have very low errors for the HREE, the intercepts are very close to zero. This causes considerable error magnification in the final calculated source pattern. Therefore, the anomalous behavior of Yb and especially Lu obtained in the garnet lherzolite model may well be caused by this large error magnification. The discrepancies between melt and source partitioning reflect also the high sensitivity of Yb and Lu to the presence of garnet in the source and may show the limited role of garnet during Kohala magmas genesis inferred by the model. As explained in Feigenson et al. (1983), the strongest constraint of this model is that negative concentrations in the source are not possible. Therefore, the calculation $C_o^i/C_o^{Ba} = (1-P^i)/I^i$ impose $P^i < 1$ as the intercepts calculated for all trace elements are positive (Fig. 4). Now the diagram of Fig. 6a shows that the values of P^{Yb} and P^{Lu} are near or equal to 1, which is mostly due to the high compatibility of these elements in garnet. For example, if we consider the $D^{Lu}_{garnet/melt} = 7$ proposed by Salters and Stracke (2004) for a peridotite under 3 GPa (Table 4), the fraction of garnet entering the melt must be less than 0.14 (and even less as clinopyroxene partition also this element) to obtain a positive initial Lu content. Consequently, the garnet fraction of 0.12 estimated for the primary melt norm appears slightly too high to produce the observed trace element compositions of Kohala lavas, which explain the anomalous negative Lu content in the estimated initial pattern. A reduction of the garnet fraction entering the melt to 0,1 would already produce initial Yb and Lu content higher than 1. The values of partition coefficient between garnet and silicate melt for Yb and Lu may also be too high and may generate this strong depletion of HREE in our calculations. Nonetheless, the depletion of Heavy REE produced by the garnet lherzolite model disagrees with a strong presence of garnet in the source mineralogy. Therefore, these new calculations on the Rare Earth Elements lead to the same conclusion as in the previous study, attesting the presence of residual clinopyroxene during the genesis of the Kohala magma, with or without small amounts of residual garnet (Feigenson et al., 1983).

The general shape of the patterns is not uniform as would be expected if the source of the Hawaiian lava were only primitive mantle, but is characterized by a positive slope on the HFSE and Light REE (Fig. 5). Highly incompatible elements (Rb, Th, U) have initial contents

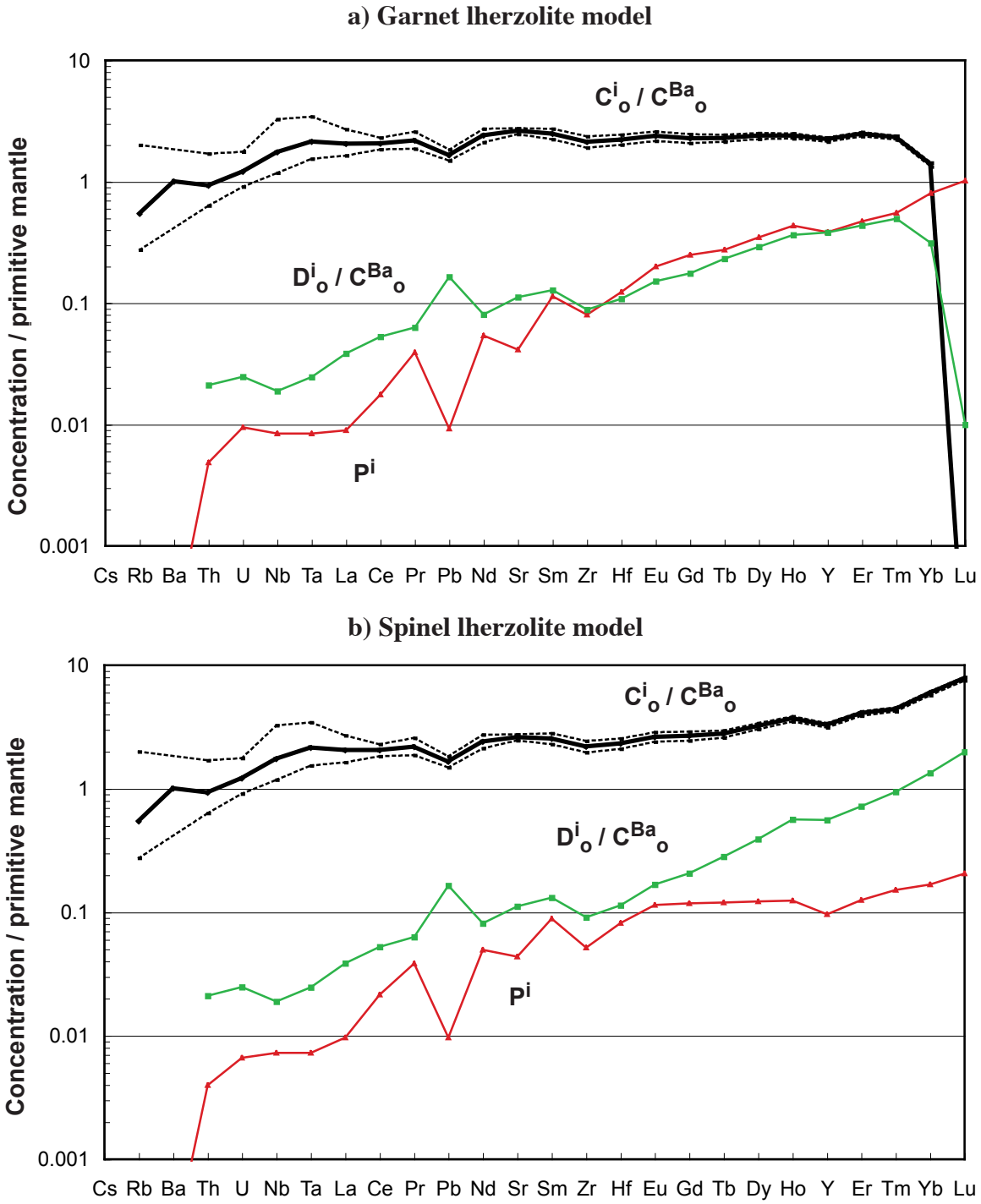

Fig. 5: *Bulk partition coefficients P^i of the melt, relative source concentrations $C^i_o/C^{Ba}_o = (1-P^i) / I^i$, and relative bulk partition coefficients of the source assemblage $D^i_o/C^{Ba}_o = S^i (1- P^i) / I^i$ for fractionation-corrected Pololu lavas and calculated for* ***a)*** *a garnet lherzolite source mineralogy and for* ***b)*** *a spinel lherzolite source mineralogy. S = slope and I = intercepts, calculated in Fig. 3 and 4. Maximum and minimum values are given for the calculated relative source concentrations and indicate growing uncertainties on the highly incompatible element that may reflect variations in the degree of partial melting during the genesis of Pololu magmas. In both model, the initial concentrations increase progressively from Ba to the HREE and suggest a source slightly depleted in incompatible elements relative to less incompatible elements for the Hawaiian lavas.*

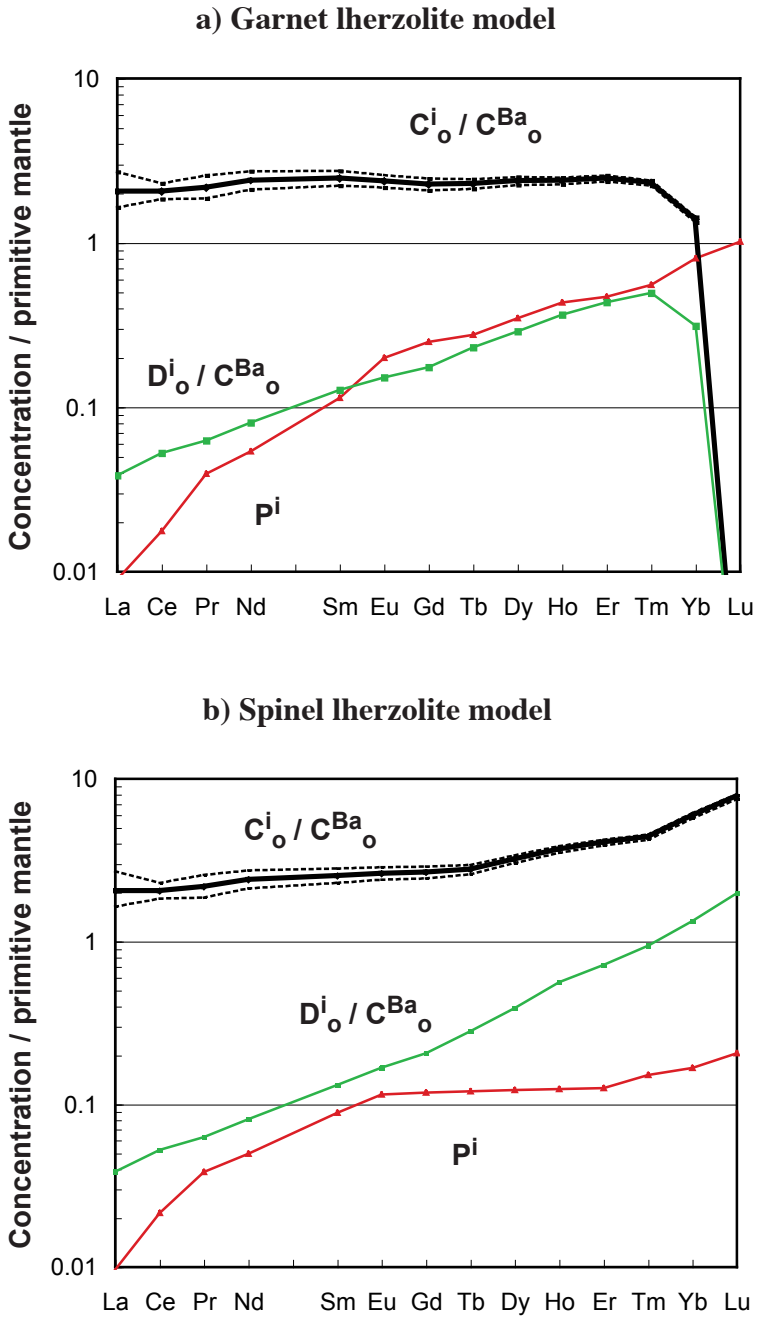

Fig. 6: *Bulk partition coefficients P^i of the melt, relative source concentrations $C^i_o / C^{Ba}_o = (1\text{-}P^i) / I^i$, and relative bulk partition coefficients of the source assemblage $D^i_o / C^{Ba}_o = S^i (1\text{-} P^i) / I^i$ for fractionation-corrected Pololu lavas and calculated for* ***a)*** *a garnet lherzolite source mineralogy and for* ***b)*** *a spinel lherzolite source mineralogy. S = slope and I = intercept, calculated in Fig. 3 and 4. Anomalously low initial Yb and Lu contents are obtained when considering a garnet lherzolite source, which may be in favor of a garnet-free (or low garnet) source for the Hawaiian lavas.*

close to that of Ba, then the pattern describe a shift towards higher abundances such as Nb/Ba ~ 2. The values grow further slightly from Nb to Sm and stabilize or slightly increase on the MREE and HREE.

Both patterns are significantly depleted in Pb relative to Ce (or Pr and Nd), slightly enriched in Sr relative to Nd and Sm and slightly depleted in Zr and Hf relative to Sm and Eu. As demonstrated in Hofmann et al. (1986), the Pb depletion relative to Pr and Nd is a general feature of all oceanic basalts and their sources and is probably due to the presence of residual sulfide. This depletion is, however, much larger for Loa-trend volcanoes than for Kea-trend volcanoes such as Kohala (see Fig. 1). The presence of such phase, having strong control on Pb during partial melting, would then explains the discrepancy observed between bulk partition coefficients of the melt and of the source for Pb (Fig. 5), as sulfide is not taken into account by our calculations. On the other hand, the slight Sr enrichment relative to Nd and Sm is a feature of the Hawaiian lavas and manifests the presence of recycled oceanic crust in the source of the Hawaiian plume via ghost plagioclase signatures (Sobolev et al., 2000). Finally, the slight depletion of Zr and Hf relative to Sm and Eu may reflect an important proportion of clinopyroxene in the source mineralogy because these elements are more incompatible than Sm in this mineral phase. This is also visible when looking at the bulk partition coefficient of the melt and the source for Zr and Hf, which are clearly lower than those of Sm.

6. Constraints on the nature of the Hawi lavas

A primary melt composition in major elements is rather difficult to estimate for the Hawi lavas because of the highly differentiated nature of these rocks and the complexity of their fractionating phases. In contrast, it is possible to verify any systematic change in the trace element compositions of the source during the post shield-building event using the process identification diagrams. Indeed, if the Hawi and Pololu lavas are derived from different degrees of partial melting of similar source composition, the primary abundances obtained from these two types of lava should form a single line in the process identification diagrams. Therefore, in order to verify any divergence in the trace element signature of the two lava groups, we corrected the trace element compositions of the Hawi lavas using the same primary magma determined previously (Table 2). Proportions of fractionating phases

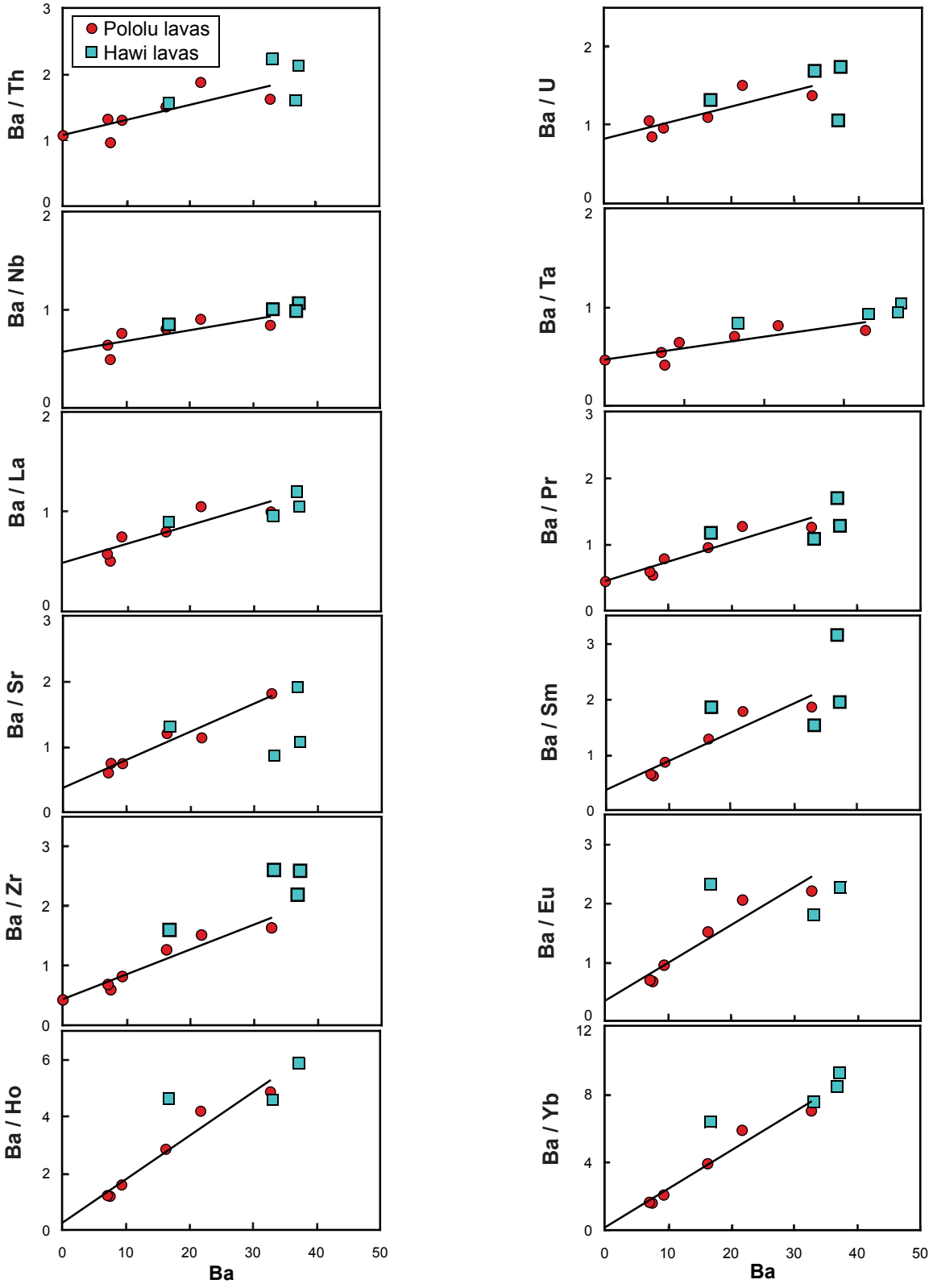

Fig. 7: *Process identification diagrams showing Ba content versus divers trace element ratios for Pololu lavas and Hawi lavas. As in Fig. 4, the trace elements abundances are corrected for fractionation and normalized to primitive mantle values. The Hawi lavas are particularly well aligned with the correlation defined by the Pololu lavas when highly incompatible elements ratios are plotted. This may indicate that the compositional change affecting the isotopic ratios between shield stage and post-shield stage of Kohala volcanism did not significantly affect the trace element compositions.*

were then calculated for each Hawi lavas composition using the least square regression method of Wright and Doherty (1970) and supposing fractionation of olivine± cpx ± ilmenite. Ilmenite and clinopyroxene compositions were taken from Feigenson et al. (1983) and olivine compositions were calculated in equilibrium with each lava sample. The results obtained are shown in Table 3, together with the corrected trace element compositions calculated further.

When reported in the process identification diagrams, primary compositions calculated for the Hawi lavas are reasonably well aligned with the pololu compositions, particularly when the most incompatible elements are plotted (Fig. 7). These elements have been only slightly disturbed during petrogenetic processes (leading to somewhat greater scatter) and alignments of their ratios indicate that the Hawi and the Pololu lavas do not possess clearly distinct trace element signatures. Slight differences in the source composition may exist during the post shield building stage of Kohala Volcano, as indicated by slightly distinct range of isotopic signatures, but the effects are not clearly visible in the trace element compositions of the lavas.

7. Conclusion

The extension of trace element composition to highly incompatible elements has first confirmed the kea-end-member signature of the Kohala lavas. On the basis of recent evaluations of primary magma compositions of Hawaiian picrites and olivine fractionation calculations, a primary magma composition with 16% MgO was inferred for the Pololu Volcanics. The larger amount of fractionating phases deduced from this primary composition has allowed a better correction of the Heavy REE and has significantly reduced the errors on these elements. However, these better constraints on primary melt compositions did not generate important changes in the calculated initial REE patterns, apart from progressive increase on Heavy REE abundances in the case of spinel lherzolite mineralogy. On the other hand, better correction of the HREE and the actual set of partition coefficient between garnet and silicate melt reported in literature provide important constraint on the role of garnet during the Kohala magmas genesis. Anomalously low Yb and Lu contents were obtained for the source when considering a garnet fraction of 0.12 in the primary melt norm, which

suggests that the amount of garnet entering the kohala magma should have been lower than 12%. These new calculations appear to validate the previous conclusions of Feigenson et al. (1983) attesting the presence of residual clinopyroxene, with or without small amounts of residual garnet, during the formation of the Kohala magma.

The calculated source patterns were extended to highly incompatible elements. They indicate a general increase of the abundances from Ba to the HREE. Therefore, these new results for Nb, Ta, Th and U confirm and extend the trend of highly-incompatible depletion of the Hawaiian source rocks. This is consistent with the isotopic signatures, which also indicate source depletion. Therefore, the incompatible element enrichments present in the melts themselves are entirely produced by partial melting effects and not by previous (metasomatic ?) source enrichments.

Finally, the slight modifications of the source composition between Hawi and Pololu volcanics suggested by isotopic data do not clearly appear in the trace elements variations of the lavas. The primary melt compositions calculated from both Hawi and Pololu lavas are relatively well aligned in the process identification diagrams of Minster and Allègre (1978) and thus imply only minor changes in the source composition during the post shield building stage of the Kohala Volcano.

References

Allègre C. J. and Minster J.-F. (1978) Quantitative models of trace element behavior in magmatic processes. *Earth Planet Sci Lett* 38, 1.

Beeson M. H. and Jackson E. D. (1970) Origin of the garnet pyroxenite xenoliths at Salt Lake Crater, Oahu. *Mineral Soc. Am. Spec. paper* 3, 95.

Bennett V. C., Norman M. D. and Garcia M. O. (2000) Rhenium and platinum group element abundances correlated with mantle source components in Hawaiian picrites: sulphides in the plume. *Earth Planet Sci Lett* 183, 513.

Chen C. Y. and Frey F. A. (1983) Origin of Hawaiian tholeiites and alkalic basalt. . *Nature* 302, 785.

Chen C. Y. and Frey F. A. (1985) Trace element and isotopic geochemistry of lavas from Haleakala Volcano, east Maui, Hawaii: Implications for the origin of Hawaiian basalts. *Journal of geophysical research* 90, 8743.

Danyushevsky L. V., Della-Pasqua F. N. and Sokolov S. (2000) Re-equilibration of melt inclusions trapped by magnesian olivine phenocrysts from subduction – related magmas : petrological implications. . *Contrib Mineral petrol* 138, 68.

Fedorowich J. S., Richards J. P., Jain J. C., Kerrich R. and Fan J. (1993) A rapid method for REE and trace-elemet analysis using laser sampling ICP-MS on direct fusion whole-rock glasses. *Chemical Geology* 106, 229.

Feigenson M. D. (1984) Geochemistry of Kauai volcanics and a mixing model for the origin of Hawaiian alkali basalts. *Contrib. Mineral. Petrol.* 87, 109.

Feigenson M. D., Hofmann A. W. and Spera F. J. (1983) Case studies on the origin of basalt II. The transition from Tholeiitic to alkalic volcanism on Kohala Volcano, Hawaii. . *Contrib Mineral petrol* 84, 390.

Hofmann A. W. and Feigenson M. D. (1983) Case studies on the origin ogf basalt. I. Theory and reassessment of Grenada basalts. *Contrib Mineral petrol* 84, 382.

Hofmann A. W., Feigenson M. D. and Raczek I. (1987) Kohala revisited. *Contrib Mineral petrol* 95, 114.

Hofmann A. W. and Jochum K. P. (1996) Source characteristics derived from very incompatible trace elements in Mauna Loa and Mauna Kea basalts, Hawaii Scientific Drilling Project. *Journal of geophysical research* 101, 11831.

Hofmann A. W., Jochum K. P., Seufert M. and White W. M. (1986) Nb and Pb in oceanic basalts: new constraints on mantle evolution. *Earth Planet Sci Lett* 79, 33.

Jochum K. P., Dingwell D. B., Rocholl A., Stoll B. and Hofmann A. W. (2000) The preparation and preliminary characterization of eight geological MPI-DING reference glasses for in-situ microanalysis. *Geostandards Newsletters* 24, 87.

Kennedy A., Kwon S. T., Frey F. A. and West H. B. (1991) The isotopic composition of postshield lavas from Mauna-Kea Volcano, Hawaii. . *Earth Planet Sci Lett* 103, 339.

Lanphere M. A. and Frey F. A. (1987) Geochemical evolution of Kohala Volcano, Hawaii. . *Contrib Mineral petrol* 95, 100.

Lassiter J. C., DePaolo D. J. and Tatsumoto M. (1996) Isotopic evolution of Mauna Kea Volcano: results from the initial phase of the Hawaii Scientific Drilling Project. *J Geophys. Res.* 101, 11769.

McDonough W. F. and Sun S. S. (1995) The composition of the Earth. *Chemical Geology* 120, 223.

McDougall I. and Swenson D. A. (1972) Potassium-Argon ages of lavas from Hawi and Pololu volcanics Series, Kohala Volcano, Hawaii. *Bull Geol Soc Am* 83, 3731.

Minster J.-F. and Allègre C. J. (1978) Systematic use of trace elements in igneous processes, part III. Inverse problem of batch melting in volcanic suites. *Contrib Mineral petrol* 68, 37.

Norman M. D. and Garcia M. O. (1999) Primitive magmas and source characteristics of the Hawaiian plume: petrology and geochemistry of shield picrites. *Earth Planet Sci Lett* 168, 27.

Roeder P. L. and Emslie R. F. (1970) Olivine-Liquid equilibrium. *Contrib Mineral petrol* 29, 275.

Salters V. J. M. and Stracke A. (2004) Composition of the depleted mantle. *Geochem. Geophys. Geosystems* 5(5), Q05004.

Shaw D. M. (1970) Trace element fractionation during anatexis. *Geochim Cosmochim Acta* 34, 237.

Sobolev A. V., Hofmann A. W. and Nikogosian I. K. (2000) Recycled oceanic crust observed in "ghost plagioclase" within the source of Mauna Loa lavas. *nature* 404, 986.

Spengler R. S. and Garcia M. O. (1988) Geochemistry of the Hawi lavas, Kohala Volcano, Hawaii. *Contrib Mineral petrol* 99, 90.

Stearn H. T. and Macdonald G. A. (1946) Geology and ground-water resources of the island of Hawaii. *Hawaii Div Hydrogr Bull* 9, 362.

Wright T. L. and Doherty P. C. (1970) A linear programming and least squares computer method for solving petrological mixing problems. *Bull Geol Soc Am* 81, 1995.

Part II

The magmatic evolution of Tubuai Island, Cook-Austral chain, South Pacific

M. JAMAIS, A. STRACKE, C. CHAUVEL, A.W. HOFMANN, C. HEMOND

Abstract

New trace element and Sr, Nd, Hf isotopic analyses have been performed on mafic lavas from Tubuai Islands in the Cook-Austral chain, South Pacific in order to constrain the geochemical and isotopic variations during the magmatic evolution of the Tubuai volcanoes.

Sr, Nd and Hf isotopic data are homogeneous and typical for the HIMU-type OIB and thus confirm the cogenetic nature of the different mafic lavas from Tubuai Island. The trace element patterns show progressive enrichment of incompatible trace elements with increasing alkaline content in the lavas, which reflects progressive decrease in the degree of partial melting towards the later volcanic events. In addition, this enrichment of incompatible trace elements is associated with relative depletion of Rb, Ba, K, Nb, Ta and Ti in the lavas, which require the presence of small amount of residual phlogopite and of a Ti-bearing phase (ilmenite or rutile) during formation of the younger analcitic and nephelinitic magmas.

Considering a garnet peridotite source mineralogy, partial melting modeling suggests that alkali basalts and basanites were produced by ~ 7 – 8 % melting and that nephelinites and one analcitite sample were produced by ~ 3% melting. Analcitites compositions suggest, however, that the degree of partial melting varied during formation of the analcitic magmas. Adding ~ 1% phlogopite to the source is sufficient to reproduce the Rb, Ba and K variations in the Tubuai lavas while adding ~ 0.6% ilmenite or ~ 0.2% rutile to the source reproduce the HFSE and most of the Ti variations in the lavas.

1. Introduction

The lavas from Tubuai Island of the Cook-Austral chain, south Pacific, together with lavas from Mangaia, Rurutu (old Volcanics), Rimatara and Raivavae islands of the Cook-Austral chain and St Helena Island in the south Atlantic, define the so-called HIMU-type ocean island basalts (OIB) (Zindler and Hart, 1986). HIMU lavas have a relatively restricted range of isotopic signatures with characteristically low $^{87}Sr/^{86}Sr$ ratios (0,7027 - 0,7032), and the most radiogenic $^{206}Pb/^{204}Pb$ (20 – 21.9), $^{207}Pb/^{204}Pb$ (15.7 – 15.8) and $^{208}Pb/^{204}Pb$ (39.2 – 40.7) isotopic ratios of all OIB. Another characteristic feature of these HIMU-type lavas is their depletion of the most incompatible elements (Cs, Rb, Ba, Th and U) relative to Nb and Ta, a pronounced depletion of K relative to Ta and La and a depletion of Pb relative to Pr and Nd. This HIMU-type signature has most often been interpreted to reflect the presence of recycled, altered oceanic crust material in the mantle source of these lavas (Chase, 1981; Hofmann and White, 1982; Palacz and Saunders, 1986; Zindler and Hart, 1986; Halliday et al., 1988; Hart, 1988; Nakamura and Tatsumoto, 1988; Vidal et al., 1989; Weaver, 1991; Chauvel et al., 1992; Reisberg et al., 1993; Hauri and Hart, 1993a; Roy-Barman and Allegre, 1995; Hauri et al., 1996; Chauvel et al., 1997; Hofmann, 1997; Lassiter and Hauri, 1998; Salters and White, 1998; Stracke et al., 2003; Stracke et al., 2005). The alkali elements such as K and Rb, but particularly Pb are though to be removed from the recycled crust either during hydrothermal processes at mid-oceanic ridges or during dehydration processes in subduction zones. The resulting high U/Pb and Th/Pb ratios lead, with time (~2 Ga), to very radiogenic Pb-isotopes ratios, whereas Sr-isotopes ratios remain relatively unradiogenic due to the low Rb/Sr ratios of the altered crust (Zindler and Hart, 1986; Weaver, 1991; Chauvel et al., 1992; Brenan et al., 1995; Kogiso et al., 1997). The apparent rarity of this HIMU component in the mantle and its occurrence at only two geographic areas remain poorly understood (Stracke et al., 2005).

Tubuai Island consists of two volcanic centers that have produced four different types of mafic lavas during their last eruption period (10 – 8.8 Ma). The isotopic homogeneity of these lavas and their progressive enrichment of incompatible elements with time have been interpreted to reflect a progressive decrease in the extent of partial melting (Maury et al., 1994). However, variations in highly incompatible element ratios, which are thought to be little affected by partial melting processes, have been observed (Vidal et al., 1984; Dupuy et al., 1988) and interpreted to reflect changes in the source composition (Dupuy et al., 1988). A systematic study of the

geochemical and isotopic variations within the Tubuai lavas could provide further constraints on the genesis and the magmatic evolution of lavas from Tubuai Island. We present new major and trace element concentrations and Sr-, Nd- and Hf-isotope data from a suite of lavas comprising all four mafic rocks types from Tubuai to better constrain the magmatic evolution of the Tubuai lavas. These new data will show that the observed compositional variations are mostly controlled by variations in the degree of partial melting of a common mantle source.

2. Geologic background

2.1 Volcanism in the South Pacific

In the South Pacific, Tertiary and Quaternary volcanism formed linear volcanic island chains such as the Cook-Austral and Pitcairn-Gambier island chains and the Samoa, Society and Marquesas Islands. These island chains are aligned in a NW-SE direction, roughly parallel to the Hawaiian-Emperor island chain further north, and are often crosscut by fracture zones or transform faults. In the vicinity of the Cook-Austral, Samoa, Marquesas and Society islands, the sea floor is anomalously shallow. The area is characterized by high heat flow and large geoid residuals (Richards and Hager, 1988) and forms a topographic swell covering approximately 18 million square meters, termed the "Super Swell" by McNutt and Fisher (1987). Seismic tomography studies show a zone of low seismic velocities (Fukao, 1992; Zhao, 2001) underneath the super-swell area. Taken together, these geophysical studies suggest that the upper mantle in the South Pacific is unusually hot and possibly partially molten, which has been interpreted to be either due to a large scale upwelling of deep mantle material (Larson, 1991) or to the presence of anomalously hot asthenospheric material (McNutt and Fisher, 1987).

The Cook-Austral island chain stretches over more than 2000 km, from the MacDonald seamount in the Southeast to the northernmost Aitutaki Island (Fig. 1). Currently, only the MacDonald seamount is volcanically active. Subaerial volcanism seized on the other Austral Islands (Marotiri, Rapa, Raivavae, Tubuai, Rurutu, Rimatara and Maria Islands) and the six southern Cook Islands (Mangaia, Rarotonga, Mauke, Mitiaro, Atiu and Aitutaki Islands). Typically, the Cook-Austral islands are shield volcanoes that rise from a depth of more than 4000 meters from the Paleocene sea-floor (Pitman et al., 1974), are extensively eroded and often

surrounded by thick coral reefs (Chubb, 1927; Obellianne, 1955; Marshall, 1957, 1968; Wood, 1978a, 1978b). A pre-existing roughly E-W trending transform fault, the Austral fracture zone (AFZ), crosses the archipelago between the islands of Raivavae and Tubuai.

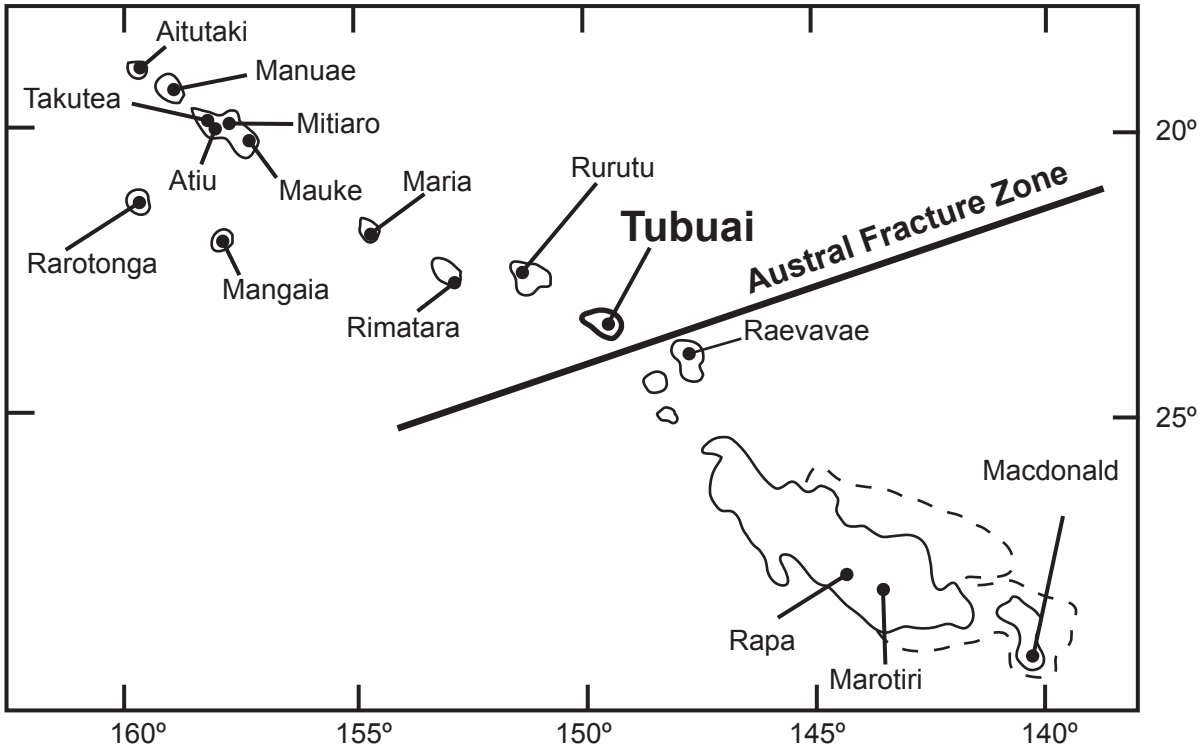

Fig. 1: *General map of the Cook-Austral Islands in the South Pacific.*

Early studies suggested a systematic progression towards older ages from the SE to the NW, which was generally thought to be consistent with the motion of the Pacific plate over a stationary hotspot (Wilson, 1963; Morgan, 1972; Duncan and McDougall, 1976). Among the southern Cook-Austral islands, however, the age progression is far more irregular than expected (Dalrymple et al., 1975; Duncan and McDougall, 1976; Bellon et al., 1980; Turner and Jarrard, 1982) and much younger ages than predicted from the plume theory have been reported from some of the Northwestern islands (Mauke, Atiu, Rarotonga, Aitutaki). Moreover, two different stages of volcanism, separated by several millions of years, have been observed on many islands (e.g. Aitutaki, Rurutu, Rimatara), and recent volcanism (< 2 Ma) is observed on islands across the entire island chain (e.g. MacDonald seamount, Rurutu, Rarotonga and Aitutaki Islands) (Dalrymple et al., 1975; Duncan and Mcdougall, 1976; Turner and Jarrard, 1982; Matsuda et al., 1984; Diraison, 1991; Barsczus et al., 1994).

Diraison (1991) and Chauvel et al. (1997) attempted to explain the age distribution along the Cook-Austral island chain by subdividing volcanism in three linear trends, thought to be

related to the presence of three independent mantle plumes. The “MacDonald trend” extends from Mangaia Island to the active MacDonald seamount and covers about 20 Ma (it includes Mangaia, old Rurutu, Tubuai, Raevavae, Rapa, Marotiri and MacDonald Volcanics). The “Atiu trend” represents 5 Ma of volcanic activity north from Tubuai (it includes old Aitutaki, Atiu, Mauke and young Rurutu Volcanics), and the “Rarotonga trend” represents recent volcanism (< 2Ma) in the northernmost part of the archipelago (it includes young Aitutaki and Rarotonga Volcanics). However, additional data on rocks from the flanks of the southernmost Marotiri and MacDonald seamounts (McNutt et al., 1997) have revealed the presence of older stages of volcanism (20 - 34 Ma) associated with the recent one. Therefore, the presence of at least four independent mantle plumes would be required to support a deep mantle origin of volcanism. In addition, the occurrence of recent volcanism (< 2 Ma) along the entire island chain, which covers an area of 2200 by 240 km, is difficult to reconcile with the idea of extensive volcanism rising off of a much larger plume head beneath the lithosphere (Morgan, 1971; Larson, 1991; Lassiter et al., 2003).

On the other hand, McNutt et al. (1997) demonstrated the presence of several periods of volcanism at the same volcanic edifice and proposed that the volume and location of volcanism are more likely to be controlled by stresses in the lithosphere than by several deep-seated mantle plumes. More recently, age determination of rocks from Austral seamounts have been interpreted by Bonneville et al. (2002) as reflecting short-lived hotspots that could be active simultaneously in a small space, appearing more consistent with local upwellings triggered by weaknesses in the lithosphere. In addition, geodynamic models for “backtracking” the proposed South Pacific hotspots to their origin have failed to demonstrate long-lived, deep-mantle plume characteristics of volcanism in the Superswell area (Wessel and Kroenke, 1997; Clouard and Bonneville, 2001). Therefore, despite the linearity of the island chains in the South Pacific and the occurrence of a seismic anomaly in the upper mantle beneath the MacDonald seamount (Ritsema and Allen, 2003), a number of authors suggested that volcanism along the Cook-Austral chain is unlikely to originate from upwelling of deep-seated mantle plumes (McNutt et al., 1997; Dickinson, 1998; Clouard and Bonneville, 2001; Lassiter et al., 2003), and instead related to zones of lithospheric weakness.

2.2 Geology of Tubuai Island

The island of Tubuai is located at the central part of the Cook-Austral chain, just North of the AFZ and about 1200 km north of the active MacDonald seamount (Fig. 2). The subaerial part of Tubuai consists of two deeply eroded volcanic edifices, the Herani and Hanareho Volcanoes, and covers an area of 9km by 5km with a maximum altitude of 400 m (Mt Taitaa) (Fig. 2). The submarine basement is by far larger (150 km by 100 km) and rests on a 65 - 70 Ma old oceanic crust.

Basaltic flows from the largest eruption centre, Herani Volcano at the East-central part of the island, are 10.04 to 8.78 Ma old (Maury et al., 2000). Two stages of volcanic activity have been described (Brousse and Maury, 1980; Maury et al., 1994; Maury et al., 2000). The first produced alkali basalts, which now form the western part of the volcano (likely from Mt Panee, 10.04 – 10 Ma) and the second produced basanites and rare analcitites at the central and eastern eruption centres (from East Herani and Mt Taitaa, 10 - 9.5 Ma).

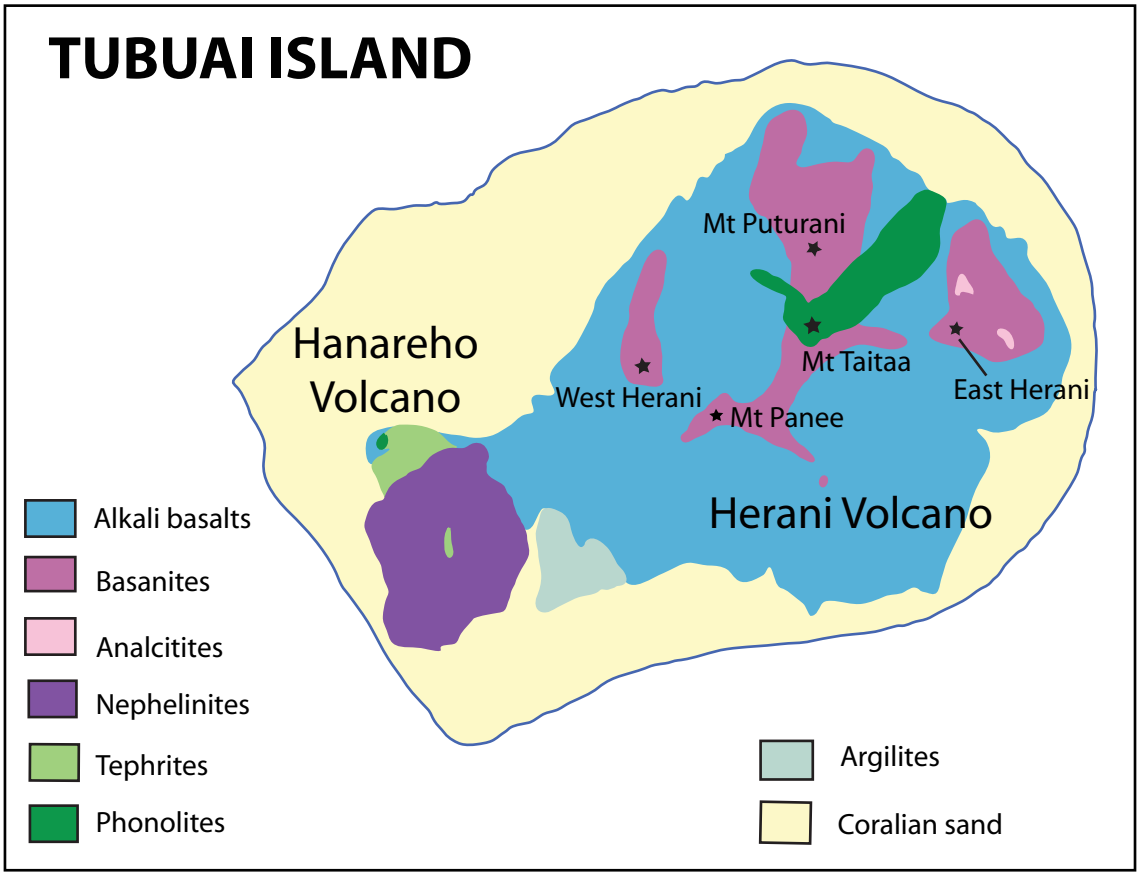

Fig. 2: *Geological map of Tubuai Island, modified from Maury et al. (1998).*

Vertical dykes of basanites and analcitites crosscut the whole stratigraphy, forming a particularly dense network around the western and northern eruption centres (respectively Mt Panee and Mt Puturani). Their main direction corresponds to the expansion vector of the oceanic crust. A later event formed the phonolitic extrusion at Mont Taitaa (8.78 Ma). Volcanic activity at Hanareho Volcano, the western volcanic edifice of Tubuai Island, is restricted to a short period between 9.68 and 8.77 Ma, contemporaneous to the waning stages of volcanism of Herani. Five hills of nephelinitic flows constitute the main part of Hanareho volcano. Towards the North, these are made up of three successive piles of tephritic flows, including xenoliths of peridotites with evidence for carbonatite metasomatism (Liotard and Barsczus, 1989; Hauri et al., 1993b). A phonolitic intrusion with similar compositions and ages compared to the Taitaa extrusion is situated at the northernmost end of the Hanareho edifices.

2.3 Petrography of mafic lavas

The mafic lavas from Tubuai Island include alkali basalts, basanites and analcitites from Herani Volcano and nephelinites from Hanareho Volcano. The nomenclature is based on the percentage of feldspathoids (foids), with increasing abundances from alkali basalts (< 5% foids) to nephelinites (> 30% foids), basanites (5% - 15% foids) and analcitites (15% - 30% foids) (Maury et al., 1994; Caroff et al., 1997). Olivine, clinopyroxene, and titanomagnetite phenocrysts are present in all these rock types (Maury et al., 1994; Caroff et al., 1997). Alkali basalts contain olivine, clinopyroxene, titanomagnetite and plagioclase in their groundmass, with precipitation of K-feldspar, ilmenite and apatite in the interstices. Additional groundmass nepheline and abundant potassic analcite are characteristic for the basanites and the analcitites respectively. The groundmass of the nephelinites is devoid of plagioclase and feldspar, but contains nepheline, analcite and sodalite.

3. Samples and analytical Methods

For this study, twenty-four lava samples (four alkali basalts, twelves basanites, two analcitites and six nephelinites) have been selected from the collection of C. Chauvel at the

University of Grenoble based on their freshness (LOI < 1%) and their relatively primitive compositions (MgO > 7%), using major element abundances reported in Caroff et al. (1997).

Lithophile trace element concentrations were determined by ICP-MS using a Plasma Quad turbo 2+ at the Laboratoire de Géodynamique des Chaines Alpines (LGCA), University of Grenoble, following a procedure modified from Barrat et al. (1996) on samples crushed and powdered in an agate mill. The analytical procedure is similar to those reported in Marini et al. (2005), except that BR was used for the calibration of the machine. The reported concentrations are relative to the average BR composition given in Table 1. This composition is in very good agreement with those reported in Eggins et al. (1997). Measurements of the international standards BHVO-2 and BE-N and the in-house standard BR24 were performed together with the samples to control the quality and accuracy of the data. Their average compositions are reported in Table 1. Repeated measurements (n = 6) of international and in-house standards reproduced to better than 4% (1 σ) for all the elements except for the Cs, Rb and Th (about 5%) measurements of the BHVO-2 standard.

Sr, Nd and Hf separations were carried out at the MPI using analytical techniques described in Hart and Brooks (1977), Pin and Zalduegui (1997) and Münker et al. (2001) respectively. Sample powders were leached in 6N HCl at 100°C for approximately 4 hours prior to Sr and Nd separation and digested in a mixture of HF-HNO_3. Sr was separated using a cation exchange resin AG50W-X8 and Nd using LN Spec resin. No leaching was performed prior to Hf separation on LN Spec resin. Sr and Nd isotope ratios were measured by thermal ionization mass spectrometry (TIMS) using a Finnigan TRITON mass spectrometer at the IUEM, University of Brest. $^{87}Sr/^{86}Sr$ and $^{143}Nd/^{144}Nd$ ratios were normalized using an exponential law mass fractionation model to $^{88}Sr/^{86}Sr = 0.1194$, and $^{146}Nd/^{144}Nd = 0.7219$, respectively. During the analysis period, repeated measurements of the SRM-NBS 987 Sr standard yielded an average $^{87}Sr/^{86}Sr$ of 0.710264 +/-20 (n = 11); the average $^{143}Nd/^{144}Nd$ of the La Jolla Nd standard yielded 0.511872 ± 30 (n = 14). This last value is high compared to the range of values usually obtained on the La Jolla standard ($^{143}Nd/^{144}Nd = 0.511840 – 0.511850$). Consequently, the Nd-isotopic results obtained on Tubuai lava samples have been readjusted to the $^{143}Nd/^{144}Nd$ value of 0.511850 for the La Jolla standard in order to compare these new results with previous isotopic data (see Table 2). Hf isotope ratios were measured on a Nu Plasma Multi-Collector ICPMS (MC-ICPMS) in static mode using a CETAC Aridus inlet system fitted with ESI Teflon nebulizer and a 50ml flow rate at the MPI. All isotope ratios were corrected with an exponential

Table 1: Major and trace element compositions of lavas from Tubuai Island. Major element data are from Caroff et al. (1997) and from C.Chauvel (pers. Comm). The measured values for standard materials are also reported and compare well to values reported in Eggins et al. (1997), Kelley et al. (2002), Garbe-Schönberg (1993) and Marini et al. (2005).

	Alkali Basalts				Basanites												Analcitites		Nephelinites						Standard averages			
	TB118	TB228	TB201	TB244	TB120	TB63	TB115	TB220	TB33	TB34	TB209	TB208	TB105	TB104	TB127	TB207	TB110	TB124	TB111	TB60	TB112	TB58	TB113	TB54	BR n = 11	BHVO-2 n = 6	BE-N n = 6	BR24 n = 6
SiO_2	45.0	45.5	47.0	45.3	44.3	44.4	44.1	44.8	44.5	44.6	43.8	43.5	43.4	44.1	43.7	43.5	42.4	40.4	41.9	41.7	42.2	42.3	41.6	42.2				
TiO_2	2.47	2.45	2.35	2.78	2.08	2.16	2.66	2.37	2.68	2.68	3.32	3.46	2.98	2.96	3.41	3.13	2.63	3.61	2.88	3.10	2.90	2.88	3.00	3.2				
Al_2O_3	12.6	12.5	12.3	13.9	9.23	10.8	12.1	11.8	12.7	12.7	13.7	13.7	13.9	12.8	15.6	14.7	12.7	13.0	12.9	12.8	13.1	12.9	13.0	13.5				
Fe_2O_3	1.39	1.37	1.29	1.48	1.37	1.41	1.42	1.36	1.47	1.46	1.52	1.53	1.48	1.43	1.56	1.49	1.48	1.66	1.61	1.64	1.62	1.63	1.61	1.6				
FeO	11.2	11.1	10.4	12.0	11.1	11.4	11.5	11.0	11.9	11.8	12.3	12.4	12.0	11.5	12.6	12.1	12.0	13.4	13.1	13.31	13.1	13.2	13.0	13.0				
MnO	0.215	0.216	0.184	0.237	0.202	0.203	0.204	0.206	0.225	0.224	0.195	0.196	0.214	0.205	0.224	0.213	0.236	0.233	0.287	0.295	0.298	0.298	0.289	0.276				
MgO	11.6	11.0	9.10	7.53	17.0	14.5	12.56	11.9	10.4	10.4	9.78	9.44	9.35	8.89	7.30	7.62	11.0	7.56	8.18	8.03	7.77	7.73	7.71	7.24				
CaO	12.0	12.2	14.1	13.1	11.9	12.0	12.0	13.0	12.2	12.0	11.1	11.8	12.1	14.3	11.1	11.9	10.6	13.0	9.52	9.84	9.73	9.988	9.60	9.48				
Na_2O	2.29	2.32	2.35	2.51	1.92	2.02	2.31	2.31	2.55	2.72	2.93	2.68	2.99	2.46	3.04	3.66	4.68	4.84	6.86	6.70	6.53	6.21	7.17	6.67				
K_2O	0.798	0.853	0.532	0.741	0.514	0.681	0.797	0.700	0.888	0.857	0.792	0.908	1.03	0.870	0.919	1.14	1.42	1.43	1.70	1.61	1.73	1.74	1.97	1.83				
P_2O_5	0.409	0.432	0.348	0.422	0.282	0.345	0.398	0.412	0.419	0.418	0.422	0.402	0.480	0.481	0.480	0.488	0.884	0.811	1.03	1.02	0.987	1.11	1.01	0.881				
Li	7.31	7.30	6.23	7.27	5.23	6.09	7.48	6.87	8.41	6.97	6.67	6.42	7.70	7.37	7.98	8.46	15.5	11.3	20.4	18.5	20.0	19.7	18.9	20.6	14.9	4.78	13.2	6.99
Rb	21.1	25.9	13.5	18.0	12.3	17.2	22.3	30.6	34.9	24.5	15.4	31.4	28.4	24.6	21.3	30.0	49.1	40.8	58.8	51.7	55.4	66.4	65.9	56.3	48.7	9.65	49.8	85.2
Sr	556	637	450	556	386	541	557	518	562	528	681	625	642	680	599	673	1055	1007	1425	1362	1415.5	1507	1358	1315	1364	412	1414	635
Y	27.6	28.7	24.5	31.1	20.6	23.6	27.1	26.4	29.9	29.2	26.5	26.2	30.3	29.8	32.1	31.9	36.4	36.5	47.0	45.3	46.4	48.4	45.3	45.6	31.5	29.6	32.0	32.3
Zr	196	206	164	229	144	166	199	190	215	206	207	203	231	230	228	240	320	353	468	467	481	511	462	481	283	184	284	313
Nb	65.7	69.0	46.5	61.8	39.3	53.1	60.8	62.8	70.7	67.8	61.3	57.1	77.3	78.3	71.3	78.3	132	130	201	191	204.5	219	194	210	119	19.8	120	41.7
Cs	0.228	0.264	0.135	0.155	0.134	0.116	0.199	0.237	0.279	0.252	0.200	0.220	0.227	0.204	0.187	0.297	0.486	0.500	0.804	0.838	0.753	0.824	1.41	0.518	0.82	0.101	0.745	0.733
Ba	266	271	196	243	162	208	251	250	297	281	295	278	303	321	286	318	572	516	757	686	751	796	713	705	1082	130	1027	385
La	42.0	42.0	31.2	38.95	25.0	32.6	39.0	39.7	46.8	42.3	36.3	34.2	47.5	51.5	44.1	49.9	101	85.1	139	134.5	141	142	136	138	82.1	15.2	81.8	34.2
Ce	86.0	86.4	64.2	82.2	53.0	67.1	80.7	81.4	93.8	86.3	78.4	75.8	95.2	103	91.2	102	185	170	252	245	252	257	246	245	152	37.9	152	73.8
Pr	9.96	9.89	7.61	9.78	6.41	8.01	9.43	9.5	11.2	10.2	9.52	9.14	11.2	12.0	10.6	11.7	20.7	19.3	27.4	26.8	27.4	28.1	27.0	26.5	17.4	5.32	17.3	9.70
Nd	38.4	38.4	30.3	38.9	26.0	31.7	37.5	37.3	43.4	39.6	38.2	37.5	42.6	46.4	41.9	45.2	73.9	73.8	96.5	94.2	95.5	98.4	94.6	92.0	66.1	24.4	66.0	40.3
Sm	7.31	7.3	6.31	7.7	5.45	6.25	7.37	7.23	8.22	7.72	7.78	7.85	8.27	8.76	8.31	8.75	12.7	13.4	16.0	15.9	15.8	16.5	15.8	15.5	12.1	6.05	12.0	8.49
Eu	2.24	2.19	1.99	2.37	1.66	1.91	2.26	2.20	2.53	2.33	2.39	2.39	2.52	2.71	2.55	2.63	3.78	3.96	4.66	4.60	4.66	4.82	4.60	4.54	3.58	2.01	3.58	2.55
Gd	6.20	6.11	5.61	6.71	4.60	5.57	6.43	6.15	7.20	6.55	6.66	6.86	7.02	7.67	7.145	7.37	10.3	10.8	12.6	12.4	12.55	12.8	12.5	12.2	9.57	5.89	9.46	7.30
Tb	0.925	0.928	0.867	1.00	0.703	0.813	0.952	0.914	1.06	0.962	0.97	0.968	1.01	1.10	1.08	1.11	1.40	1.51	1.73	1.72	1.75	1.79	1.72	1.71	1.29	0.933	1.27	1.08
Dy	4.97	4.92	4.52	5.46	3.7	4.21	5.09	4.81	5.62	5.21	5.05	4.85	5.49	5.68	5.73	5.80	7.06	7.26	8.92	8.71	8.84	9.07	8.78	8.65	6.3	5.16	6.24	5.75
Ho	0.936	0.938	0.843	1.04	0.702	0.784	0.936	0.891	1.09	0.975	0.902	0.869	1.01	1.02	1.08	1.08	1.22	1.24	1.58	1.52	1.57	1.61	1.56	1.56	1.09	0.988	1.07	1.07
Er	2.43	2.44	2.14	2.72	1.76	2.04	2.40	2.26	2.72	2.59	2.20	2.16	2.53	2.55	2.81	2.75	2.98	2.84	3.88	3.77	3.89	4.01	3.84	3.83	2.59	2.56	2.56	2.74
Yb	1.95	1.97	1.64	2.215	1.36	1.51	1.85	1.78	2.25	2.05	1.6	1.56	1.98	1.92	2.19	2.09	2.11	1.94	2.89	2.76	2.89	3.01	2.83	2.81	1.8	1.97	1.79	2.14
Lu	0.285	0.291	0.238	0.322	0.196	0.212	0.255	0.257	0.331	0.291	0.231	0.218	0.287	0.272	0.3155	0.302	0.279	0.259	0.4	0.383	0.395	0.422	0.384	0.386	0.255	0.279	0.244	0.309
Hf	4.40	4.47	3.86	5.06	3.25	3.72	4.57	4.33	5.18	4.79	5.00	5.07	4.92	5.34	5.12	5.33	6.49	7.63	9.08	9.04	9.19	9.71	8.78	8.98	5.62	4.30	5.58	6.71
Ta	3.71	3.84	2.54	3.52	2.21	2.86	3.40	3.41	4.2	3.84	3.47	3.16	4.16	4.46	3.99	4.45	6.80	7.08	10.9	10.4	11.1	11.7	11.1	11.4	5.79	1.17	5.75	2.44
Pb	2.81	3.09	2.32	2.49	1.54	2.36	2.75	2.27	3.53	2.65	2.16	1.98	2.99	2.96	2.60	2.90	6.97	4.23	9.39	8.85	10.3	13.0	3.33	10.3	4.77	1.64	4.05	3.65
Th	4.91	5.13	3.64	4.41	2.72	3.65	4.57	4.69	5.58	5.01	3.76	3.40	5.67	6.03	5.04	5.90	13.8	10.2	18.6	19.1	20.6	21.5	19.5	21.9	10.9	1.28	10.8	4.74
U	1.24	1.30	0.835	1.09	0.661	1.03	1.13	1.15	1.38	1.18	0.904	0.818	1.39	1.46	1.245	1.32	3.26	2.48	3.81	4.49	4.87	5.09	4.91	5.25	2.46	0.410	2.40	1.20

Table 2: Sr, Nd and Hf isotopic compositions of lavas from Tubuai Island. Transition metal data reported in Caroff et al. (1997) for the same samples are also presented here.

		$^{87}Sr/^{86}Sr$	2σ	$^{143}Nd/^{144}Nd$	2σ	$^{143}Nd/^{144}Nd$ readjusted *	$^{176}Hf/^{177}Hf$	2σ	Sc	Cr	Co	Ni
TB 118	Alkali Basalt	0.702805	5	0.512899	2	0.512877	0.282932	4				
TB 228	Alkali Basalt	0.702820	6	0.512912	5	0.512890	0.282922	3	33	690	56	216
TB 201	Alkali Basalt	0.702792	5	0.512935	4	0.512913	0.282950	3	38	370	52	136
TB 244	Alkali Basalt						0.282942	2	34	220	54	89
TB 120	Basanites	0.702798	9	0.512936	5	0.512914	0.282968	3				
TB 63	Basanites	0.702810	7	0.512917	5	0.512895	0.282957	3				
TB 115	Basanites	0.702820	5	0.512924	4	0.512902	0.282953	3				
dup-TB 115		0.702815	7									
TB 220	Basanites	0.702844	7	0.512938	7	0.512916	0.282949	3	33	685	60	280
TB 33	Basanites	0.702804	4	0.512895	7	0.512873	0.282929	2	34	480	65	176
dup-TB 33		0.702803	12									
TB 34	Basanites	0.702803	5	0.512923	4	0.512901	0.282932	3	35	500	66	178
TB 209	Basanites	0.702809	3	0.512924	6	0.512902	0.282954	3	26	282	63	200
dup-TB 209				0.512909	11	0.512887						
TB 208	Basanites	0.702814	6	0.512921	5	0.512899	0.282951	2	27	265	45	190
TB 105	Basanites	0.702821	6	0.512919	3	0.512897	0.282955	3	22	290	61	188
TB 104	Basanites	0.702832	4	0.512922	5	0.512900	0.282962	3				
dup-TB 104		0.702820	9									
TB 127	Basanites	0.702804	3	0.512933	5	0.512911	0.282947	3	21	74	53	51
TB 207	Basanites	0.702819	5	0.512938	5	0.512916	0.282948	3	23	217	56	128
TB 110	Analcitites	0.702821	6	0.512964	4	0.512942	0.282951	2			53	
TB 124	Analcitites	0.702824	4	0.512931	4	0.512909	0.282948	2	19	112	55	80
TB 111	Nephelinites	0.702834	5	0.512941	6	0.512919	0.282961	2				
TB 60	Nephelinites	0.702833	3	0.512919	4	0.512897	0.282954	2	16	166	45	128
TB 112	Nephelinites	0.702821	6	0.512935	5	0.512913	0.282961	3				
TB 58	Nephelinites	0.702835	6	0.512944	5	0.512922	0.282955	2	16	162	45	128
TB 113	Nephelinites						0.282966	2	15	140	42	110
TB 54	Nephelinites	0.702834	7	0.512929	4	0.512907	0.282961	3	16	155	42	125

* : $^{143}Nd/^{144}Nd$ readjusted to a value of the La Jolla standard $^{143}Nd/^{144}Nd = 0.511850$ (see analytical methods).

fractionation law using $^{179}Hf/^{177}Hf$ = 0.7325. During the analysis period, repeated measurements of the JMC 475 Hf standard averaged $^{176}Hf/^{177}Hf$ = 0.282158 (2SD = 0.000008, n = 13) and are in good agreement with the long-term average of 0.282161 (2SD = 0.000016, n = 415).

4. Results

4.1 Sr-, Nd- and Hf-isotopes

Sr, Nd and Hf isotopic ratios are reported in Table 2. All the lavas are younger than 10.1 Ma, so the measured Sr, Nd and Hf isotopic ratios are identical, within error, to the initial ratios. Sr, Nd and Hf isotopic ratios obtained on the entire lava series define a limited range (0.70278 – 0.70284, 0.51289 – 0.51296 and 0.28292 – 0.28297 respectively). The new Sr and Nd isotopic data are within the range of previous isotope data on Tubuai lavas (Fig. 3) and overlap those of other HIMU-type OIB from Mangaia and St Helena, for example. Small differences between HIMU-type OIB arise when Pb isotopes are considered (Fig. 4), with Mangaia showing the most extreme Pb isotopic signature and St Helena having more moderate Pb isotopic ratios. Pb isotope values of Tubuai lavas (Vidal, 1984; Chauvel, 1992; Hauri, 1993) are between those of Mangaia and St Helena.

This new set of Sr, Nd, and Hf isotopic ratios limits the range of $^{87}Sr/^{86}Sr$ previously measured (Fig. 3). Though values obtained on nephelinites are among the highest values of Sr and Hf isotopic ratios, they entirely overlap those of basanites and there is no clear isotopic distinction between the different rock types (Fig. 3), which confirms the isotopic homogeneity of the Tubuai lavas pointed out previously (Vidal et al., 1984; Chauvel et al., 1992; Hauri and Hart, 1993a).

4.2 Major elements and transitional metals

Major element concentrations of some of these samples have been measured previously by C. Chauvel and are reported in Table 1 (unpublished data) together with major and transition metal element concentrations taken from Caroff et al. (1997). In addition to these data,

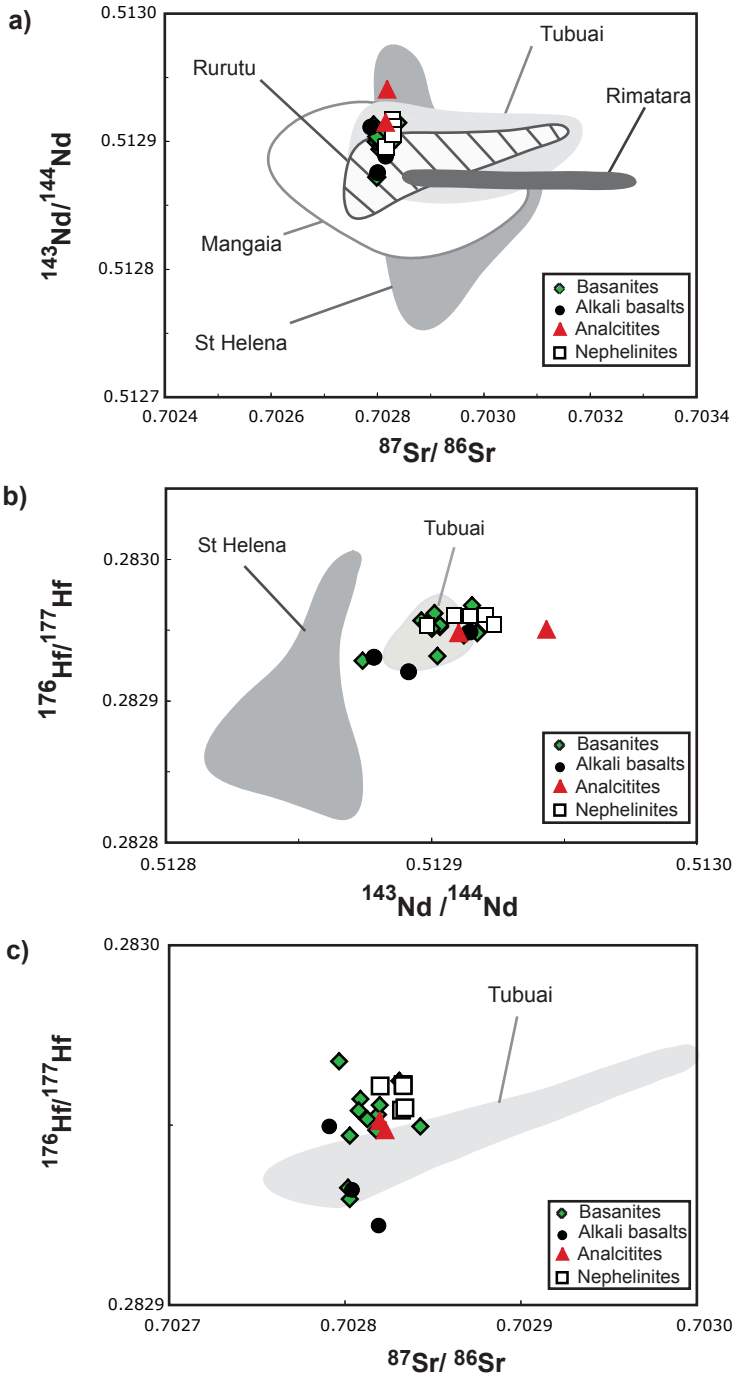

Fig. 3: a) *^{87}Sr / ^{86}Sr versus ^{143}Nd / ^{144}Nd diagram showing the isotopic compositions of Tubuai lavas together with available data from literature on Tubuai and other HIMU-type OIBs (see compilation data in Stracke et al., 2003). Due to the high value of the LaJolla standard measured in this study (0.511872), the set of ^{143}Nd / ^{144}Nd ratios obtained on Tubuai lavas were readjusted to a lower value of Lajolla standard (0.511850) in order to compare these new data with previous isotopic compositions (see Table 2). The new data overlap the HIMU field defined by previous data and display a narrow range of values in the left side of the Tubuai field.* ***b)*** *$^{143}Nd/^{144}Nd$ versus $^{176}Hf/^{177}Hf$ diagram showing the same new and literature data. The new data extend the Tubuai field towards slightly higher Nd isotopic compositions. c) $^{87}Sr/^{86}Sr$ versus ^{176}Hf / ^{177}Hf diagram showing new and literature compositions of Tubuai lavas. The new data display slightly higher Hf isotopic compositions for a given Sr isotopic composition.*

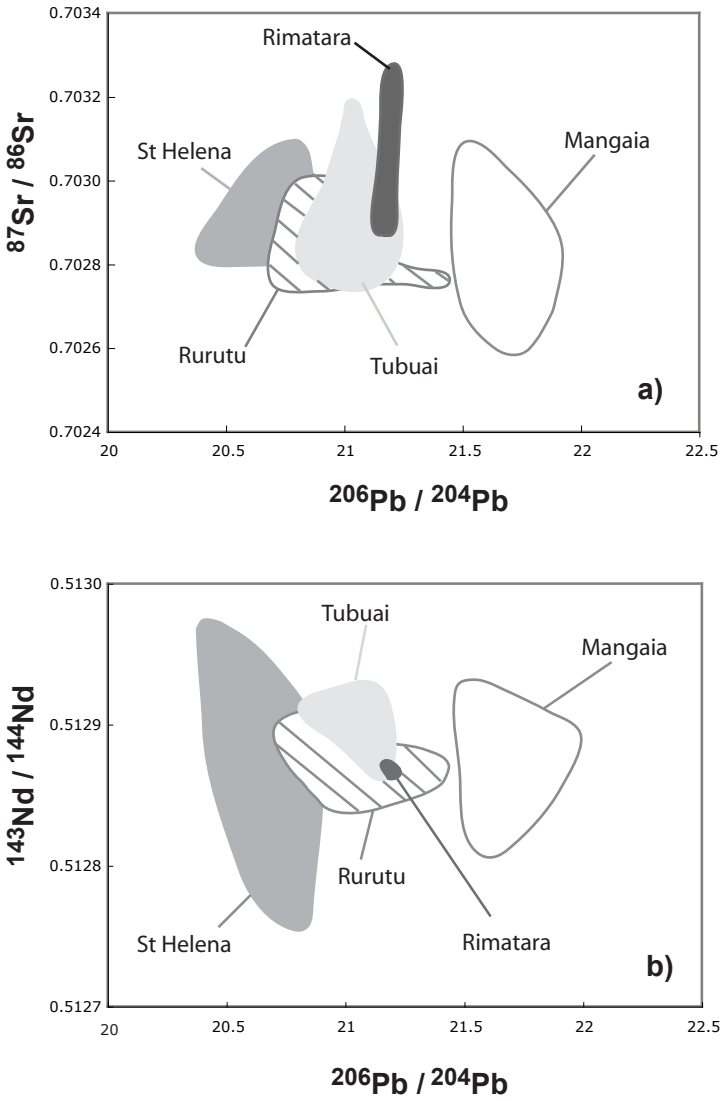

Fig. 4: a) *$^{206}Pb/^{204}Pb$ versus $^{87}Sr/^{86}Sr$ diagram and* ***b)*** *$^{206}Pb/^{204}Pb$ versus $^{143}Nd/^{144}Nd$ diagram showing small variations in the isotopic composition of the different HIMU-type OIBs. Pb isotopic values of Tubuai lavas are higher than those of St Helena, South Atlantic, but are less extreme than those of Mangaia Island in the Cook-Austral chain. See compilation data in Stracke et al. (2003).*

compositions of other Tubuai samples reported in Caroff et al. (1997) and in Chauvel et al. (1992) are also presented in diagrams of Fig. 5 and Fig. 6.

The silica content decreases progressively from the alkali basalts (SiO_2 = 45 - 47 %) to the basanites (SiO_2 = 43 - 45 %), analcitites (SiO_2 = 40 - 42 %) and nephelinites (SiO_2 = 41 - 42 %). It is accompanied by a progressive decrease in CaO and Sc and a progressive increase in FeO, Na_2O and K_2O concentrations (Fig. 5). The P_2O_5 and MnO contents are distinctively higher in the nephelinites and display intermediate values in the analcitites, but all the lavas have similar ranges of Al_2O_3, TiO_2, Ni and Cr concentrations.

Within the basanites, decreasing MgO content is accompanied by slightly decreasing SiO_2

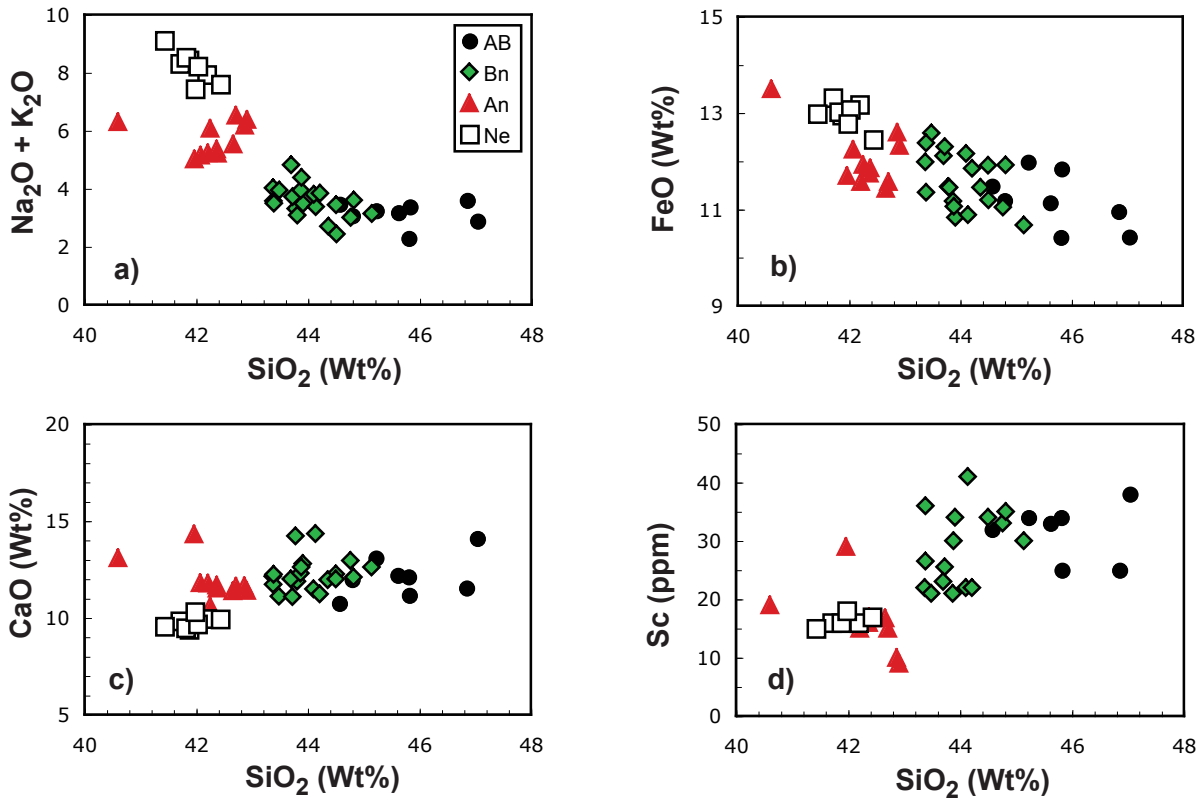

Fig. 5: *Plots of several major and transitional elements (**a**) Na_2O+K_2O, **b**) FeO, **c**) CaO, and **d**) Sc) as a function of SiO_2 showing the evolution of lava compositions during the magmatic activity of Tubuai Volcanoes. From the early volcanics (alkali basalts) to the late volcanics (nephelinites), progressive silica under-saturation is accompanied by an increase in alkaline and FeO contents and a decrease in CaO and Sc contents. AB = alkali basalt, Bn = basanite, An = analcitite and Ne = nephelinite. All data are from Caroff et al. (1997) and Chauvel et al. (1992).*

and CaO contents as well as Sc, Cr and Ni concentrations, and by increasing Al_2O_3, TiO_2, FeO, Na_2O, K_2O and P_2O_5 concentrations (Fig. 6), suggesting progressive fractionation of clinopyroxene with subordinate olivine (Chauvel et al., 1992). On the other hand, the SiO_2 concentrations are rather constant in the alkali basalts and Sc decrease only moderately with decreasing MgO contents in these lavas, suggesting that the proportion of olivine was more important in the mineral assemblage during alkali basalt differentiation. Major elements variations in analcitites are not well constrained but seem to be parallel to the basanites trend, suggesting a similar fractionation history.

4.3 Trace elements

The trace element compositions are presented in Table 1. Values obtained on samples previously analyzed by Caroff et al. (1997) are in good agreement with those reported in this

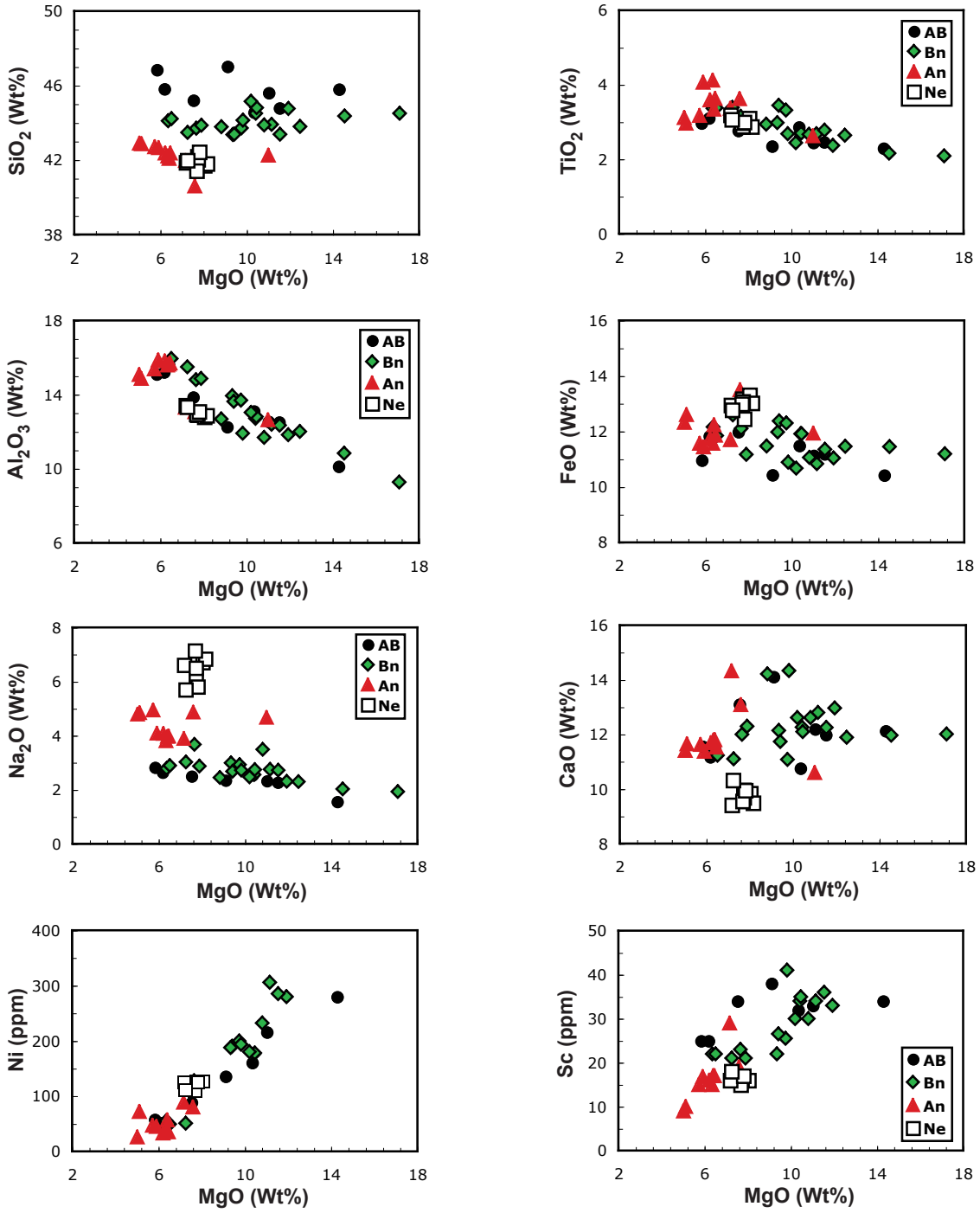

Fig. 6: *Plots of several major and transitional elements (SiO_2, TiO_2, Al_2O_3, FeO, CaO, Na_2O, Ni and Sc) as a function of MgO showing compositional variations during magma differentiation. In the basanites, the slight decrease in SiO_2 and CaO, the moderate decrease in Ni and Sc and the increase in FeO, TiO_2, Al_2O_3 and Na_2O with decreasing MgO content reflect a dominant role of clinopyroxene fractionation. Variations in the alkali basalts indicate more moderate decrease in SiO_2 and Sc with decreasing MgO contents and suggest higher proportion of olivine in the mineral assemblage (see text). AB = alkali basalt, Bn = basanite, An = analcitite and Ne = Nephelinite. All data are from Caroff et al. (1997) and Chauvel et al. (1992).*

study for the rare earth elements (REE) and Th, but are systematically higher for Nb, Zr and Y. Values reported for the USGS standard BE-N by Caroff et al. (1997) show similar discrepancies for Nb, Zr and Y contents compared to the BE-N measurements presented here. Nb and Zr concentrations obtained for the BE-N, BHVO-2 and BR24 standard are in good agreement with the values reported in Garbe-Schönberg (1993), Kelley et al. (2003) and Marini et al. (2005) respectively. On the other hand, the Y contents are slightly higher compared to these reference values and likely over-estimate the Y contents of the lavas.

All trace element patterns of the Tubuai lavas are typical HIMU-like (Chauvel et al., 1992; Willbold and Stracke, 2006), with increasing concentrations from Lu to Nb, but depletions of U, Th, Ba, Rb, and Cs relative to Nb, Ta and La, of K relative to Ta and La, of Pb relative to Pr and Nd, of Hf relative to Zr and Sm and of Ti relative to Eu and Gd (Fig. 7). Sr is slightly enriched relative to Nd and Zr.

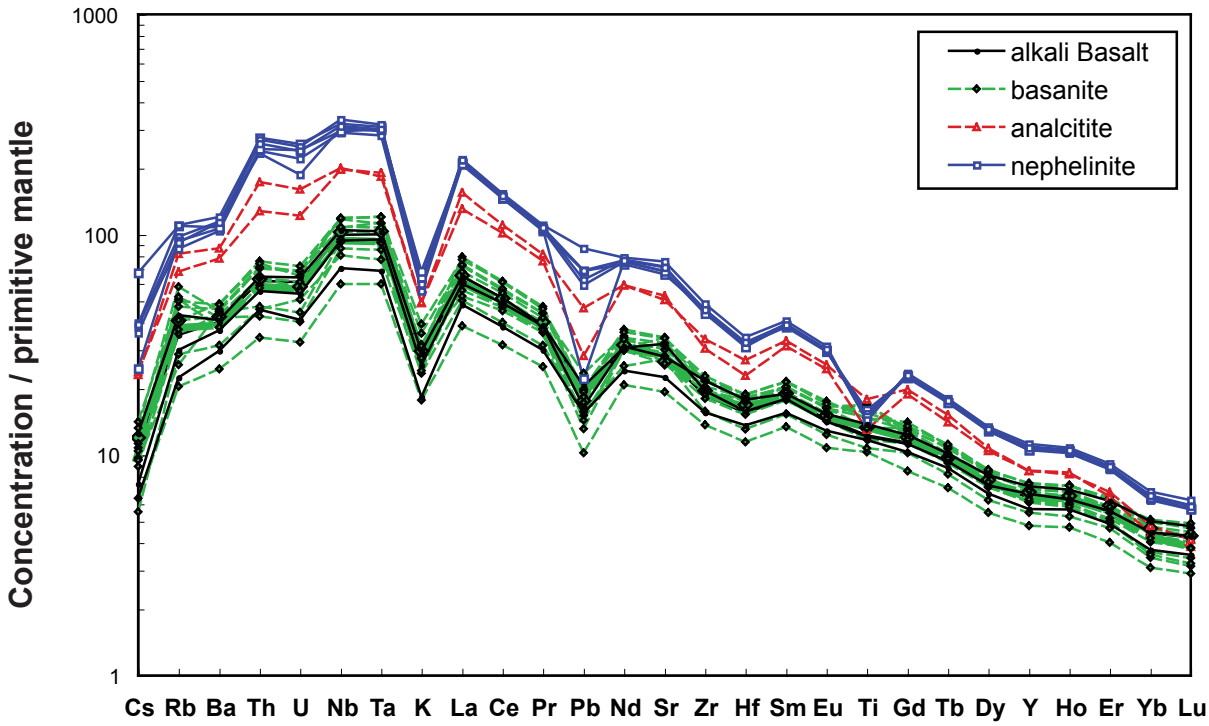

Fig. 7: *Trace element concentrations normalized to primitive mantle values (McDonough and Sun, 1995). The patterns have a typical HIMU-type OIB shape with enrichment in Nb and Ta relative to L-REEs, progressive depletion in highly incompatible elements from U to Cs relative to Nb and Ta and depletion of potassium relative to Ta and La. Progressive enrichment in highly incompatible elements is accompanied by silica under-saturation in the lavas: alkali basalts and basanites have very similar concentrations, analcitites and nephelinites have compositions distinctively enriched in Light REE and highly incompatible elements.*

The highly incompatible trace elements and the REEs increase with increasing degree of silica under-saturation in the lavas (from alkali basalts to nephelinites, Fig. 7). The alkali basalts and basanites have similar concentration ranges for all trace elements, with, for example, $(Sm/Yb)_N$ = 3.69 ± 0.16 and 4.18 ± 0.24 (2σ) and $(La/Sm)_N$ = 5.37 ± 0.43 and 5.30 ± 0.27 (2σ), respectively. While the HREE concentrations in the analcitites overlap those of the alkali basalts and basanites (Ho – Lu), they are distinctively more enriched in MREE ($(Sm/Yb)_N$= 6.46 ± 0.89 (2σ)), in LREEs ($(La/Sm)_N$= 7.15 ± 1.6 (2σ)) and highly incompatible elements. The nephelinites have the highest concentrations for all trace elements with the strongest enrichment in LREE and highly incompatible elements relative to less incompatible elements ($(Sm/Yb)_N$ = 5.56 ± 0.09 and $(La/Sm)_N$ = 8.7 ± 0.15 (2σ)) of all rock types. A conspicuous feature is the increasing negative Ti anomaly in the patterns from basanites to nephelinites, caused by similar titanium contents in all rock types but progressively increasing MREE concentrations (Fig. 6 and 7), suggesting that Ti is buffered during melt generation and evolution of the Tubuai magmas.

Within the basanite series, the trace elements concentrations increase progressively with increasing magmatic differentiation (e.g. decrease of MgO content), whereas the alkali basalts have very homogeneous trace elements concentrations that do not show any systematic variation with MgO content, although the small number of samples may not be representative enough. The two analcitites have similar compositions, showing slight scatter among the highly incompatible elements and for Pb content (Fig. 7). The nephelinite samples have nearly identical trace element concentrations with increasing scatter towards the most incompatible elements.

Fig. 8 is a plot of fluid-mobile element concentrations such as Cs, Rb, U and Pb versus less mobile elements (Ba, Th and Nb). Correlations described by the whole set of data are very well constrained and confirm the freshness of the selected samples. Rare discrepancies appear, however, and emphasize Pb loss in TB113 (TB113 has significantly lower Pb content than the others with an anomalously high Ce/Pb ratio of 70 compared to Ce/Pb between 20 and 27 in all other nephelinites) as well as slight enrichment of Rb in the basanites TB220, TB33 and TB208. The Cs-Nb correlation highlights also some Cs loss in TB54 as well as an anomalously high concentration of Cs in TB113. All these divergences are most likely due to surface alteration and these data will not be used in the following.

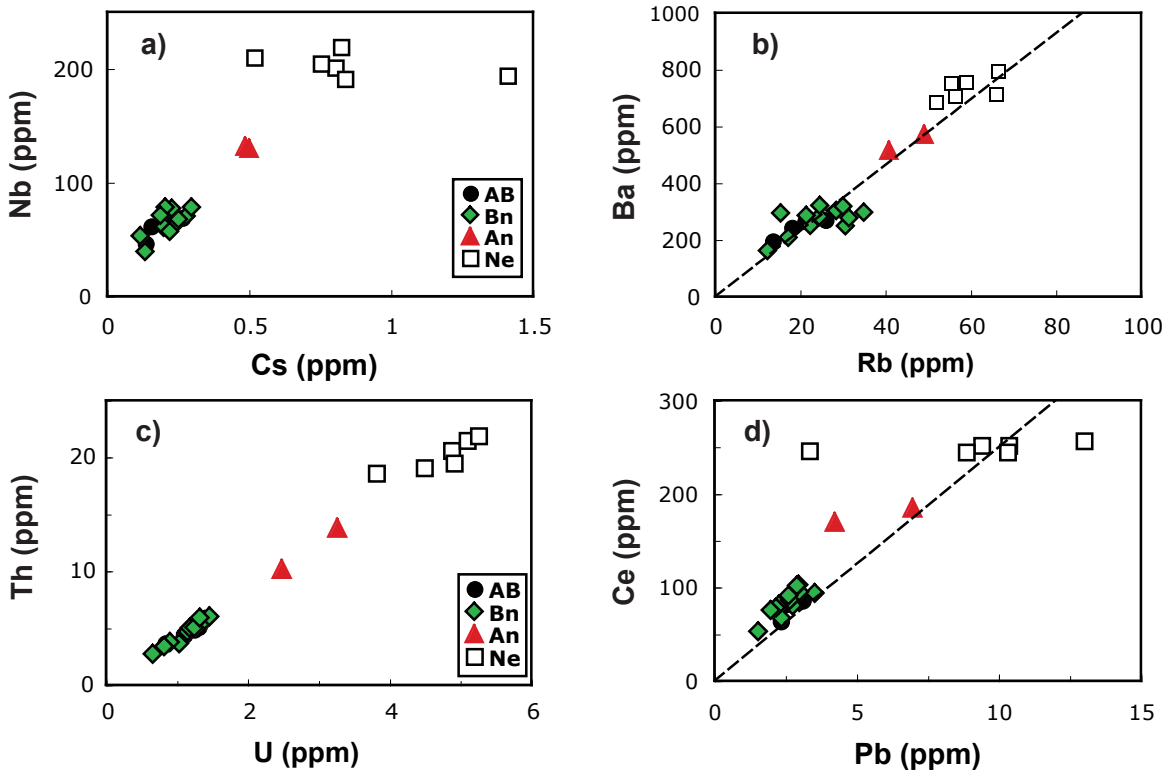

Fig. 8: *Diagrams plotting fluid-mobile elements such as* ***a)*** *Cs,* ***b)*** *Rb, and* ***c)*** *U versus less mobile element such as Ba, Th, Nb. With the exception of rare discrepancies, the data show a consistent behavior of fluid mobile and immobile elements and thus confirm the freshness of the selected samples;* ***d)*** *plot of Pb versus Ce variations in the Tubuai lava series showing anomalously low Pb content in the nephelinite TB113, while other samples show regular Pb - Ce correlation. Trend lines on the Rb versus Ba diagram and on the Pb versus Ce diagram represent average ocean basalt Ba / Rb = 11.6 (Hofmann and White, 1983) and Ce / Pb = 25 (Hofmann et al., 1986). AB = alkali basalt, Bn = basanite, An = analcitite and Ne = nephelinite.*

4.4 Trace element distinctions between the different rock types

The basanites are the most numerous samples among the lava series and are, similarly to the alkali basalts, the most trace element depleted samples. Therefore, we use an average trace element composition of the basanite for comparison with those of the other lava groups. Fig. 9a presents the average trace element patterns for each group of lavas normalized to primitive mantle values (McDonough and Sun, 1995). The patterns in Fig. 9b are obtained by dividing the average composition of a rock type by the average composition of basanites and thus highlight the differences between the alkali basalts, analcitites, nephelinites and the basanites.

There are only minor differences between the average alkali basalt and basanite compositions, which disappear when comparing samples with the same degree of fractionation (e.g. the same MgO content). The nephelinites are enriched in all trace elements compared to the basanites, with abundances ranging from 1.5 (Lu) to 4.4 (Th) times higher than in the basanites

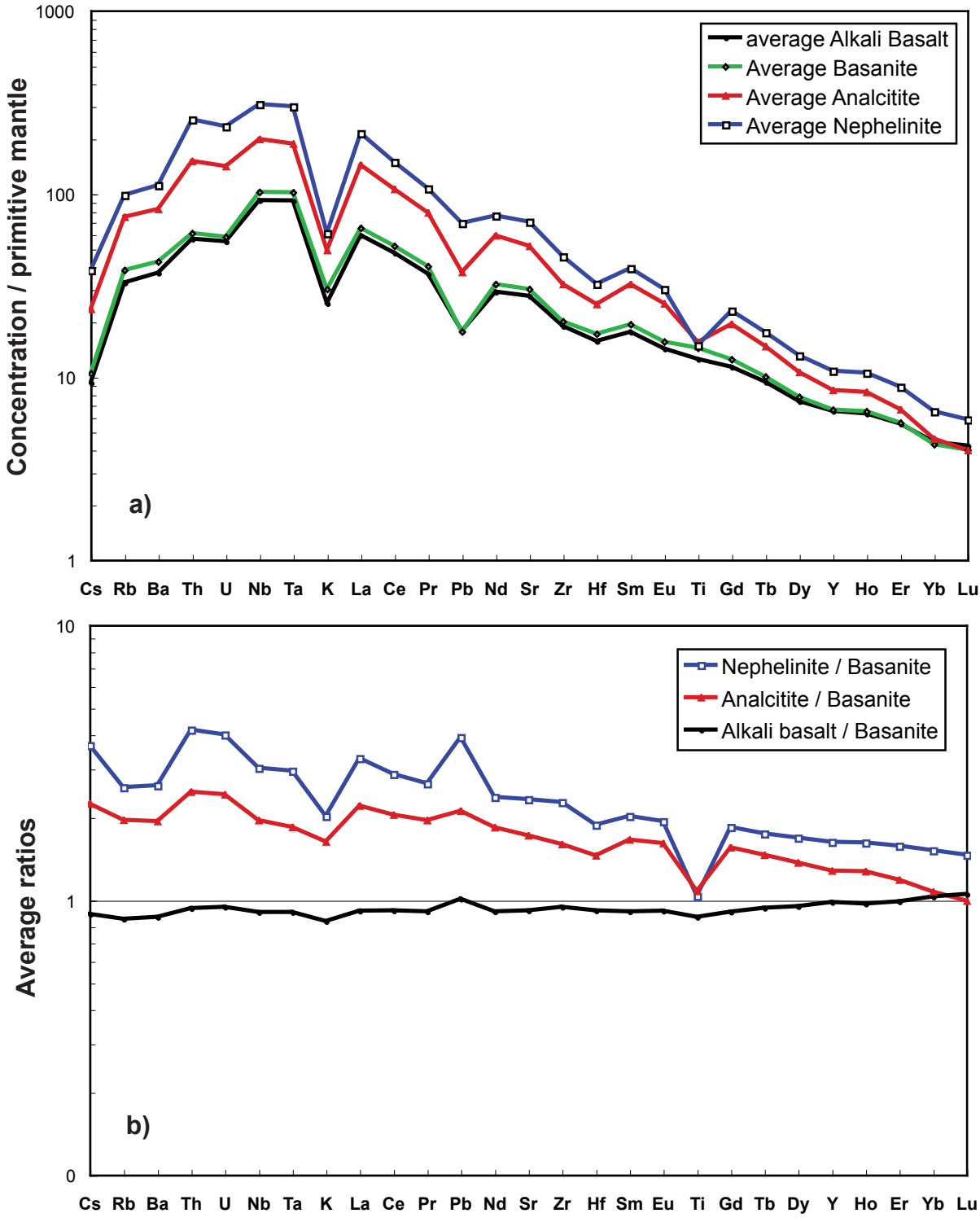

Fig. 9: a) *Average trace element patterns of the different group of lavas from Tubuai Island. The concentrations are normalized to primitive mantle values (McDonough and Sun, 1995). Average concentrations emphasize similar trace element compositions in the alkali basalts and basanites and progressive enrichment of incompatible elements and MREE from basanites to nephelinites, while the Ti content is constant in all the lavas.* ***b)*** *Average concentrations of the alkali basalts, analcitites or nephelinites normalized to the average basanite concentrations. These patterns allow direct comparison between the average compositions of the different groups of lavas and the average composition of the basanites. For example, the nephelinite / basanite pattern highlights lower proportion of Rb and Ba relative to Cs and Th in the nephelinites compared to the basanites.*

(Fig. 9b). In addition to the progressive enrichment of the most incompatible trace elements, the comparative nephelinite / basanite pattern shows a stronger depletion of Rb and Ba relative to Cs and Th in the nephelinites than in the basanites (Fig. 9b), which is confirmed by their lower Rb/Cs and Ba/Th ratios (Table 3 and Fig. 10a, b). The comparative pattern also indicates a slight depletion of Nb and Ta relative to U and La, which is emphasized by lower Nb/U and La/Ta ratios in nephelinites compared to basanites (Table 3 and Fig. 10c,d). It reveals also stronger depletion of K relative to Ta and La, stronger enrichment of Pb relative to Pr and Nd, and a pronounced depletion of Ti relative to Eu and Gd in the nephelinites (Fig. 9b). These differences are confirmed in Table 3 and Fig. 10 because the nephelinites have distinctively lower K/Ta and K/La ratios, slightly lower Pr/Pb ratios, as well as lower Ti/Eu and Ti/Gd ratios compared to the basanites. Finally, the comparative nephelinite / basanite pattern highlights a slight depletion of Hf relative to Zr and Sm in the nephelinites (Fig. 9a and 9b), which is confirmed by the higher Zr/Hf and Hf/Sm ratios of the nephelinites (Table 3 and Fig. 10g, h).

Table 3: Average values of trace element ratios for each group of lavas.

	Alkali basalt	Basanite	Analcitite	nephelinite
Ba / Rb	12.8	11.7	12.1	12.5
Th / U	4.07	4.09	4.17	4.29
Nb / Ta	17.9	17.8	18.9	18.3
Sr / Nd	15.0	15.0	14.0	14.7
Rb / Sr	0.035	0.042	0.043	0.042
La / Yb	19.8	22.0	45.9	48.2
Sm / Yb	3.69	4.18	6.46	5.56
La / Sm	5.37	5.29	7.15	8.70
Sm / Gd	1.16	1.16	1.24	1.27
Gd / Yb	3.18	3.60	5.22	4.37
La / Th	8.53	8.82	7.83	6.88
Rb / Cs	101	115	91.3	74.07
Ba / Th	54.0	59.3	46.0	36.48
Nb / U	54.5	57.6	46.4	43.30
La / Ta	11.4	11.2	13.4	12.47
K / Ta	1778	1992	1703	1317
K / La	156	179	128	105
Ce / Pb	29.8	33.2	33.4	24.5
Pr / Pb	3.49	3.93	3.77	2.69
Zr / Hf	44.6	43.52	47.8	52.3
Sm / Hf	1.61	1.62	1.86	1.74
Ti / Eu	6854	7471	4817	3867
Ti / Gd	2446	2662	1767	1435

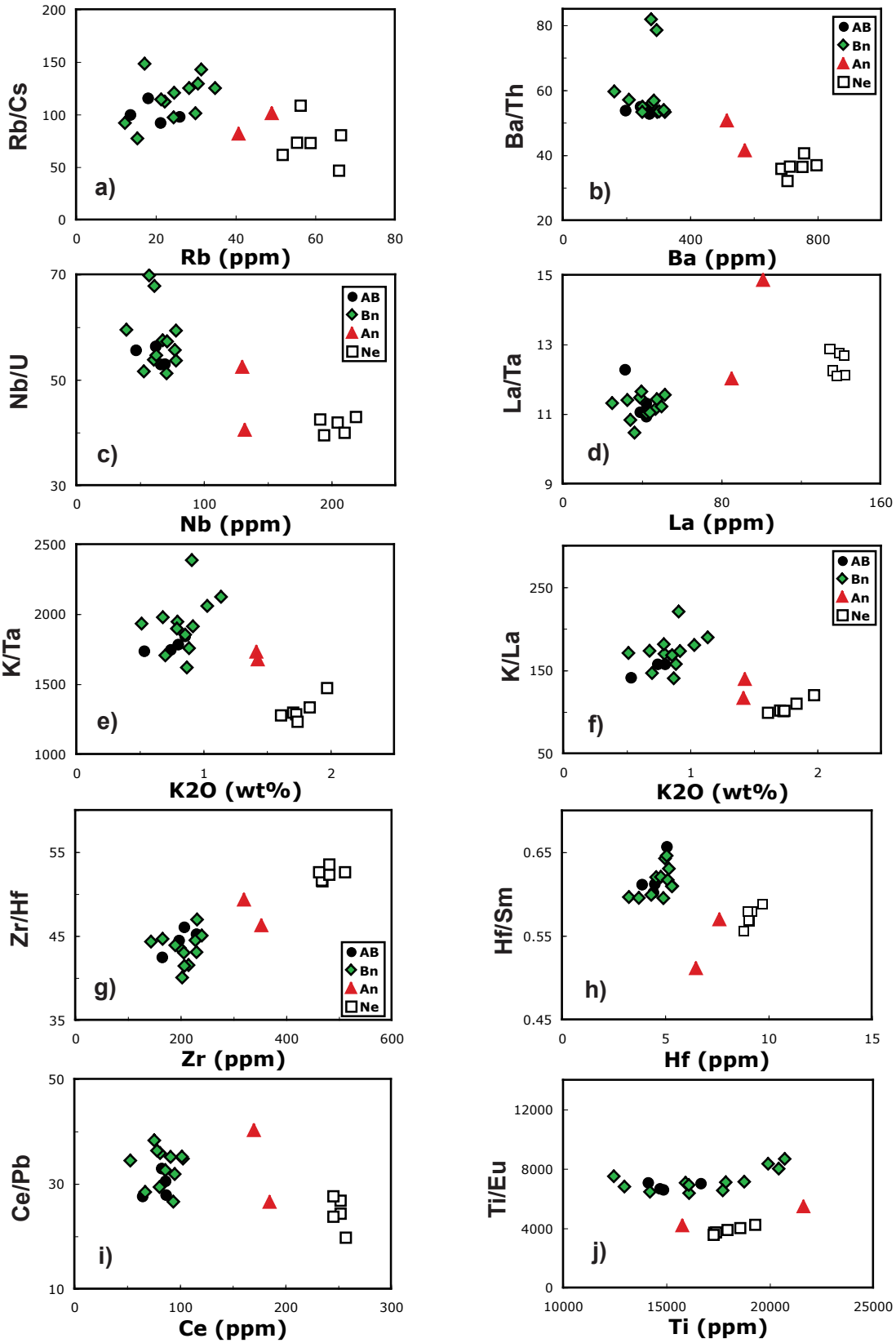

Fig. 10: *Plots of various incompatible element ratios as a function of the most incompatible element, emphasizing progressive depletion of Rb and Ba relative to Cs and Th (Fig 10 a and b), of Nb and Ta relative to U and La (Fig. 10c and d), of K relative to Ta and La (Fig. 10e and f), of Hf relative to Zr and Sm (Fig. 10g and h). Fig. 10j emphasize the progressive enrichment of Pb relative to Ce with enrichment of lavas compositions and Fig. 10j emphasize the similar Ti content in all the lava types despite progressive enrichment of Eu from alkali basalts and basanites to nephelinites.*

Analcitites have intermediate compositions between basanites and nephelinites, with trace element abundances from 1 up to 2.6 times higher than abundances in basanites (Fig. 9b). As for the nephelinites, the comparative analcitites / basanites pattern of Fig. 9b and the trace element ratios reported in Table 3 and Fig. 10 suggest a relative depletion of Rb, Ba, Nb, Ta, K, Hf and Ti and relative enrichment of Pb in analcitites compared to basanites. The relative depletion of Rb, Ba, K and Ti as well as the relative enrichment of Pb are less pronounced in the analcitites compared to the nephelinites, which is confirmed by intermediate values of Ba/Th, K/Ta, Pr/Pb and Ti/Eu ratios between those of the basanites and the nephelinites (Table 3 and Fig. 10). However, the analcitite values of Nb/U and Hf/Sm ratios are similar, or even slightly lower than the nephelinite values, emphasizing a similar amount of depletion in Nb, Ta and Hf in these two rock types.

5. The role of petrogenetic processes

The Tubuai lavas series analyzed in this study have homogeneous Sr, Nd and Hf isotopic compositions confirming the cogenetic nature of the different mafic rocks from Tubuai Island (Fig. 3). However, these different rock types are clearly distinguished by their major and trace element abundances, indicating a range of possible parental lava compositions. The effect of the different petrogenetic processes on the lava compositions is examined in the following in order to understand which mechanisms cause the observed variations.

5.1 The effect of fractional crystallization

Fractional crystallization of clinopyroxene and olivine affected the major element compositions of the alkali basalt, basanites and analcitites. The limited range of compositions displayed by the nephelinites (in this study and other study as well) is not sufficient to geochemically constrain the dominant mineral phases removed from the nephelinitic magmas. However, clinopyroxene, olivine and titanomagnetite are the dominant phenocrysts in these lavas, similarly to the alkali basalts and basanites (see paragraph 2, and Brousse and Maury, 1980; Maury et al., 1994)). Thus, the mineral assemblage clinopyroxene ± olivine ±

titanomagnetite is most likely to represent the dominant crystallizing phases in all the mafic lavas from Tubuai.

Fig. 6 shows that, for a given MgO content, analcitites and particularly nephelinites have distinctively higher Na_2O contents (and also higher K_2O, P_2O_5 and MnO contents, not shown in Fig. 6) and distinctively lower SiO_2 and CaO contents compared to alkali basalts and basanites. Higher proportions of clinopyroxene in the mineral assemblage of the nephelinitic magmas would decrease, as observed, the CaO, SiO_2 and Sc contents and increase the Na_2O contents of the lavas (Fig. 6). However, the total amount of fractionated minerals required to produce the observed variations in alkali contents is incompatible with the other major element concentrations. For example, at least 70% of clinopyroxene fractionation would be required for a basanite with 12% MgO to reach the Na_2O contents of the nephelinites, but only 30 % of clinopyroxene fractionation would be required to reach the CaO contents (see paragraph 6.1 for the calculations). This indicates that first, other processes than fractional crystallization alone must be involved, and second, that the nephelinites and analcitites cannot be derived by fractional crystallization from the same parental magmas than the basanites and alkali basalts.

5.2 Decreasing degree of partial melting

The early alkali basalt flows are likely to be produced by similar degrees of partial melting than the basanitic flows because these two rock types display a similar range of trace element concentrations (Fig. 7). As suggested in previous studies on Tubuai lavas (Dupuy et al., 1988; Vidal et al., 1989; Maury et al., 1994), the regular increase in incompatible trace element concentrations and ratios (e.g. La/Sm or La/Yb) with increasing alkali contents in the younger lavas further suggests a decrease in the degree of partial melting during the late volcanic events of Tubuai (Fig. 5 and 7).

It is, however, more difficult to explain variations in ratios of highly incompatible elements such as Ba/Th, Nb/U or K/La that should be little affected by different extends of partial melting. One possible way to explain variations in such incompatible element ratios is the role of residual phases that preferentially incorporate one or several elements that are usually highly incompatible during partial melting of typical mantle mineral assemblages.

5.3 Minor phases in the mantle source?

In the Tubuai lavas, variations in Ba/Th and Cs/Rb ratios show a significant depletion of Rb and Ba relative to Cs and Th in the analcitites, and particularly in the nephelinites, compared to the early alkali basaltic and basanitic lavas. This indicates that the compatibility of Rb and Ba increased compared to those of Cs and Th with decreasing degree of partial melting. Similarly, the progressive depletions of Nb and Ta relative to U and La, of K relative to Ta and La, of Hf relative to Zr and Sm and of Ti relative to Eu and Gd pointed out by the comparative trace element patterns (Fig. 9b) indicate an increasing compatibility of Nb, Ta, K, Hf, and Ti with decreasing degree of partial melting.

The occurrence of residual phlogopite at low degrees of partial melting has previously been suggested to explain the pronounced K depletion in the Tubuai lavas (Chauvel et al., 1992). In our lava suites, the K depletion increases from the basanites to the nephelinites, suggesting that a K-rich phase may have played a role during early stages of partial melting and disappeared at larger extent of partial melting. Phlogopite is rich in Rb and Ba and contains small amounts of titanium. Consequently, the presence of phlogopite in the mantle source of the Tubuai lavas may have influenced the observed variations in K, Rb and Ba between the different lava groups. Some Ti-rich amphiboles also have higher partition coefficients for K, Rb and Ba compared to other highly incompatible elements (Adam et al., 1993; Latourette et al., 1995; Adam and Green, 2003). However, compared to phlogopite, the absolute values of the partition coefficients are significantly lower in amphibole ($D_{K, Rb, Ba\ (amphibole/basanitic\ melt)} < 0,5$ and $D_{K, Rb, Ba\ (phlogopite/basanitic\ melt)} = 1\text{-}7$; Adam et al., 1993; Latourette et al., 1995; Adam and Green, 2006) so that considerable amounts of amphibole in the source would be necessary to generate the observed K, Rb and Ba variations. In addition, amphibole is not stable beyond lithospheric mantle conditions (Class and Goldstein, 1997), while phlogopite might be more stable at asthenospheric pressures (Foley, 1993).

While the presence of residual phlogopite could explain the Ba, Rb and K variations, it cannot account for the increasing compatibility of Nb, Ta, Hf and Ti. Especially the observed buffering of the Ti concentrations suggests the additional presence of a Ti-rich phase with high partition coefficient values for the high field strength elements (HFSE) Nb, Ta, Hf and Zr. This Ti-rich phase could either be rutile or ilmenite, which are Ti-bearing phases with relatively high partition coefficients for the HFSE (Mccallum and Charette, 1978; Green, 2000; Bennett et al.,

2004; Klemme et al., 2006). In the following, we quantitatively investigate the influence of minor abundances of phlogopite and rutile / ilmenite on the trace element composition of the Tubuai lavas.

6. Modeling the genesis of Tubuai magmas

6.1 Correction for fractional crystallization

Although the selected samples have relatively primitive compositions, i.e. they have high MgO contents, the effect of fractional crystallization on the trace element concentrations is significant, particularly for the nephelinites. The HREE behave compatibly during partial melting of garnet-bearing sources and are not very sensitive to small variations (or tend to be less abundant by large variations) in the degree of partial melting. Thus, on the basis of the isotopic evidence that all mafic lavas from Tubuai are derived from a similar mantle source, the parental compositions of the different lava types should have similar HREE abundances (at least in Er, Yb and Lu). Therefore, the observed enrichment of the HREE in the nephelinites compared to the basanites is most likely caused by fractional crystallization (Fig. 9a) and the composition of these lavas needs to be corrected before modeling partial melting processes.

The method of Hofmann and Feigenson (1983) is used to correct the trace element abundances of the nephelinites for fractional crystallization effects. This method involves, in a first step, to calculate the amount of mineral phases removed from the major element composition of a primary magma, and subsequently to calculate the trace element contents of the inferred parental magma using the Rayleigh fractionation law:

$$C^i_m / C^i_{mo} = F_m^{D-1}$$

where C^i_m is the measured concentration of element i, C^i_{mo} is the concentration of element i in the primary magma, F_m is the fraction of residual liquid and D the bulk partition coefficient ($D = F_\alpha D^i_\alpha + F_\beta D^i_\beta + \ldots$ with D^i_α the partition coefficient between mineral α and melt for element i and F_α the fraction of mineral α).

The basanite sample TB115, containing 12.5% MgO, is considered to be the most likely candidate for a near-parental melt composition for the basanites. Assuming that the parental magma of the nephelinites has similar HREE abundances than TB115, its trace element composition is estimated by adding variable amounts of clinopyroxene and olivine to the average nephelinite composition until the HREE abundances match those of TB115. Fig. 11a shows the calculated trace element patterns using different proportions of clinopyroxene and olivine and the partition coefficients between mineral and melt reported in Table 4. The best match is obtained using a mineral assemblage consisting of 30% clinopyroxene and 10% olivine.

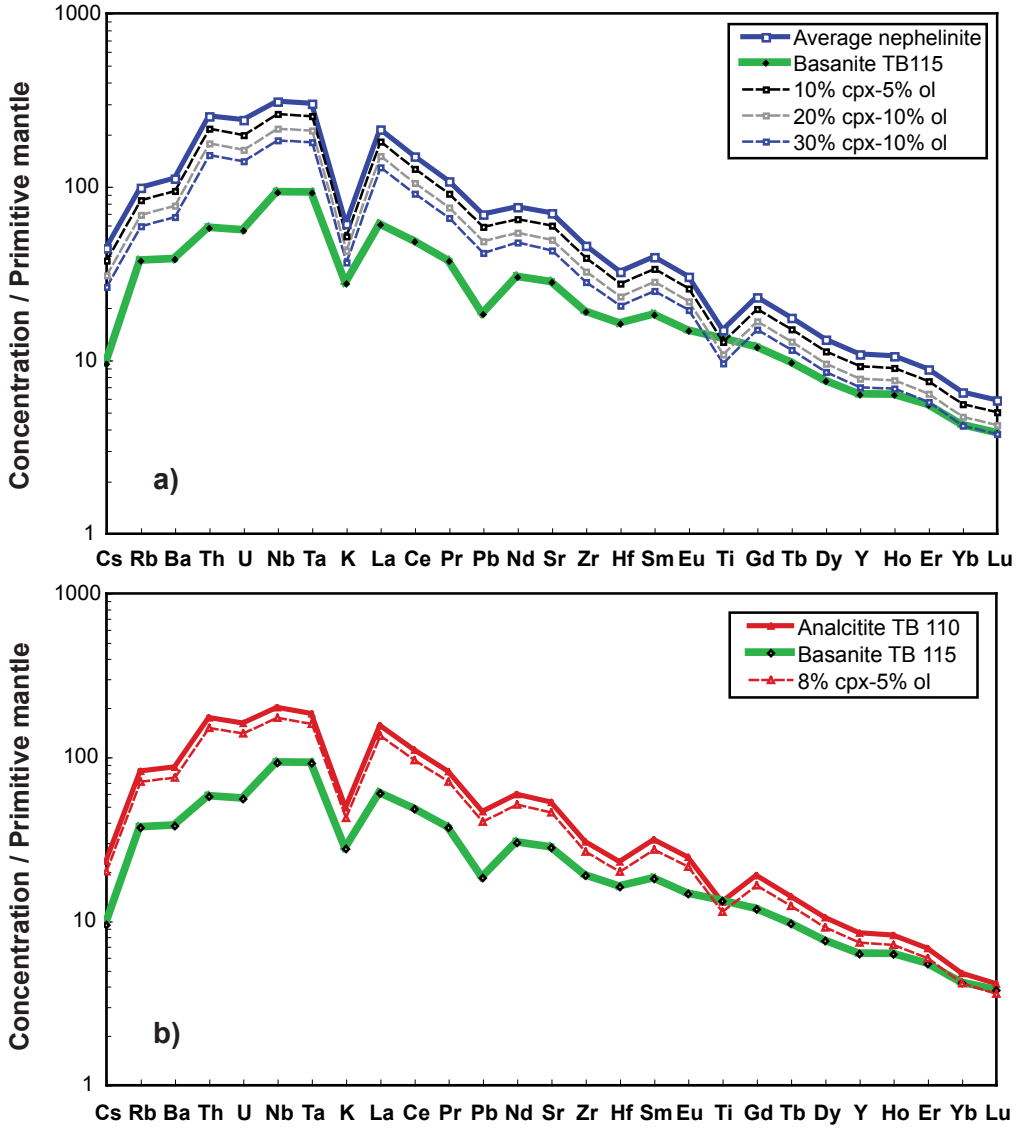

Fig. 11: *Trace element patterns showing the effects of trace element correction for fractionation using different mineral assemblages (see text).* ***a)*** *The HREE contents of the average nephelinite pattern reach the HREE contents of the basanite TB115 when adding 30% clinopyroxene and 10% olivine to the average nephelinite composition. This corrected composition may be a good estimation of a primary melt composition for the nephelinites.* ***b)*** *The HREE contents of the analcitite TB110 reach those of the basanite TB115 when adding 8% clinopyroxene and 5% olivine to its composition.*

Table 4: Partition coefficients between mineral and melt used to model fractional crystallization (1 GPa) and partial melting (3 GPa) processes.

	D olivine/melt 1GPa a	D Cpx/melt 1GPa a	D olivine/melt 3 Gpa b	D opx/melt 3 Gpa b	D Cpx/melt 3 Gpa b	D Garnet/melt 3 Gpa b	D Phlogopite/melt 2.7 Gpa c	D Ilmenite/melt 3 Gpa d	D Rutile/melt 3 Gpa e
Rb	0.0004	0.00008	0.0003	0.0002	0.0004	0.0002	4.5	0	0
Sr	0.001	0.111	0.00004	0.0007	0.091	0.0007	0.16	0.005	0
Y	0.003	0.51	0.018	0.05	0.2	2	0.003	0.029	0
Zr	0.002	0.2	0.0005	0.014	0.09	0.27	0.012	0.78	2.1
Nb	0.00007	0.005	0.0005	0.004	0.01	0.015	0.055	1.9	6.1
Cs	0.0002	0.00007	0.0015	0.0001	0.0025	0.0001	0.004	0	0
Ba	0.0001	0.00015	0.000005	0.000006	0.0004	0.00007	3.1	0	0
La	0.0001	0.07	0.0005	0.004	0.02	0.0007	0.0004	0	0
Ce	0.001	0.12	0.0005	0.004	0.05	0.02	0.0003	0.0047	0
Pr	0.002	0.18	0.0005	0.008	0.07	0.03	0.0006	0	0
Nd	0.003	0.27	0.00042	0.012	0.1	0.064	0.0009	0	0
Sm	0.002	0.42	0.0011	0.02	0.16	0.3	0.0007	0.0051	0
Eu	0.0005	0.48	0.0011	0.06	0.16	0.4	0.0007	0	0
Gd	0.0011	0.54	0.0011	0.065	0.16	1	0.0007	0.007	0
Tb	0.004	0.56	0.00324	0.065	0.165	1.2	0.0007	0	0
Dy	0.007	0.56	0.0027	0.065	0.17	2	0.0007	0	0
Ho	0.009	0.55	0.008	0.065	0.175	2.5	0.0009	0	0
Er	0.0132	0.5	0.013	0.065	0.18	3	0.0012	0	0
Yb	0.05	0.47	0.02	0.08	0.25	5.5	0.035	0	0
Lu	0.041	0.43	0.02	0.12	0.276	7	0.0017	0.16	0
Hf	0.004	0.42	0.0022	0.024	0.14	0.4	0.015	1	3.1
Ta	0.0004	0.021	0.0005	0.004	0.01	0.015	0.062	2.3	**7**
Pb	0.001	0.008	0.003	0.009	0.009	0.005	0.089	0	0
Th	0.0003	0.007	0.00005	0.002	0.006	0.009	0.0004	0.0006	0
U	0.0003	0.006	0.00038	0.002	0.011	0.028	0.0033	0.006	0
K	0.00002	0.001	0.00002	0.0001	0.001	0.013	**8**	0	0
Ti	0.015	0.46	0.015	0.086	0.14	0.6	1	**20**	**39**

a: partition coefficients between mineral and basanitic melt under 1 GPa reported in Adam et al. (2006); b: partition coefficients between mineral and silicate melt under 3 GPa reported in Salters and Stracke. (2004);

c: partition coefficients between phlogopite and basanitic melt under 2.7 GPa reported in Adam et al. (2006); d: partition coefficients between ilmenite and basaltic melt reported in Klemme et al (2006), except for Ti (see te

e: partition coefficients between rutile and basaltic melt under 3 Gpa reported in Green et al. (2000), except values for Ta and Ti (see text).

It is now possible to estimate the primary composition in major element associated with the removal of this mineral assemblage, and thereby verify the relevance of our calculations. In addition, the effects of small amounts of titanomagnetite fractionation (see paragraph 5.1), although negligible for most other trace element concentrations, should be significant on titanium and need to be taken into account. According to petrographic descriptions of Tubuai lavas (Brousse and Maury, 1980; Caroff et al., 1997), a maximum amount of 1% titanomagnetite is likely to have fractionated from the nephelinitic magmas and is added to the previous mineral assemblage in our calculations. Using the composition of clinopyroxene, olivine and titanomagnetite phenocrysts in nephelinites reported by Brousse and Maury (1980) (see Table 5), the major element composition of the parental nephelinitic magma is determined for each oxide considering that:

$$C^x_{mo} = C^x_m F_m + C^x_{cpx} F_{cpx} + C^x_{ol} F_{ol} + C^x_{Ti\text{-}mg} F_{Ti\text{-}mg}$$

with C^x_{mo} being the proportion of oxide x in the primary melt and C^x_m the proportion of oxide x in the average nephelinite composition. The resulting major and trace element composition of the primary nephelinite is reported in Table 5. This calculated parental nephelinite has very similar SiO_2, TiO_2, MnO and MgO concentrations compared to TB115, but has lower Al_2O_3 and higher FeO, CaO and particularly Na_2O, K_2O and P_2O_5 contents (Table 5). This shows that our calculations lead to reasonable parental lava compositions and also confirms the earlier conclusion that the nephelinites and basanites are derived from different parental magmas.

In a similar fashion, a parental analcitite composition was obtained by adding a mineral assemblage of 8% clinopyroxene and 5% olivine to the composition of the analcitite sample TB110 (Fig. 11b). The primitive composition of this sample (11% MgO) infers no or negligible amount of titanomagnetite fractionation. The resulting major and trace element composition of the primary analcitite is reported in Table 5. This composition is similar to that of the parental nephelinite, indicating that these two lava types are derived from similar parental magmas. Slight differences are observed for the HFSE and Rb, Ba, K and MREE (Fig. 12). We note, however, that the incompatible trace element concentrations of the analcitite sample TB124, which has similar MgO content than the nephelinites (7 - 8 wt.%), are not only distinctively lower than the nephelinite compositions (Fig. 7), but are also lower than those of the analcitite

Table 5: Phenocryst compositions used and calculated primary melt composition for the analcitic and nephelinitic magmas. The basanite sample TB115 is reported here for comparison.

	phenocrysts compositions reported in Brousse et al. (1980)					calculated primary melt		
Sample	**107s (1)**	**110y (1)**	**Tu 4**	**Tu 4**	**Tu 4**			**TB115**
rock type	analcitite	analcitite	nephelinite	nephelinite	nephelinite	analcitite	nephelinite	basanite
mineral	**Cpx**	**Olivine**	**Cpx**	**Olivine**	**magnetite**			
SiO_2	48.43	39.1	50.83	37.98	-	42.7	43.9	44.1
TiO_2	1.76		1.93	-	22.91	2.43	2.58	2.66
Al_2O_3	4.35		3.81	-	0.22	11.4	8.84	12.1
Fe_2O_3	2.89		-	-	23.31	1.52	1.19	1.42
FeO	8.73	19.3	6.56	23.02	49.84	12.1	12.6	11.5
MnO	0.20		0.17	-	0.13	0.222	0.224	0.204
MgO	10.04	41.9	12.73	37.55	1.14	12.5	12.2	12.56
CaO	22.05		23.27	-	0.91	11.0	12.7	12.0
Na_2O	0.90		0.56	-	0.13	4.15	4.12	2.31
K_2O	0.08		-	-	-	1.24	1.04	0.797
P_2O_5			-	-	-	0.769	0.593	0.398
X Cpx *						0.08	0.3	
X ol *						0.05	0.1	
X Ti-mg *							0.01	
Rb						39.6	34.6	22.3
Sr						965	960	557
Y						30.3	30.3	27.1
Zr						301	305	199
Nb						114	122	60.8
Cs						0.535	0.535	0.199
Ba						486	433	251
La						92.9	92.9	39.0
Ce						161	162	80.7
Pr						17.3	17.3	9.43
Nd						62.0	62.0	37.5
Sm						10.2	10.2	7.37
Eu						3.05	3.05	2.26
Gd						8.01	8.01	6.43
Tb						1.16	1.16	0.952
Dy						5.80	5.80	5.09
Ho						1.03	1.03	0.936
Er						2.59	2.59	2.40
Yb						1.85	1.85	1.85
Lu						0.250	0.250	0.255
Hf						5.94	6.19	4.57
Ta						6.16	6.63	3.40
Pb						6.70	6.66	2.75
Th						12.0	12.0	4.57
U						2.79	2.79	1.13

*: fraction of the different phases in the mineral assemblage estimated to have been removed from the primary magma calculated. Cpx = clinopyroxene, ol = olivine, Ti-mg = titanomagnetite.

TB110 (with 11% MgO). This suggests that the analcitites have been generated by slightly variable extends of partial melting.

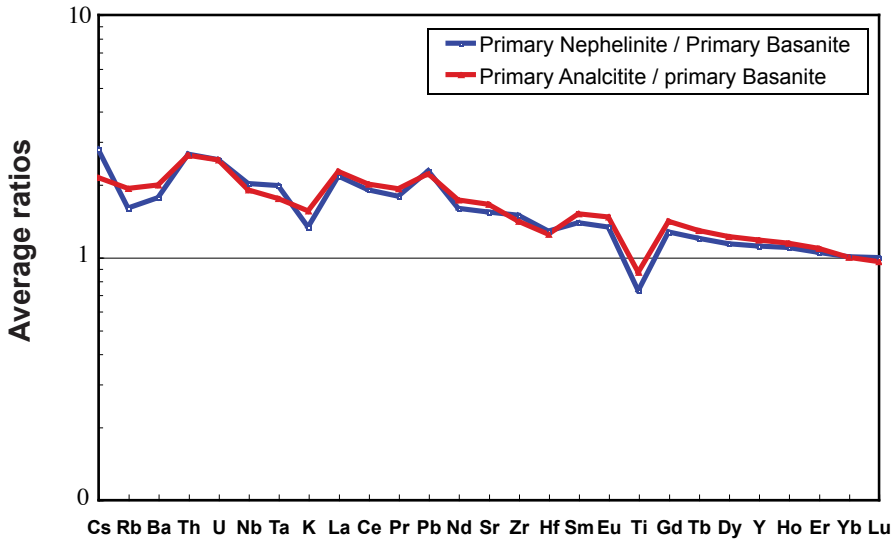

Fig. 12: *Comparative trace element patterns between the estimated primary compositions either of analcitites or nephelinites and the estimated primary composition of basanites. Discrepancies between the estimated primary nephelinite and basanite compositions on one hand, and between estimated primary analcitite and basanite compositions on the other hand, show similar enrichment of incompatible elements. This indicates a similar degree of partial melting during formation of the analcitic and nephelinitic magmas. However, the relative depletion of Rb, Ba and K is less pronounced and the relative depletion of Nb and Ta is more pronounced in the primary analcitite composition than they are in the primary nephelinite composition.*

6.2 Variations in the degree of partial melting

In order to investigate the effects of variable degrees of partial melting and the potential role of minor K- and Ti-bearing phases, the source composition of basanites is calculated in a first step, assuming that TB115 has been produced by moderate degrees of partial melting (5 - 8%) from a typical garnet-peridotite (the source, melting mode and the bulk partition coefficients are taken from Salters and Stracke (2004)). With the assumption of constant partition coefficient values during partial melting processes, the trace element composition of the basanite source is calculated using the equation for accumulated fractional melting from Shaw (1970):

$$C^i_{mo} = C^i_o / F * [1-(1- P^i * F / D^i_o)]$$

where C^i_{mo} is the concentration of element i in the primary melt, C^i_o is the concentration of element i in the source, D^i_o is the bulk partition coefficient of element i in the source such as

$D^i_o = F_{\alpha o}D^i_\alpha + F_{\beta o}D^i_\beta + \ldots$ with $F_{\alpha o}$ the fraction of mineral α in the source and D^i_α the partition coefficient between mineral α and melt under ~ 3 GPa, F is the fraction of melt produced and P^i is the bulk partition coefficient of element i in the melt such as $P^i = F_{\alpha m}D^i_\alpha + F_{\beta m}D^i_\beta + \ldots$ with $F_{\alpha m}$ the fraction of mineral α entering the melt.

Thereafter, in an attempt to reproduce the general shape of the primary analcitite and nephelinite patterns, a range of melt compositions is calculated from the inferred source composition of the basanite using the same parameters as in the calculation above but smaller degrees of melting (1 - 5%). The closest match is obtained for F ~ 7 - 8% melting for the basanites and F = 3 % melting for the analcitites and nephelinites (Fig. 13).

These calculated melting patterns also show that decreasing degree of melting generates a progressive enrichment of Pb relative to Pr and Nd, which is due to lower partition coefficient values of Pb in the peridotite minerals compared to those of Pr and Nd. On another hand, these results confirm that the depletion of Rb, Ba, Nb, Ta, K and Ti relative to their respective neighbors in the patterns cannot be produced by variable degrees of a simple four phase garnet peridotite (Fig. 13) and thus require the presence of additional minor phases.

6.3 Residual phlogopite and rutile/ilmenite

Adding small quantities of phlogopite to the source considerably increases the bulk partition coefficients for Cs, Rb, Ba and K, and also slightly increases the bulk partition coefficient for Ti (partition coefficient values for phlogopite-melt are taken from Adam and Green (2006) and assuming a $D_{phlogopite/melt} = 8$ for K; Table 4). About 1% of residual phlogopite is required to reproduce the Rb, Ba and K contents of the primary nephelinite pattern (Table 6 and Fig. 13a). The primary analcitite pattern has slightly higher Rb, Ba and K contents compared to the nephelinite pattern (Fig. 12), so that even lower amounts of phlogopite in the source (0.7%) are sufficient (Table 6 and Fig. 15a). This emphasizes the sensitivity of Rb, Ba and K to this mineral phase and indicates that variability in Cs, Rb, Ba and K concentrations can be caused by almost minute variations in the abundance of residual phlogopite.

Although residual phlogopite has a substantial effect on the bulk alkali element partition coefficients, it does not significantly influence the bulk partition coefficients of the HFSE. As indicated by the apparent buffering of Ti during petrogenetic processes, an additional Ti-bearing phase with high partition coefficient values for the HFSE is required. This could either be rutile

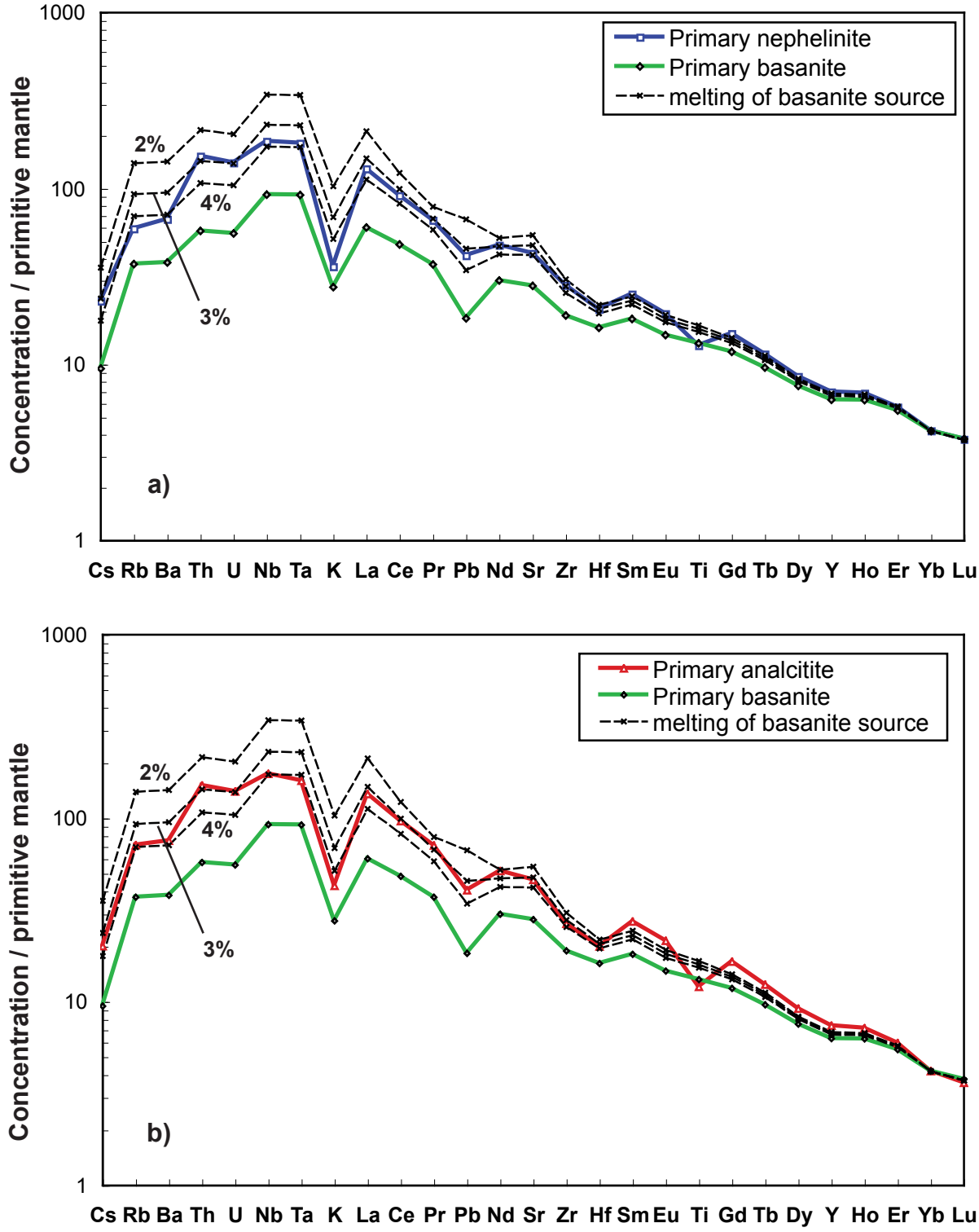

Fig. 13: *Garnet peridotite melting model. Calculated melting patterns of the basanite source, supposing that the basanitic melts were formed by 7.5% melting of a garnet peridotite and using parameters of Table 4 and 6. The primary nephelinite pattern in* ***a)*** *and the primary analcitite pattern in* ***b)*** *are most closely matched by 3% melting of the basanite source. The Rb, Ba, Nb, Ta, K and Ti contents of the primary nephelinite and analcitite patterns are, however, not reproduced, showing that the relative depletion of these elements in these lavas are not generated by a simple decrease in the degree of melting. On the other hand, the relative Pb enrichment in the analcitites and nephelinites compared to the basanites is reproduced when decreasing the degree of partial melting in the lavas.*

or ilmenite. In order to investigate the possible role of each of these phases on Tubuai lavas composition, the partitioning of Ti between rutile / melt and between ilmenite / melt need to be estimated.

Rutile is a titanium oxide, constituted of nearly 100% TiO_2 (Ionov et al., 1999; Xiong et al., 2005). Therefore, a maximum partition coefficient value for Ti between rutile and melt can be estimated such as:

$$D^{Ti}_{rutile/melt} = C^{Ti}_{rutile} / C^{Ti}_{melt} = C^{TiO2}_{rutile} / C^{TiO2}_{melt} = 100 / C^{TiO2}_{melt}$$

Considering the average value of 2.56 % TiO_2 content for the primary melt calculated above (Table 6),

$$D^{Ti}_{rutile/melt} = 100 / 2.56 = 39$$

On the other hand, ilmenite contains around 50% TiO_2 (Ionov et al., 1999; Klemme et al., 2006) and maximum partition coefficient value for Ti between ilmenite and melt can be estimated such as:

$$D^{Ti}_{ilmenite\ /\ melt} = 50 / 2.56 = 20$$

Having calculated these partitioning values for Ti, the effects of small quantities of each of these phases in the source are evaluated using the partition coefficient for HFSE of Green (2000) and Klemme et al. (2006), respectively, which are reported in Table 4. About 0.6% of residual ilmenite is required to reproduce the Ti and HFSE contents of the primary nephelinite pattern (Table 6 and Fig. 14b). The primary analcitite pattern has slightly lower HFSE contents compared to the nephelinite pattern (Fig. 12), so that slightly higher amounts of ilmenite in the source (0.8%) are necessary (Table 6 and Fig. 15b). On the other hand, only 0.2% of residual rutile is necessary to reproduce the Ti, Nb, Hf and Zr contents of the primary nephelinite pattern and 0.25% of residual rutile reproduces those of the primary analcitite pattern (Table 6 and Fig. 14c and 15c). The $D^{Ta}_{rutile/melt}$ of 14 proposed by Green (2000) seems, however, too high to match the Ta content of both primary lava compositions. As the Nb/Ta ratio do not vary significantly in the Tubuai lavas (Table 3), a $D^{Ta}_{rutile/melt}$ of ~ 7, more similar to the $D^{Nb}_{rutile/melt}$, would be required to reproduce the Ta variations in the lavas. This might argue against the presence of rutile in the source of Tubuai lavas as the $D^{Ta}_{rutile/melt}$ is often reported to be

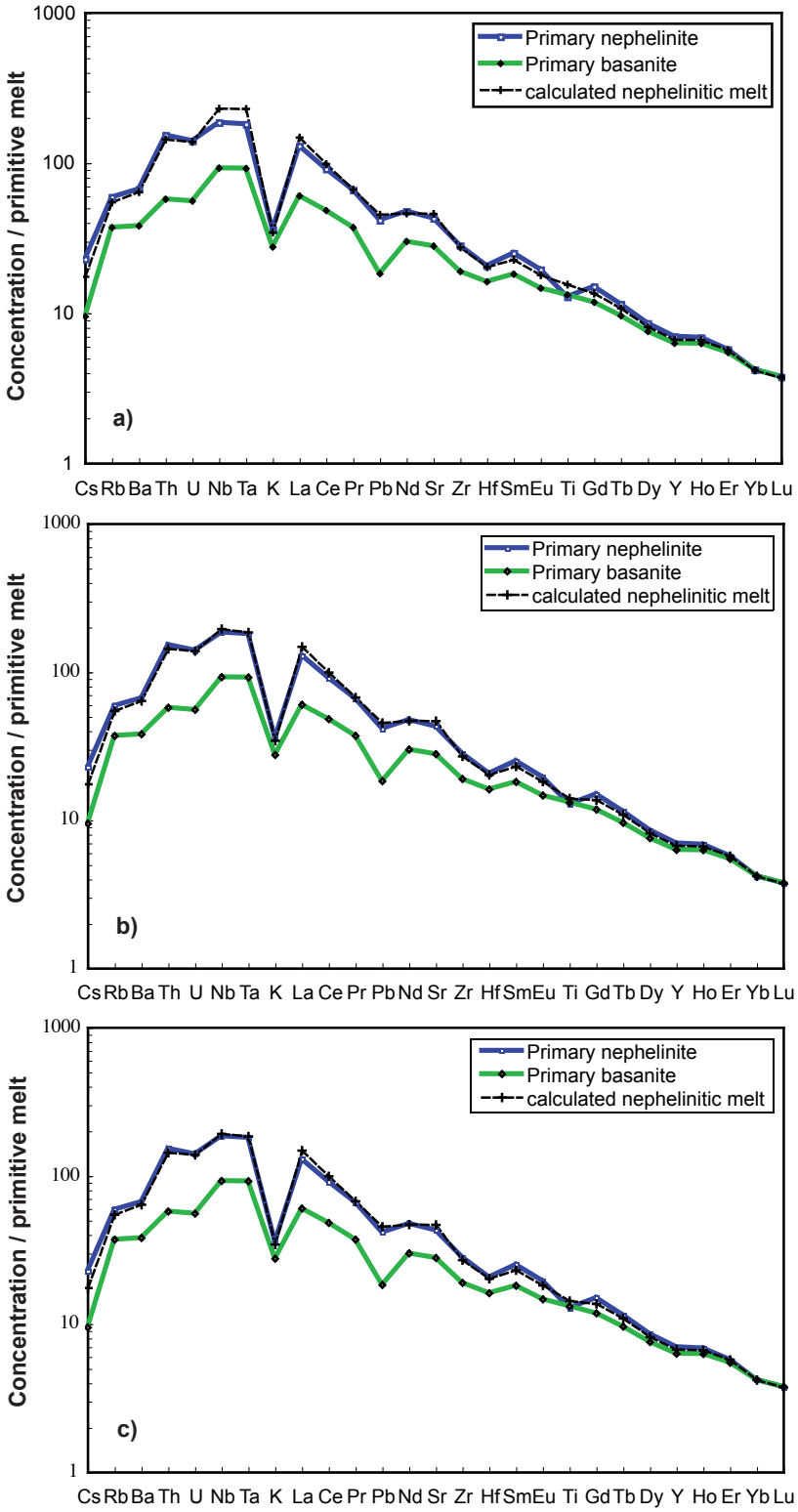

Fig. 14: *Calculated melting patterns of the basanite source, supposing F = 7.5% melting for the basanitic magma and F = 3% melting for the nephelinitic magma.* ***a)*** *1% phlogopite is added to the basanitic source and is residual during the production of the nephelinitic magma. The Rb, Ba and K contents of the nephelinite pattern are now reproduced.* ***b)*** *1% phlogopite and 0.6 % ilmenite are added to the basanitic source and are residual during the production of the nephelinitic magma. These mall amounts of ilmenite reproduce the HFSE and Ti contents of the nephelinite pattern.* ***c)*** *1% phlogopite and 0.2 % rutile are added to the basanitic source and are residual during the production of the nephelinitic magma. The HFSE and Ti contents of the primary nephelinite pattern are also well reproduced.*

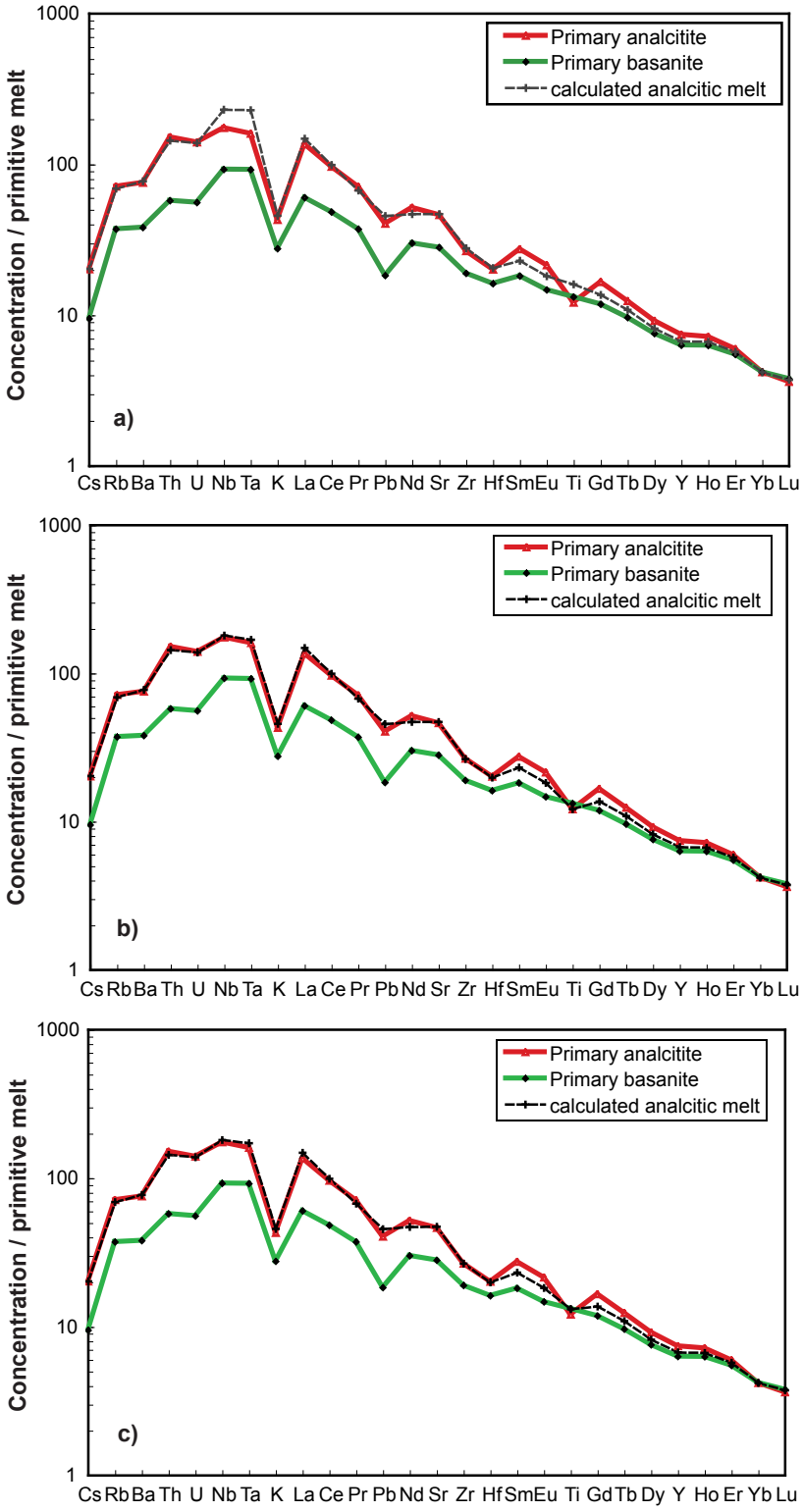

Fig. 15: *Calculated melting patterns of the basanite source, supposing F = 7.5% melting for the basanitic magma and F = 3% melting for the analcitic magma.* ***a)*** *The Rb, Ba and K contents of the analcitite pattern are well reproduced when supposing 0.7% residual phlogopite.* ***b)*** *The HFSE and Ti contents of the analcitite pattern are well reproduced for 0.8 % residual ilmenite.* ***c)*** *The HFSE and Ti contents of the analcitite pattern are also well reproduced for 0.25 % residual rutile.*

significantly higher than the $D^{Nb}_{rutile/melt}$ in the literature (Jenner et al., 1993; Green, 2000; Schmidt et al., 2004; Xiong et al., 2005). In addition, rutile is most often present in mafic rocks or metasomatized peridotites and might not be stable in ultramafic rocks. However, the stability of rutile in mantle rocks and the partitioning of HFSE between rutile and silicate melt is not really well constrained and the presence of small quantities of rutile in the source of Tubuai lavas cannot be entirely rule out.

Table 6: Primary melt norms and source norms used in the model

Rock type	Basanite	Analcitite	nephelinite		Basanite	Analcitite	nephelinite
F	0.075	0.03	0.03		0.075	0.03	0.03
melt mode				melt mode			
olivine	0.05	0.05	0.05	olivine	0.05	0.05	0.05
opx	-0.49	-0.49	-0.49	opx	-0.49	-0.49	-0.49
cpx	1.294	1.31	1.31	cpx	1.298	1.31	1.31
garnet	0.13	0.13	0.13	garnet	0.13	0.13	0.13
phlogopite	0.01	0	0	phlogopite	0.01	0	0
ilmenite	0.006	0	0	rutile	0.002	0	0
source mode				source mode			
olivine	0.514	0.515	0.514	olivine	0.518	0.5205	0.518
opx	0.08	0.08	0.08	opx	0.08	0.08	0.08
cpx	0.34	0.34	0.34	cpx	0.34	0.34	0.34
garnet	0.05	0.05	0.05	garnet	0.05	0.05	0.05
phlogopite	0.01	0.007	0.01	phlogopite	0.01	0.007	0.01
ilmenite	0.006	0.008	0.006	rutile	0.002	0.0025	0.002

Both rutile and ilmenite have a strong influence on Nb, Ta and Ti abundances (and those of Hf and Zr in a lesser extent) and the addition of very small quantities of either of these phases in the source reproduce the variations in Nb, Ta and Ti observed within the Tubuai lavas. Consequently, variations in compatibility of Rb, Ba, K, HFSE and Ti recorded in the Tubuai lavas can be explained by the presence of small quantities of phlogopite (0.7 – 1%) and small quantities of either ilmenite (0.6 – 0.8 %) or rutile (0.2 – 0.25 %) in the source. These minor phases may have been entirely consumed during generation of the early alkali basaltic and basanitic magmas but may have remained residual at the comparatively lower degrees of partial melting that lead the production of the analcitic and nephelinitic magmas.

7. Conclusions

This systematic study of the geochemical and isotopic variations within the Tubuai lavas confirms the cogenetic nature of the different mafic lavas from Tubuai Island. This new set of $^{87}Sr/^{86}Sr$ (0.70278 – 0.70284), $^{143}Nd/^{144}Nd$ (0.51289 – 0.51296) and $^{176}Hf/^{177}Hf$ (0.28292 – 0.28297) isotopic compositions also emphasize the very homogeneous signature of these HIMU-type OIB. Most of the geochemical variations observed in the lavas can further be explained by variations in the degree of partial melting followed by fractional crystallization processes. A progressive enrichment of incompatible elements in the lavas from old volcanics (alkali basalts and basanites) to younger volcanics (nephelinites) reflects a progressive decrease in the degree of partial melting towards late volcanic events. Analcitites and nephelinites are also relatively depleted in Rb, Ba, K, Nb, Ta and Ti compared to alkali basalts and basanites, which suggests the presence of residual phlogopite and a Ti-bearing phase (either ilmenite or rutile) during formation of the analcititic and nephelinitic magmas. In contrast, these minor phases are likely to have been consumed at the comparative higher degree of melting that lead to the formation of the early alkali basaltic and bananitic magmas.

The presence of these phases in the source of Tubuai lavas will need to be further understood. Phlogopite may reflect the presence of water in the source and these minor phases may have stabilized during initial stages of partial melting, then be consumed at sufficiently large extents of partial melting. Better constrains on the stability of rutile and ilmenite under upper mantle conditions and trace element partitioning in these phases would also help to constrain which Ti-bearing phase was present in the source of the Tubuai lavas.

References

Adam J. and Green T. (2003) The influence of pressure, mineral composition and water on trace element partitioning between clinopyroxene, amphibole and basanitic melts. *Eur.J.Mineral.* 15, 831-841.

Adam J. and Green T. (2006) Trace element partitioning between mica- and amphibole-bearing garnet lherzolite and hydrous basanitic melt: 1. Experimental results and the investigation of controls on partitioning behavior. *Contrib. Mineral. Petrol.* 152, 1-17.

Adam J., Green T. H. and Sie S. H. (1993) Proton microprobe determined partitioning of Rb, Sr, Ba, Y, Zr, Nb and Ta between experimentally produced amphiboles and silicate melts with variable F contents. *Chem. Geol.* 109, 29-49.

Barrat J. A., Keller F. and Amosse J. (1996) Determination of Rare Earth Elements in sixteen silicate reference samples by ICP-MS after Tm addition and Ion exchange separation. *Geostandards Newsletters* 20(1), 133-139.

Barsczus H. G., Guille G., Maury R., Chauvel C. and Guillou H. (1994) Two magmatic sources at Rurutu Island (Austral Islands, French Polynesia) and The Austral "hotline". *Eos Trans. AGU* 75(16, spring Meet. Suppl.), 3231.

Bellon H., Brousse R. and Pantaloni A. (1980) Ages de l'ile de Tubuai: l'alignement des Australes et des Cook. . *Cahiers Indo-Pacifique* 2(4), 219-240.

Bennett S. L., Blundy J. D. and Elliott T. (2004) The effect of sodium and titanium on crystal-melt partitioning of trace elements. *Geochim. Cosmochim. Acta* 68, 2335-2347.

Bonneville A., Le Suave R., Audin A., Clouard V., Dosso L., Gillot P. Y., Jannet P., Jordahl K. and Maamaatuaiahutapu K. (2002) Arago Seamount: The missing hotspot found in the Austral Islands. *Geology* 30, 1023-1026.

Brenan J. M., Shaw H. F., Ryerson F. J. and Phinney D. L. (1995) Mineral-aqueous fluid partitioning of trace elements at 900ºC and 2.0 GPa: Constraints on the trace element chemistry of mantle and deep crustal fluids. *Geochim. Cosmochim. Acta* 59, 3331-3350.

Brousse R. and Maury R. (1980) Volcanisme et petrologie de l'ile de Tubuai dans les iles Australes (Pacifique Sud). *Cahiers Indo-Pacifique* 2, 131-193.

Caroff M., Maury R., Guille G. and Cotten M. (1997) Partial melting below Tubuai (Austral Islands, French Polynesia). *Contrib. Mineral. Petrol.* 127, 369-382.

Chase C. G. (1981) Oceanic island Pb: two-stage histories and mantle evolution. *Earth Planet. Sci. Lett.* 52, 227-284.

Chauvel C., Hofmann A. W. and Vidal P. (1992) HIMU-EM: The French Polynesian connection. *Earth Planet Sci Lett* 110, 99-119.

Chauvel C., McDonough W., Guille G., Maury R. and Duncan R. (1997) Contrasting old and young volcanism in Rurutu Island, Austral chain. *Chem. Geol.* 139, 125-143.

Chubb L. J. (1927) The geology of Tubuai of the Austral Islands. *Geol. Soc. London Quart. J.* 83, 294-316.

Class C. and Goldstein S. L. (1997) Plume-lithosphere interactions in the ocean basins: constraints from the source mineralogy. *Earth Planet. Sci. Lett.* 150, 245-260.

Clouard V. and Bonneville A. (2001) How many pacific hotspots are fed by deep-mantle plumes? *Geology* 29(8), 695-698.

Dalrymple G. B., Jarrard R. D. and Clague D. A. (1975) K-Ar ages of some volcanic rocks from the Cook and Austral Islands. *Geol. Sci. Amer. Bull.* 86, 1463-1467.

Dickinson W. R. (1998) Geomorphology and geodynamics of the Cook-Austral Island-Seamount chain in the South Pacific Ocean: Implications for hotspots and plumes. *International Geology Review* 40, 1039-1075.

Diraison C. (1991) Le volcanisme aerien des archipelss polynesiens de la Societe, des Marquises et des Australes-Cook. Tephrostratigraphie, datation isotopique et geochimique comparees. Contribution a l'etude des origines du volcanisme intraplaque du pacifique centrale., Univ. Bretagne Occidentale.

Duncan R. and McDougall I. (1976) Linear volcanism in French Polynesia. *Journ. Volcanol. Geoth. Res.* 1, 197-227.

Dupuy C., Barsczus H. G., Liotard J. M. and Dostal J. (1988) Trace element evidence for the origin of ocean island basalts: an example from the Austral Islands (French Polynesia). *Contrib. Mineral. Petrol.* 98, 293-302.

Eggins S. M., Woodhead J. D., Kinsley L. P. J., Mortimer G. E., Sylvester P., McCulloch M. T., Hergt J. M. and Handler M. R. (1997) A simple method for the precise determination of > 40 trace elements in geological samples by ICPMS using enriched isotope internal standardisation. *Chem. Geol.* 134, 311-326.

Foley S. F. (1993) An experimental study of olivine lamproite: First results from the diamond stability field. *Geochim. Cosmochim. Acta* 57, 483-489.

Fukao Y. (1992) Seismic tomogram of the Earth's mantle: Geodynamic implications. *Science* 258, 625-630.

Garbe-Schönberg C. D. (1993) Simultaneous determination of thirty-seven trace elements in twenty-eight international rock standards by ICP-MS. *Geostandards Newsletters* 17(1), 81-97.

Green T. H. (2000) New partition coefficient determinations pertinent to hydrous melting processes in subduction zones. In *State of the Arc 2000: Processes and Timescales* (ed. J. P. Davidson, J. A. Gamble, and R. C. Price), pp. 92-95.

Halliday A. N., Dickin A. P., Fallick A. E. and Fitton J. G. (1988) Mantle dynamics: a Nd, Sr, Pb and O isotopic study of the Cameroon Line volcanic chain. *J. Petrol.* 29, 181-211.

Hart S. R. (1988) Heterogeneous mantle domains: Signatures, genesis and mixing chronologies. *Earth Planet. Sci. Lett.* 90, 273-296.

Hart S. R. and Brooks C. (1977) Geochemistry and evolution of early precambrian mantle. *Contrib. Mineral. Petrol.* 61(2), 109-128.

Hauri E. and Hart S. R. (1993a) Re-Os isotope systematics of HIMU and EMII oceanic island basalts from the south Pacific Ocean. *Earth Planet. Sci. Lett.* 114, 353-371.

Hauri E., Shimizu N., Dieu J. J. and Hart S. R. (1993b) Evidence for hotspot-related carbonatite metasomatism in the oceanic upper mantle. *Nature* 365, 221-226.

Hauri E. H., Lassiter J. C. and DePaolo D. J. (1996) Osmium isotope systematics of drilled lavas from Mauna Loa, Hawaii. *J Geophys. Res.* 101(B5), 11793-11806.

Hofmann A. W. (1997) Mantle geochemistry: The message from oceanic volcanism. *Nature* 385, 219-229.

Hofmann A. W. and Feigenson M. D. (1983) Case studies on the origin ogf basalt. I. Theory and reassessment of Grenada basalts. *Contrib. Mineral. Petrol.* 84, 382-389.

Hofmann A. W. and Jochum K. P. (1996) Source characteristics derived from very incompatible trace elements in Mauna Loa and Mauna Kea basalts, Hawaii Scientific Drilling Project. *Journal of geophysical research* 101, 11831-11839.

Hofmann A. W. and White W. M. (1982) Mantle plumes from ancient oceanic crust. *Earth Planet. Sci. Lett.* 57, 421-436.

Hofmann A. W. and White W. M. (1983) Ba, Rb and Cs in the Earths mantle. *Zeitschrift fur naturforschung section A-A journal of physical sciences* 38(2), 256-266.

Ionov D. A., Grégoire M. and Prikhod'ko V. S. (1999) Feldspar-Ti-oxide metasomatism in off-cratonic continental and oceanic upper mantle. *Earth Planet. Sci. Lett.* 165, 37-44.

Jenner G. A., Foley S. F., Jackson S. E., Green T. H., Fryer B. J. and Longerich H. P. (1993) Determination of partition coefficients for trace elements in high pressure-temperature experimental run products by laser ablation microprobe-inductively coupled plasma-mass spectrometry (LAM-ICP-MS). *Geochim. Cosmochim. Acta* 57, 5099-5103.

Kelley K. A., Plank T., Ludden J. and Staudigel H. (2003) Composition of altered oceanic crust at ODP Sites 801 and 1149. *Geochem. Geophys. Geosystems* 4(6).

Klemme S., Günther D., Hametner C., Prowatke S. and Zack T. (2006) The partitioning of trace elements between ilmenite, ulvospinel, armalcolite and silicate melts with implications for the early differentiation of the moon. *Chem. Geol.* 234, 251-263.

Kogiso T., Tatsumi Y., Shimoda G. and Barsczus H. G. (1997) High μ (HIMU) ocean island basalts in southern Polynesia: new evidence for whole mantle scale recycling of subducted oceanic crust. *J. Geophys. Res.* 102(B4), 8085-8103.

Larson R. L. (1991) Evidence for a mid-cretaceous superplume. *Geology* 19, 547-550.

Lassiter J. C., Blichert-Toft J., Hauri E. and Barsczus H. G. (2003) Isotope and trace element variations in lavas from Raivavae and Rapa, Cook-Austral islands: constraints on the nature of HIMU- and EM-mantle and the origin of mid-plate volcanismm in French Polynesia. *Chem. Geol.* 202, 115-138.

Lassiter J. C. and Hauri E. H. (1998) Osmium-isotope variations in Hawaiian lavas : evidence for recycled oceanic lithosphere in the Hawaiian plume. *Earth Planet Sci Lett* 164, 483-496.

LaTourette T., Hervig R. L. and Holloway J. R. (1995) Trace element partitioning betwen amphibole, phlogopite, and basanite melt. *Earth Planet. Sci. Lett.* 135, 13-30.

Liotard J. M. and Barsczus H. G. (1989) Genese des foïdites phonolitiques de Tubuai (archipel des Australes, Ocean Pacific Sud): Intervention d'un magma d'affinite carbonatitique. *C.R. Acad. Sci. Paris* 308(2), 1261-1266.

Marini J. C., Chauvel C. and Maury R. (2005) Hf isotope composition of northern Luzon arc lavas suggest involvment of pelagic sediments in their source. *Contrib. Mineral. Petrol.* 149, 216-232.

Marshall P. (1957) Geology of Mangaia. *B. P. Bischop Mus. Bull.* 36, 1-48.

Marshall P. (1968) Geology of Rarotonga and Aitutaki. *Royal Soc. New Zealand Trans.* 41(new ser.), 98-100.

Matsuda J. I., Notsu K., Okano J., Yaskawa K. and Chungue L. (1984) Geochemical implications from Sr isotopes and K-Ar age determinations for the Cook-Austral Islands chain. *Tectonophysics* 104, 145-154.

Maury R., El Azzouzi M., Bellon H., Liotard J. M., Guille G., Barsczus H. G., Chauvel C., Diraison C., Dupuy C., Vidal P. and Brousse R. (1994) Geologie et petrologie de l'ile de Tubuai (Australes, Polynesie francaise). *C.R. Acad. Sci. Paris* 318(2), 1341-1347.

Maury R., Guille G., Guillou H., Blais S., Chauvel C. and Brousse R. (2000) Notice explicative, feuille Rurutu et Tubuai, Polynesie francaise (1154). In *Carte geologique France*. BRGM.

Maury R. C., Guille G., Blais S., Guillou H. and Brousse R. (1998) Carte géologique du Territoire de Polynesie francaise, feuille au 1/25 000ème de Rurutu et Tubuai. *Editions du B.R.G.M.*

McCallum I. S. and Charette M. P. (1978) Zr and Nb partition coefficients: Implications for the genesis of mare basalts, kreep, and sea floor basalts. *Geochim. Cosmochim. Acta* 42, 859-869.

McDonough W. F. and Sun S. S. (1995) The composition of the Earth. *Chemical Geology* 120, 223-253.

McNutt M. K., Caress D. W., Reynolds J., Jordahl K. A. and Duncan R. (1997) Failure of the plume theory to explain midplate volcanism in the southern Austral islands. *Nature* 389, 479-482.

McNutt M. K. and Fisher K. M. (1987) The South Pacific superswell. In *Seamounts, Islands, and Atolls*. (ed. B. H. Keating, P. Fryer, R. Batiza, and G. W. Boehlert), pp. 25-34. Am. Geophys. union Geophys. Monogr.

Morgan W. J. (1971) Convection plumes in the lower mantle. *Nature* 230, 42-43.

Morgan W. J. (1972) Deep mantle convection plumes and plate motions. *Bull. Amer. Assoc. Petrol. Geol.* 56, 203-213.

Münker C., Weyer S., Scherer E. and Mezger K. (2001) Separation of high field strength elements (Nb, Ta, Zr, Hf) and Lu from rock samples for MC-ICPMS measurements. *Geochem. Geophys. Geosystems* 2.

Nakamura Y. and Tatsumoto M. (1988) Pb, Nd, and Sr isotopic evidence for a multicomponent source for rocks of Cook-Austral Islands and heterogeneities of mantle plumes. *Geochim. Cosmochim. Acta* 52, 2909-2924.

Obellianne J. M. (1955) Contribution a l'etude geologique des iles des etablissements francais de l'oceanie. *Sci. de la terre* 3, 1-148.

Palacz Z. A. and Saunders A. D. (1986) Coupled trace element and isotope enrichment in the Cook-Austral-Samoa islands, southwest Pacific. *Earth Planet. Sci. Lett.* 79, 270-280.

Pin C. and Zalduegui J. F. S. (1997) Sequential separation of light rare-earth elements, thorium and uranium by miniaturized extraction chromatography: Application to isotopic analyses of silicate rocks. *Analytica chimica acta* 339(1-2), 79-89.

Pitman W. C., Larson R. L. and Herron E. M. (1974) The age of the ocean basins. *Geol. Soc. Am. Map series MC-6*.

Reisberg L. C., Zindler A., Marcantonio F., White W. M., Wyman D. and Weaver B. (1993) Os isotope systematics in ocean island basalts. *Earth Planet Sci Lett* 120, 149-167.

Richards M. A. and Hager B. H. (1988) The Earth's geoid and the large-scale structure of mantle convection. In *The physics of the planets* (ed. S. K. Runcorn), pp. 247-272. Wiley, New York.

Ritsema J. and Allen R. M. (2003) The elusive mantle plume. *Earth Planet. Sci. Lett.* 207, 1-12.

Roy-Barman M. and Allegre C. J. (1995) 187Os/186Os in oceanic island basalts: Tracing oceanic crust recycling in the mantle. *Earth Planet. Sci. Lett.* 129, 145-161.

Salters V. J. M. and Stracke A. (2004) Composition of the depleted mantle. *Geochem. Geophys. Geosystems* 5(5).

Salters V. J. M. and White W. M. (1998) Hf isotope constraints on mantle evolution. *Chem. Geol.* 145, 447-460.

Schmidt M. W., Dardon A. C., G. and Vannucci R. (2004) The dependance of Nb and Ta rutile-melt partitioning on melt composition and Nb/Ta fractionation during subduction processes. *Earth Planet. Sci. Lett.* 226, 415-432.

Shaw D. M. (1970) Trace element fractionation during anatexis. *Geochim. Cosmochim. Acta* 34, 237-243.

Stracke A., Bizimis M. and Salters V. J. M. (2003) Recycling oceanic crust: Quantitative constraints. *Geochem. Geophys. Geosystems* 4(3).

Stracke A., Hofmann A. W. and Hart S. R. (2005) FOZO, HIMU, and the rest of the mantle zoo. *Geochem. Geophys. Geosystems* 6(5).

Turner D. L. and Jarrard R. D. (1982) K-Ar dating of the Cook-Austral Island chain: a test of the hot-spot hypothesis. *Journ. Volcanol. Geoth. Res.* 12, 187-220.

Vidal P., Chauvel C. and Brousse R. (1984) Large mantle heterogeneity beneath French Polynesia. *Nature* 307, 536-538.

Vidal P., Rocaboy A. and Dupuy C. (1989) Composition du manteau: le reservoir HIMU. *C.R. Acad. Sci. Paris* 308(2), 635-639.

Weaver B. L. (1991) The origin of ocean island basalt end-member compositions: Trace element and isotopic constraints. *Earth Planet. Sci. Lett.* 104, 381-397.

Wessel P. and Kroenke L. (1997) A geometric technique for relocating hotspots and refining absolute plate motions. *Nature* 387, 365-369.

Willbold M. and Stracke A. (2006) Trace element composition of mantle end-members: Implications for recycling of oceanic and upper and lower continental crust. *Geochem. Geophys. Geosystems* 7(4).

Wilson J. T. (1963) Evidence from islands of the spreading of the ocean floors. *Nature* 197, 536-538.

Wood C. P. (1978a) Petrology of Aitutaki, Cook Islands. *N. Z. J. Geol. Geophys.* 21, 761-765.

Wood C. P. (1978b) Petrology of Atiu and Mangaia, Cook Islands. *N. Z. J. Geol. Geophys.* 21, 767-771.

Xiong X. L., Adam J. and Green T. H. (2005) Rutile stability and rutile/melt HFSE partitioning during partial melting of hydrous basalt: Implications for TTG genesis. *Chem. Geol.* 218, 339-359.

Zhao D. (2001) Seismic structure and origin of hotspots and mantle plumes. *Earth Planet. Sci. Lett.* 192, 251-265.

Zindler A. and Hart S. R. (1986) Chemical geodynamics. *Annu. Rev. Earth Planet. Sci.* 14, 493-571.

Conclusions

Various inverse modeling approaches have been used throughout this entire study in order to constrain the effects of divers petrogenetic processes (partial melting, fractional crystallization, wall-rock assimilation) on the mantle composition sampled in both the Hawaiian and the Tubuai lavas. Using the AFC modeling of DePaolo (1981) on Os isotopic variations, we have been able to quantify the amount of wallrock material assimilated during the Hawaiian magma differentiation and to measure the effects on Sr and Nd isotopic tracers. Using the inverse modeling approach of Hofmann and Feigenson (1983) on trace element variations, we have further estimated most of the trace element pattern of the source of Kohala Volcano. Finally, the geochemical variations in lavas from Tubuai Island have been successfully reproduced using fractional crystallization and partial melting modeling, improving thereby our knowledge about the mantle source composition of Tubuai lavas and its evolution. In the following, I will summarize the main conclusions and give some perspectives for each study.

1. AFC processes during the Kohala magma differentiation

The study of PGE variations in lavas from Kohala Volcano has first revealed that Os and other PGE behavior change during the Hawaiian magma differentiation. The Hawaiian magma most likely reaches sulfur saturation as its composition evolves through ~ 8% MgO, inducing the formation of sulfide phases in evolved magma. Since the PGE are extremely compatible in sulfides ($D^{PGE}_{sulfide/melt} \sim 10^4 - 10^5$, Fleet et al., 1996; Roy-Barman et al., 1998; Sattari et al., 2002), a strong and simultaneous decline of all PGE abundances in lavas containing less than ~8% MgO results. Correlations between MgO and each PGE contents described by the Kohala lavas and other Hawaiian lavas clearly show that PGE behave incompatibly (bulk $D_{Ir, Pt, Pd} \leq 0.5$) or slightly compatibly ($D_{Os, Ru} \sim 3 - 6$) in lavas containing more than 8% MgO, but become all very compatible ($30 < D_{PGE} > 50$) in evolved lavas with less than 8 % MgO. Around 0.1 – 0.3 % sulfide would be sufficient to generate the high bulk D_{PGE} values estimated in evolved lavas. These values of bulk D_{PGE} and the proportion of sulfide phases inferred are, however, associated with relatively large errors due to the poor PGE data set on Hawaiian lavas. Additional PGE data on Hawaiian lavas would be therefore helpful to accurately constrain the PGE partitioning in both sulfur under-saturated and sulfur saturated condition.

The study of $^{187}Os/^{188}Os$ variations in the same suites of lavas from Kohala Volcano has further indicated that small amounts of upper pacific crust material (< 8%) have been assimilated during the shield stage of Kohala volcanic activity. Os-isotopes ratios strongly depend on the abundance of Os in the magma and their sensitivity to any radiogenic contaminant increases as the Os content decreases in the magma. Therefore, Os isotopic compositions measured in lavas with more than 8% MgO, and high Os concentrations are very homogeneous (0.130 – 0.133) and most likely reflect the true mantle signature of Kohala lavas. In contrast, Os isotopic compositions measured in evolved lavas with less than 8% MgO and low Os concentrations have a large range of radiogenic values (0.137 – 0.196) that are clearly the result of contamination with crustal Os. Similar processes have affected lavas from the postshield stage of volcanism of Kohala Volcano ($^{187}Os/^{188}Os$ = 0.131 - 0.223).

The magma chamber of Kohala Volcano may thus be situated in the upper level of the oceanic crust, which is in agreement with previous geophysical estimations of shallow magma reservoir in Mauna Loa and Kilauea Volcanoes (Ryan et al., 1981; Decker et al., 1983; Thurber, 1984, 1987; Rowan and Clayton, 1993). On the other hand, AFC modeling has shown that the Sr and Nd isotopic compositions of the Hawaiian lavas are only susceptible to change significantly beyond 30 % of upper crust assimilation. Therefore, this study demonstrates that shallow level assimilation processes are not responsible for the Sr and Nd isotopic heterogeneities observed within the Kohala lavas and possibly within individual Hawaiian Volcanoes in general.

2. Trace element variations in Kohala lavas and source composition.

The extension of trace element composition to highly incompatible elements has first confirmed the “Kea trend” signature of the Kohala lavas. Most of the trace element pattern of their mantle source has been further estimated using the trace element variations and the inverse modeling method of Hofmann and Feigenson (1983). This calculated initial trace element pattern has confirmed and extended the highly-incompatible depletion of the Hawaiian source rocks and has shown that the incompatible element enrichments present in the Hawaiian melts are entirely produced by partial melting processes.

More accurate corrections for fractional crystallization have been obtained on the HREE when updating the primary magma composition for the Kohala lavas, which has reduced the errors obtained on the initial HREE concentrations compared to the previous work of Feigenson et al. (1983). The shape of the calculated initial REE patterns is, however, similar to those obtained by Feigenson et al. (1983), which validate the previous conclusions regarding the presence of residual clinopyroxene, with or without small amounts of residual garnet, during the formation of the Kohala magma.

The same method of calculations has been applied to the postshield lavas and has suggested that, contrary to isotopic data, only minor changes have affected the source composition during the post shield building stage of Kohala Volcano.

Better constrains on the source composition of these Hawaiian lavas could be obtained, however, with additional trace element data on both the Pololu and Hawi lavas from Kohala Volcano.

3. The magmatic evolution of Tubuai Island

In contrast with the previous study on Hawaiian lavas, it has been shown here that the different mafic lavas from Tubuai Island have been produced by different degrees of partial melting and do not derive from a single parental magma composition. The study of $^{87}Sr/^{86}Sr$, $^{143}Nd/^{144}Nd$ and $^{176}Hf/^{177}Hf$ variations in these lavas has confirmed their co-genetic nature and the very homogeneous isotopic signature of these HIMU-type OIB. However, a progressive decrease in the degree of partial melting has affected their geochemical compositions and generated enrichment of incompatible major and trace elements from the early volcanics (alkali basalts and basanites) to the later volcanics (nephelinites). The study of trace element variations between the different lava types has further revealed the presence of small quantities of phlogopite and a Ti-bearing phase (ilmenite or rutile) in the source of the Tubuai lavas. These minor phases are entirely consumed during the early volcanic events but remain residual during formation of the late analcitic and nephelinitic magmas, causing a relative depletion of Rb, Ba, K, HFSE and Ti in the lava compositions.

The presence of these phases in the source of Tubuai lavas will need further to be understood. Phlogopite may reflect the presence of water in the source and these minor phases

may have stabilized during initial stages of partial melting and be consumed during formation of the early volcanics. Better constrains on the stability of rutile and ilmenite under mantle condition and trace element partitioning in these phases would also help to determine which Ti-bearing phase was present in the source of the Tubuai lavas.

References

Decker R. W., Koyanagi R. Y., Dvorak J. J., Lockwood J. P., Okamura A. T., Yamashita K. M. and Tanigawa W. R. (1983) Seismicity and surface deformation of Mauna Loa Volcano, Hawaii. *EOS* 64, 545-547.

DePaolo D. J. (1981) Trace element isotopic effects of combined wallrock assimilation and fractional crystallisation. *Earth Planet Sci Lett* 53, 189-202.

Feigenson M. D., Hofmann A. W. and Spera F. J. (1983) Case studies on the origin of basalt II. The transition from Tholeiitic to alkalic volcanism on Kohala Volcano, Hawaii. . *Contrib Mineral petrol* 84, 390-405.

Fleet M. E., Crocket J. L. and Stone W. E. (1996) Partitioning of platinum-group elements (Ir, Os, Ru, Pt, Pd) and Gold between sulfide liquid and basalt melt. *Geochim Cosmochim Acta* 60, 2397-2412.

Hofmann A. W. and Feigenson M. D. (1983) Case studies on the origin ogf basalt. I. Theory and reassessment of Grenada basalts. *Contrib. Mineral. Petrol.* 84, 382-389.

Rowan L. R. and Clayton R. W. (1993) The three-dimensional structure of Kilauea Volcano, Hawaii, From travel time tomography. *J Geophys. Res.* 98, 4355-4375.

Roy-Barman M., Wasserburg G. J., Papanastessiou D. A. and Chaussidon M. (1998) Osmium isotopic compositions and Os concentrations in sulfide globules from basaltic glasses. . *Earth Planet Sci Lett* 154, 331-347.

Ryan C. G., Koyanagi R. Y. and Fiske R. S. (1981) Modeling the three-dimensional structure of macroscopic magma transport systems: Applications to Kilauea Volcano, Hawaii. *J Geophys. Res.* 86, 7111-7129.

Sattari P., Brenan J. M., Horn I. and McDonough W. F. (2002) Experimental constraints on the Sulfide- and Chromite-Silicate melt: partitioning behavior of rhenium and platinum-group elements. *Econ. Geol.* 97, 385-398.

Thurber C. H. (1984) Seismic detection of the summit magma complex of Kilauea Volcano, Hawaii. *Science* 223, 165-167.

Thurber C. H. (1987) Seismic structure and tectonics of Kilauea Volcano, Hawaii. *US Geol Surv Prof Pap* 1350, 919-934.